

# Game of Coding for Vector-Valued Computations

Hanzaleh Akbari Nodehi, Parsa Moradi, Soheil Mohajer, and Mohammad Ali Maddah-Ali  
 University of Minnesota, Twin Cities  
 Minneapolis, MN, USA  
 Email: {akbar066, moradi, soheil, maddah}@umn.edu

## Abstract

The game of coding is a new framework at the intersection of game theory and coding theory; designed to transcend the fundamental limitations of classical coding theory. While traditional coding theoretic schemes rely on a strict trust assumption, that honest nodes must outnumber adversarial ones to guarantee valid decoding, the game of coding leverages the economic rationality of actors to guarantee correctness and reliable decodability, even in the presence of an adversarial majority. This capability is paramount for emerging permissionless applications, particularly decentralized machine learning (DeML). However, prior investigations into the game of coding have been strictly confined to scalar computations, limiting their applicability to real world tasks where high dimensional data is the norm. In this paper, we bridge this gap by extending the framework to the general  $N$ -dimensional Euclidean space. We provide a rigorous problem formulation for vector valued computations and fully characterize the equilibrium strategies of the resulting high dimensional game. Our analysis demonstrates that the resilience properties established in the scalar setting are preserved in the vector regime, establishing a theoretical foundation for secure, large scale decentralized computing without honest majority assumptions.

## I. INTRODUCTION

Consider a scenario comprising a data collector (DC) and a set of  $M$  external worker nodes. The DC outsources a (perhaps approximate) computational task, such as the calculation of a gradient in a machine learning model, to these workers, who return their results to the DC for aggregation. The

The work of Mohammad Ali Maddah-Ali, Hanzaleh Akbari Nodehi, and Parsa Moradi has been partially supported by the National Science Foundation under Grant CCF-2348638.

network consists of two disjoint sets of workers: a set of honest nodes, denoted by  $\mathcal{H}$ , who faithfully adhere to the protocol, and a set of adversarial nodes, denoted by  $\mathcal{T}$ . We assume that these sets partition the network, such that  $\mathcal{H} \cap \mathcal{T} = \emptyset$  and  $\mathcal{H} \cup \mathcal{T} = \{1, \dots, M\}$ .

Standard coding-theoretic frameworks rely on a fundamental trust assumption: valid decoding is only guaranteed when honest workers sufficiently outnumber their adversarial counterparts. This honest-majority constraint is evident across various schemes. For example, repetition coding mandates  $|\mathcal{H}| \geq |\mathcal{T}| + 1$  for error-free recovery. In the context of polynomial-based computations, the requirements are even more stringent; Reed-Solomon  $(K, M)$  codes [1] require  $|\mathcal{H}| \geq |\mathcal{T}| + K$ , while Lagrange coding [2] with degree  $d$  necessitates  $|\mathcal{H}| > |\mathcal{T}| + (K - 1)d$ . Similar hard thresholds govern recoverability in analog coding settings [3]–[6]. In all these cases, a fundamental trust assumption is imposed: the honest workers must outnumber the adversaries. Consequently, if the majority of the network is adversarial, classical approaches fail to produce a decoded result.

This limitation is particularly problematic in the emerging landscape of Web3 [7]–[9], specifically in decentralized machine learning (DeML). In DeML, training or inference is often coordinated by smart contracts on a blockchain to ensure transparency and accountability [10]–[16]. However, given that blockchains cannot handle the heavy computational loads of modern AI, tasks must be outsourced to off-chain networks of volunteer workers [17]. We highlight two critical characteristics of these networks that challenge standard modeling assumptions. First, these systems are inherently permissionless. Since the network allows unrestricted access to any contributor, the conventional assumption that the majority of nodes are honest is difficult to justify. Second, the behavior of worker nodes is primarily governed by economic incentives. In blockchain-based environments, participants are motivated by cryptocurrency rewards; they act as rational agents optimizing for profit, rather than as purely malicious adversaries intent on system destruction.

If we model the adversarial nodes as *rational* players rather than purely malicious ones, the problem changes fundamentally. In this setting, the DC announces a reward policy: computations satisfying specific acceptance conditions are rewarded, while others are rejected. For example, the DC may require that any two reported results lie within a specific small distance of each other, or that all submitted vectors satisfy a particular mathematical constraint, such as lying on a specific polynomial or manifold. Rational adversaries face a conflict of interest: they wish to maximize their utility by injecting error into the DC’s final estimate, but they also desire the financial reward, which is contingent on their results being accepted. Unlike malicious actors who aim solely to destroy system *liveness*, defined here as the probability that the system accepts a result and remains functional, rational players optimize their strategy based on the probability of acceptance and the magnitude

of the error they can successfully inject. Conversely, the DC seeks to maximize this probability of acceptance while minimizing the estimation error. This interaction creates a game-theoretic scenario, formally introduced as the *game of coding* framework in [18]–[21].

The game of coding framework offers a viable alternative to existing outsourcing solutions for DeML:

- **Verifiable Computing:** This approach guarantees correctness of the results by requiring workers to generate cryptographic proof of correctness along with their results [22], [23]. However, this method is often computationally prohibitive [24]–[28] and is restricted to exact computation [28]–[31], which conflicts with the approximate nature of AI.
- **Optimistic Verification:** This common approach assumes computations are correct by default and relies on a challenge-response mechanism to ensure correctness [32], [33]. In this model, the system assumes a result is correct unless a node acting as a challenger sends a fraud proof message to the blockchain claiming the computation is incorrect; the blockchain then initiates a judgment procedure to determine which party, either the worker who performed the computation or the challenger, is acting maliciously. The honest party is rewarded while the malicious one is punished. The primary failure of this method is that it suffers from delayed finality, because it requires a sufficiently large window of time to allow for the submission of a fraud proof message, and critically, this mechanism does not support approximate computing.
- **Classical Coded Computing:** This method utilizes algorithmic redundancy to manage latency and approximation [2], [3], [34]. While effective, it lacks resilience against an adversarial majority, making it unsuitable for permissionless environments.

To overcome the limitations of the aforementioned approaches, the game of coding emerged as a powerful alternative. As established in [18], this framework lies at the intersection of game theory and coding theory. The initial investigation in [18] laid the theoretical foundation by analyzing computation over scalar values. A key finding of this work was that accurate estimation and reliable decodability are achievable even when the majority of the network is adversarial; a feat impossible under classical coding theory. Following this, subsequent research sought to capture critical practical considerations necessary for real-world deployment. Specifically, [19] addressed the threat of attackers masquerading as multiple workers to gain unfair influence, known as a Sybil attack; the work proved that the framework is inherently Sybil resistant, which means it maintains robustness even if an attacker creates numerous fake identities to manipulate the system. Furthermore, to handle scenarios where the DC does not know the adversary’s strategy in advance, [20] employed bandit algorithms;

these are machine learning techniques that allow the system to learn the most effective reward policies over time by observing the adversary's behavior and adapting to it dynamically. A comprehensive summary of these motivations and comparisons is available in [21].

### A. Contributions of This Paper

While all prior research on the game of coding was limited to scalar computations, in this paper we extend the framework to the general  $N$ -dimensional Euclidean space. This extension is critical for practical applicability, since most real-world computations, such as gradient calculations in machine learning, involve vector-valued results rather than scalars.

In this work, we provide a rigorous problem formulation for the high-dimensional setting; we formally define the utility functions that each player seeks to maximize and define the equilibrium of this game. In this strategic interaction, the DC first commits to a *parametric* acceptance policy, comprising a specific decision rule governed by a tunable free parameter. For any given parameter setting, the adversary chooses a noise distribution that maximizes its own utility, balancing the trade-off between the probability of passing the acceptance policy and the magnitude of the injected error. The DC, anticipating this rational behavior, can effectively predict the adversary's optimal strategy, along with the resulting system state, for any choice of the parameter. By evaluating the expected outcome across the parameter space, the DC identifies and commits to the optimal parameter value that maximizes its own utility.

We assume very minimal and natural assumptions for these utility functions to ensure the framework captures a wide range of practical scenarios. However, in this interaction, finding the equilibrium is directly related to the specific forms of these utility functions; it is a significant challenge to find the equilibrium if we stick to such minimal assumptions for the utilities. To resolve this issue, we define an intermediary optimization problem in (19) which is independent of the specific utility functions of the players. Then, in Theorem 1, we prove that by having access to the result of that optimization problem, one can find the equilibrium of the game very readily using a 2D searching procedure defined in Algorithm 1. It is worth noting that this is a fundamentally important contribution, since it converts an optimization problem over infinitely-many dimension (the space of adversarial noise distributions and acceptance policies) to a problem with a two-dimensional feasible set. Consequently, the remaining task is to solve the intermediary optimization problem introduced in (19), which is achieved in Theorem 2.

Furthermore, we present detailed numerical examples to clarify the theoretical findings and visualize the system dynamics. Throughout this paper, we significantly extend the scope of the game of

coding framework, capturing a critical aspect of real-world decentralized applications where multi-dimensional data is the norm.

### B. Organization of The Paper

The remainder of this paper is organized as follows. Section II formally introduces the problem formulation, the utility functions for both the DC and the adversary, and the game-theoretic formulation of the problem. In Section III, we present the main theoretical findings of this work. The detailed mathematical proofs of the main theorems are provided in Section IV and Section V. Section VI provides numerical examples across different cases to visualize the equilibrium and demonstrate the impact of different strategies. Finally, Section VII concludes the paper and discusses potential directions for future research.

### C. Notation

We denote random variables using uppercase letters and deterministic values (or realizations) using lowercase letters. Furthermore, we distinguish vectors from scalars by using boldface type for the former and standard type for the latter. For example,  $\mathbf{X}$  represents a random vector, whereas  $\mathbf{x}$  denotes a deterministic vector. Similarly,  $X$  represents a scalar random variable, while  $x$  denotes a deterministic scalar. Unless stated otherwise, all vectors are elements of the  $N$ -dimensional Euclidean space  $\mathbb{R}^N$ , and we denote the standard Euclidean ( $\ell_2$ ) norm of a vector  $\mathbf{x} = (x_1, \dots, x_N)$  by  $\|\mathbf{x}\|_2 = \sqrt{\sum_{i=1}^N x_i^2}$ .

The symbol  $\Gamma(\cdot)$  denotes the Euler Gamma function, which generalizes the factorial function to real and complex arguments. For any real number  $x > 0$ , it is defined by the integral

$$\Gamma(x) = \int_0^\infty t^{x-1} e^{-t} dt. \quad (1)$$

If  $n$  is non-negative integer, we know that  $\Gamma(n+1) = n!$ , and,  $\Gamma(n + \frac{1}{2}) = (n - \frac{1}{2}) \cdot (n - \frac{3}{2}) \cdots \frac{1}{2} \cdot \sqrt{\pi}$ .

We define the  $N$ -dimensional closed ball of radius  $r > 0$  centered at a point  $\mathbf{c} \in \mathbb{R}^N$  as

$$\mathcal{B}_N(r, \mathbf{c}) \triangleq \left\{ \mathbf{x} \in \mathbb{R}^N : \|\mathbf{x} - \mathbf{c}\|_2 \leq r \right\}. \quad (2)$$

For simplicity, when the center is at the origin (i.e.,  $\mathbf{c} = \mathbf{0}$ ), we denote the ball by  $\mathcal{B}_N(r)$ . The volume of an  $N$ -ball depends only on its radius and is independent of its center. We denote this volume by  $V_N(r)$ , which is given by

$$V_N(r) = \frac{\pi^{N/2}}{\Gamma(\frac{N}{2} + 1)} r^N. \quad (3)$$

Accordingly, we define the uniform distribution over this ball, denoted by  $\mathbf{X} \sim \text{Unif}(\mathcal{B}_N(r))$ , as the distribution characterized by the probability density function (PDF)  $f_{\mathbf{X}}(\mathbf{x}) = 1/V_N(r)$  for  $\mathbf{x} \in \mathcal{B}_N(r)$  and 0 otherwise.

Let  $\mathbb{R}^*$  denote the Euclidean space of arbitrary dimension. For any set  $\mathcal{S} \subseteq \mathbb{R}^*$  and an arbitrary function  $f : \mathcal{S} \rightarrow \mathbb{R}$ , the notation  $\arg \max_{x \in \mathcal{S}} f(x)$  represents the set comprising all elements  $x$  in  $\mathcal{S}$  that maximize  $f(x)$ . Similarly we define  $\arg \min_{x \in \mathcal{S}} f(x)$ . For  $a, b \in \mathbb{R}$ , the notation  $[a, b]$  represents the closed interval  $\{x \in \mathbb{R} : a \leq x \leq b\}$ .

## II. PROBLEM FORMULATION

In this section, we establish the formal mathematical framework for the  $N$ -Dimensional game of coding. We consider a setting comprised of a data collector (DC) and a set of  $K = 2$  computational nodes<sup>1</sup>, denoted by  $\mathcal{K} \triangleq \{1, 2\}$ , operating in an  $N$ -dimensional Euclidean space  $\mathbb{R}^N$ . The system architecture is illustrated in Figure 1. Let  $\mathbf{U} \in \mathbb{R}^N$  be a random vector representing the ground truth, which is characterized by a probability density function  $f_{\mathbf{U}}(\mathbf{u})$ . The ultimate goal of the DC is to compute/estimate  $\mathbf{U}$ , which can be found from the data available to the computing nodes. However, the DC does not have direct access to the realization of  $\mathbf{U}$  and must instead rely on the reports provided by the nodes to estimate its value.

The set of nodes is partitioned into two disjoint singleton sets: an honest node  $\mathcal{H} = \{h\}$  and an adversarial node  $\mathcal{T} = \{a\}$ . Thus,  $\mathcal{K} = \{h, a\}$ . The identity of the adversary is unknown to the DC, and we assume the adversary is selected uniformly at random from  $\mathcal{K}$ . Each node  $k \in \mathcal{K}$  transmits a report  $\mathbf{Y}_k \in \mathbb{R}^N$  to the DC. The honest node reports a noisy version of the ground truth, denoted by  $\mathbf{Y}_h$ , where

$$\mathbf{Y}_h = \mathbf{U} + \mathbf{N}_h, \quad (4)$$

and  $\mathbf{N}_h \in \mathbb{R}^N$ . This noise represents inherent noise of approximate computing, measurement error, quantization and compression, or oracle inaccuracy. The noise is uniformly distributed within an  $N$ -dimensional ball of radius  $\Delta$ , denoted as  $\mathcal{B}_N(\Delta)$ , where  $\Delta > 0$ . Specifically, we have

$$\mathbf{N}_h \sim \text{Unif}(\mathcal{B}_N(\Delta)). \quad (5)$$

The parameter  $\Delta$  is assumed to be universally known at all parties. This distribution implies that the honest node provides an unbiased approximation within a strictly defined accuracy radius.

<sup>1</sup>While a two-node system may appear structurally simple, it represents the fundamental unit of our strategic interaction; even in this minimal setting, the game-theoretic dynamics exhibit significant technical complexity and provide the necessary intuition for larger networks.

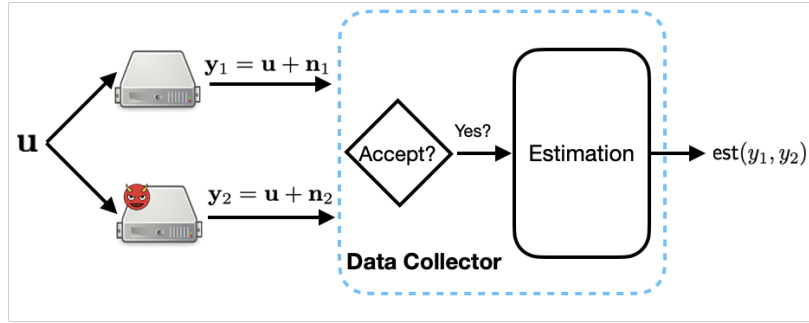


Fig. 1. System model for the  $N$ -Dimensional game of coding. The network consists of one honest node and one adversarial node. Each node reports a noisy version of the ground truth  $\mathbf{U}$  to the DC. For the honest node, the noise  $\mathbf{N}_h$  is uniformly distributed within  $\mathcal{B}_N(\Delta)$ , while for the adversarial node, the noise  $\mathbf{N}_a$  follows an arbitrary distribution  $g(\cdot)$  chosen by the adversary. Upon receiving the data, the DC decides whether to accept or reject the inputs based on a consistency threshold  $\eta$ . If accepted, the DC outputs an estimate of  $\mathbf{U}$ . In this game, the DC acts as the leader choosing  $\eta$ , and the adversary acts as the follower choosing  $g(\cdot)$ .

Conversely, the adversarial node possesses knowledge of the exact realization of  $\mathbf{U}$  and generates a report denoted by  $\mathbf{Y}_a$ , where

$$\mathbf{Y}_a = \mathbf{U} + \mathbf{N}_a. \quad (6)$$

The adversarial noise  $\mathbf{N}_a$  is drawn from an arbitrary PDF  $g(\cdot)$  chosen by the adversary, which is kept private from the DC. We assume that both noise components  $\mathbf{N}_h$  and  $\mathbf{N}_a$  are independent of the ground truth  $\mathbf{U}$  and are also independent of each other.

The DC collects the reports into a tuple  $\underline{\mathbf{Y}} \triangleq (\mathbf{Y}_1, \mathbf{Y}_2)$  and processes them in two stages: **Acceptance** and **Estimation**.

- 1) **Acceptance via Consistency Check:** The DC accepts the computation if and only if the Euclidean distance between the reports does not exceed a threshold scaled by the honest noise bound  $\Delta$ . More precisely, the acceptance event, denoted by  $\mathcal{A}_\eta$ , occurs if

$$\mathcal{A}_\eta : \quad \|\mathbf{Y}_1 - \mathbf{Y}_2\|_2 \leq \eta\Delta, \quad (7)$$

where  $\eta$  is a scalar parameter controlling the strictness of the check. The probability of acceptance (PA) is defined as

$$\text{PA}(g(\cdot), \eta) \triangleq \Pr(\mathcal{A}_\eta) = \Pr(\|\mathbf{Y}_1 - \mathbf{Y}_2\|_2 \leq \eta\Delta), \quad (8)$$

where the probability is evaluated over the randomness of  $\mathbf{U}$ ,  $\mathbf{N}_a$  and  $\mathbf{N}_h$ .

2) **Estimation:** When the reported vectors are accepted, the DC estimates the ground truth using the average of the two reported vectors. More precisely, we have

$$\hat{\mathbf{U}} = \frac{\mathbf{Y}_1 + \mathbf{Y}_2}{2}. \quad (9)$$

The performance of this estimator is measured by the mean squared error (MSE), as

$$\text{MSE}(g(\cdot), \eta) \triangleq \mathbb{E} \left[ \left\| \mathbf{U} - \frac{\mathbf{Y}_1 + \mathbf{Y}_2}{2} \right\|_2^2 \mid \mathcal{A}_\eta \right]. \quad (10)$$

The threshold parameter  $\eta$  governs the fundamental compromise between the system's liveness, the probability to accept the computation and produce an output, and the accuracy of the final estimate. If  $\eta$  is set to a very large value, the system achieves near-perfect liveness, but this allows the adversary to introduce unbounded error into the estimate of  $\mathbf{U}$ . On the other hand, setting a strict and small threshold for  $\eta$  limits the error magnitude. However, this strictness makes the system vulnerable to denial-of-service (DoS) attacks. A rational adversary could intentionally provide data that slightly violates the threshold, causing the DC to reject the inputs and preventing the system from producing any estimate.

Furthermore, the choice of  $\eta$  directly influences the adversary's behavior. In many decentralized applications, such as oracle networks and decentralized machine learning (DeML) [35]–[37], the adversary only receives rewards when their input is accepted. If the system rejects the data, the adversary gains no rewards and exerts no influence on the outcome. This structure creates a partial alignment of interests: to maximize the error, the adversary should choose a large noise; however, the adversary must first ensure that the system remains functional and its reported vector is accepted. Consequently, the adversary is incentivized to keep their induced noise within a range that satisfies the acceptance criteria, rather than simply forcing the system to shut down.

To rigorously capture this mechanism, we model the interaction between the DC and the adversary as a **Stackelberg game** [38]. In game theory, a Stackelberg model describes a sequential hierarchy where a **leader** commits to a strategy first, and a **follower** moves only after observing the leader's action. This stands in contrast to a standard Nash equilibrium in simultaneous games, where players act at the same time without observing the opponent's choice.

In our context, the DC acts as the **leader**. This role is mandated by the practical implementation of the system: the DC typically operates as a smart contract. Due to the inherent transparency of blockchain technology, the DC's acceptance policy, specifically the threshold parameter  $\eta$ , is a public code. The adversary, acting as the **follower**, can inspect the smart contract to see the exact value of  $\eta$  before generating any data. Because the adversary chooses their strategy with full knowledge of the DC's commitment, the interaction is inherently sequential rather than simultaneous.

To formalize the game, we define the admissible action sets for both players. To choose the action set for the DC, we note that even in the hypothetical and optimistic case where both nodes are honest, the inherent approximate nature of the computation implies that each report  $\mathbf{Y}_i$  may deviate from the ground truth by up to  $\Delta$ ; consequently, the distance  $\|\mathbf{Y}_1 - \mathbf{Y}_2\|_2$  can be as large as  $2\Delta$ . To ensure that the DC does not reject these honest reports, the threshold parameter  $\eta$  must be at least  $2$ .<sup>2</sup> Thus, the DC's action set is defined as

$$\Lambda_{\text{DC}} \triangleq [2, \infty). \quad (11)$$

The adversary, in turn, selects a noise distribution from the action set  $\Lambda_{\text{AD}}$ , which consists of all valid probability density functions over the noise space  $\mathbb{R}^N$ . More precisely, we have

$$\Lambda_{\text{AD}} \triangleq \left\{ g : \mathbb{R}^N \rightarrow \mathbb{R}_{\geq 0} \middle| \int_{\mathbb{R}^N} g(\mathbf{x}) d\mathbf{x} = 1 \right\}. \quad (12)$$

The players aim to maximize their respective utility functions. These objectives are captured by the following utility functions

$$U_{\text{DC}}(g(\cdot), \eta) \triangleq Q_{\text{DC}}(\text{MSE}(g(\cdot), \eta), \text{PA}(g(\cdot), \eta)), \quad (13)$$

$$U_{\text{AD}}(g(\cdot), \eta) \triangleq Q_{\text{AD}}(\text{MSE}(g(\cdot), \eta), \text{PA}(g(\cdot), \eta)), \quad (14)$$

where  $Q_{\text{DC}}$  is monotonically non-increasing in MSE and non-decreasing in PA, while  $Q_{\text{AD}}$  is strictly<sup>3</sup> increasing in both arguments. In contrast, for the DC, we rely only on the natural assumption of non-decreasing monotonicity to encompass the broadest range of practical scenarios. We assume that functions  $Q_{\text{DC}}$  and  $Q_{\text{AD}}$  are publicly known by all the parties.

<sup>2</sup>While exploring  $\eta < 2$  could offer an interesting trade-off between the risk of rejecting honest nodes and the potential for tighter error control, such an extension does not fundamentally alter the core analysis of this paper and can be viewed as a complementary direction for future research.

<sup>3</sup>To determine the game equilibrium, we utilize an intermediate optimization problem defined in (19), which is independent of  $U_{\text{DC}}$  and  $U_{\text{AD}}$ . Theorem 1 establishes that by solving (19), we can determine the optimal strategies for both players, specifically, the noise distribution for the adversary and the acceptance parameter for the DC. The strict monotonicity of  $Q_{\text{AD}}$  is a necessary condition for the validity of this theorem (see Section IV for details). Intuitively, this condition ensures that any adversarial best response must maximize the induced error for a given probability of acceptance, as the adversary would otherwise have a strict incentive to further increase the system error.

The game is resolved via backward induction. First, for any fixed threshold  $\eta \in \Lambda_{\text{DC}}$  committed to by the leader, the follower identifies the set of optimal strategies to maximize its own utility function; this strategic response is captured by the adversary's best response set, which we define as

$$\mathcal{B}_{\text{AD}}^\eta \triangleq \arg \max_{g(\cdot) \in \Lambda_{\text{AD}}} U_{\text{AD}}(g(\cdot), \eta). \quad (15)$$

It is crucial to observe that the adversary is indifferent among all strategies within  $\mathcal{B}_{\text{AD}}^\eta$ , as they all yield the same maximal utility. However, these strategies may produce different utilities for the DC. To ensure a robust security guarantee, we adopt a conservative worst-case formulation. We assume that, among the adversary's optimal strategies, the specific  $g(\cdot)$  chosen is the one most detrimental to the DC. We therefore define the set of worst-case adversarial responses as

$$\bar{\mathcal{B}}_{\text{AD}}^\eta \triangleq \arg \min_{g(\cdot) \in \mathcal{B}_{\text{AD}}^\eta} U_{\text{DC}}(g(\cdot), \eta). \quad (16)$$

Note that the DC can also solve the optimization problem in (16), and hence, it knows that for every acceptance parameter  $\eta$ , what noise density function  $g(\cdot)$  will be chosen by the adversary. Finally, the DC acts as the leader by selecting the optimal threshold  $\eta^*$  that maximizes its utility under this worst-case noise, introduced by the adversary. More precisely, for any  $\eta$ , let  $g_\eta^*(\cdot)$  be an arbitrary noise distribution in  $\bar{\mathcal{B}}_{\text{AD}}^\eta$ . Since every noise in  $\bar{\mathcal{B}}_{\text{AD}}^\eta$  provides the same utility for the DC, we have

$$\eta^* = \arg \max_{\eta \in \Lambda_{\text{DC}}} U_{\text{DC}}(g_\eta^*(\cdot), \eta). \quad (17)$$

The Stackelberg equilibrium is therefore characterized by the pair  $(\eta^*, g_{\eta^*}^*(\cdot))$ , where  $g_{\eta^*}^*(\cdot)$  is any noise in the set  $\bar{\mathcal{B}}_{\text{AD}}^{\eta^*}$ . The corresponding MSE, probability of acceptance, and utility values for this equilibrium are denoted by  $\text{MSE}^* = \text{MSE}(g_{\eta^*}^*(\cdot), \eta^*)$ ,  $\text{PA}^* = \text{PA}(g_{\eta^*}^*(\cdot), \eta^*)$ ,  $U_{\text{DC}}^* = U_{\text{DC}}(g_{\eta^*}^*(\cdot), \eta^*)$ , and  $U_{\text{AD}}^* = U_{\text{AD}}(g_{\eta^*}^*(\cdot), \eta^*)$ , respectively.

### III. MAIN RESULTS

Based on (15), (16), and (17), The DC's optimal threshold  $\eta^*$  is determined by solving the following optimization problem

$$\eta^* = \arg \max_{\eta \in \Lambda_{\text{DC}}} \min_{g(\cdot) \in \mathcal{B}_{\text{AD}}^\eta} Q_{\text{DC}}(\text{MSE}(g(\cdot), \eta), \text{PA}(g(\cdot), \eta)). \quad (18)$$

The optimization problem in (18) is formidable to solve directly due to two fundamental challenges.

- 1) **Minimal Assumptions on Utility Functions:** We aim to solve the game for a broad class of utility functions. We make no restrictive mathematical assumptions, such as convexity or concavity, on  $Q_{\text{DC}}$  or  $Q_{\text{AD}}$ , defined in (13) and (14), respectively. Our only requirement is that they satisfy the intuitive, common-sense monotonicity properties defined earlier (e.g., the

adversary always prefers higher error). This generality precludes the use of standard convex optimization tools that rely on specific functional forms.

2) **Infinite-Dimensional Strategy Space:** The adversary's optimization domain is vast. The inner minimization in (18) requires searching over  $\Lambda_{\text{AD}}$ , which contains *every* possible probability density function on  $\mathbb{R}^N$ . Since the adversary is free to shape the noise distribution arbitrarily, without being restricted to parametric families like Gaussian or uniform, identifying the worst-case attack requires a variational approach rather than simple parameter tuning.

To circumvent these obstacles, we define an intermediate optimization problem that is **independent of the utility functions**  $Q_{\text{DC}}$  and  $Q_{\text{AD}}$ . Consider a scenario where the adversary is constrained to maintain a specific level of system liveness. That is, for a fixed threshold  $\eta$  and a minimum target acceptance probability  $\alpha \in (0, 1]$ , we determine the maximum MSE the adversary can strictly enforce. This defines the system's characteristic function, denoted by  $c_\eta(\alpha)$ . More precisely, for a fixed threshold  $\eta \in \Lambda_{\text{DC}}$  and a given probability of acceptance  $\alpha \in (0, 1]$ , we define the intermediary optimization problem as

$$c_\eta(\alpha) \triangleq \max_{g(\cdot) \in \Lambda_{\text{AD}}} \text{MSE}(g(\cdot), \eta) \quad \text{subject to } \text{PA}(g(\cdot), \eta) \geq \alpha. \quad (19)$$

Intuitively,  $c_\eta(\alpha)$  traces the Pareto frontier of the attack surface, representing the maximum damage (error) the adversary can inflict for any required probability of acceptance. We first note that  $c_\eta(\alpha)$  is a non-increasing function of  $\alpha$ . This follows from the fact that if a noise distribution  $g(\cdot)$  satisfies  $\text{PA}(g(\cdot), \eta) \geq \alpha_1$ , it necessarily satisfies  $\text{PA}(g(\cdot), \eta) \geq \alpha_2$  for any  $\alpha_2 < \alpha_1$ ; consequently, the optimization domain in (19) for  $\alpha_2$  is a superset of that for  $\alpha_1$ , implying  $c_\eta(\alpha_2) \geq c_\eta(\alpha_1)$ .

As illustrated in Figure 2, the  $c_\eta(\alpha)$  curve demarcates the feasible region of attacks. Point A (in red) represents an inefficient strategy for a rational adversary; suppose that for a committed  $\eta$ , an adversarial noise  $g_A(\cdot)$  achieves the outcome at A. By replacing it with the noise  $g_B(\cdot)$  corresponding to point B (in black), the adversary maintains the same probability of acceptance while inducing a strictly higher MSE. Since the adversary's utility  $U_{\text{AD}}$ , defined in (14), is strictly increasing with respect to the induced error, a rational follower will always prefer point B over point A. Conversely, point C (in gray) in Figure 2 represents an outcome that is strictly unattainable. By the definition of  $c_\eta(\alpha)$  in (19), there exists no feasible noise distribution  $g(\cdot) \in \Lambda_{\text{AD}}$  capable of inducing the level of MSE shown at C without violating the corresponding probability of acceptance constraint. Thus, a rational adversary will always restrict its strategy set to the frontier defined by  $c_\eta(\alpha)$ .

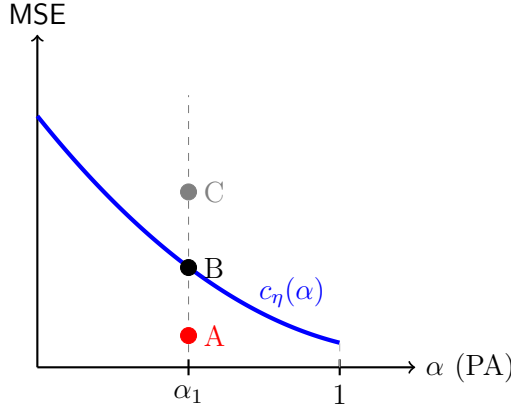


Fig. 2. The Pareto frontier  $c_\eta(\alpha)$  and adversarial rationality. Point A (red) is inefficient compared to point B (black), while Point C (gray) lies in the unattainable region beyond the maximum possible error for  $\alpha_1$ .

Perhaps surprisingly, it can be shown that characterizing (19) is sufficient to resolve the entire game. More precisely, by leveraging  $c_\eta(\alpha)$ , we can collapse the complex, infinite-dimensional search over probability distributions in (18), into a tractable, finite-dimensional scalar optimization. This reduction is formalized in Algorithm 1, which takes the utility functions and the derived curve  $c_\eta(\cdot)$  as inputs to efficiently compute the optimal strategy  $\hat{\eta}$ . The following theorem establishes that this scalar reduction is exact and that the output of Algorithm 1 corresponds precisely to the Stackelberg equilibrium of the original game.

**Theorem 1.** *The optimal threshold for the DC in the Stackelberg game formulated in (18) is given by the output of Algorithm 1, denoted as  $\hat{\eta}$ . That is,  $\eta^* = \hat{\eta}$ .*

The comprehensive proof of Theorem 1 is provided in Section IV; however, we outline the underlying intuition here. When the DC commits to a threshold  $\eta$ , a rational adversary responds by selecting a noise distribution that maximizes their utility, resulting in a (PA, MSE) pair. As discussed earlier and illustrated in Figure 2, the curve  $c_\eta(\alpha)$  serves as the boundary of the feasible attack space. Any point situated below this frontier, such as point A (red), is suboptimal for the adversary, as they could achieve a higher utility at point B (black) for the same acceptance probability. Conversely, points above the curve, such as point C (gray), are strictly unattainable. Consequently, for a fixed  $\eta$ , the adversary's optimal choice must lie on the frontier  $c_\eta(\cdot)$ , which allows the DC to characterize the adversary's behavior through the simplified optimization in (20). By anticipating this rational response, the DC can then optimize its own utility across all possible values of  $\eta$  by solving (21), ensuring the equilibrium strategy is captured.

---

**Algorithm 1** Determination of the Optimal Threshold  $\eta^*$ 


---

1: **Input:** Utility functions  $U_{AD}(\cdot, \cdot)$ ,  $U_{DC}(\cdot, \cdot)$ , and the function  $\{c_\eta(\cdot) : \eta \in \Lambda_{DC}\}$ .

2: **Output:** Optimal threshold  $\hat{\eta}$ .

3: **Step 1: Follower's Rational Response**

4: For any fixed  $\eta$ , determine the set of optimal acceptance probabilities  $\mathcal{L}_\eta$  that maximize the adversary's utility along the curve  $c_\eta(\alpha)$ :

$$\mathcal{L}_\eta = \arg \max_{0 < \alpha \leq 1} U_{AD}(c_\eta(\alpha), \alpha). \quad (20)$$

5: **Step 2: Leader's Strategic Choice**

6: The DC identifies  $\hat{\eta}$  by maximizing its utility, accounting for the adversary's best response:

$$\hat{\eta} = \arg \max_{\eta \in \Lambda_{DC}} \left( \min_{\alpha \in \mathcal{L}_\eta} U_{DC}(c_\eta(\alpha), \alpha) \right). \quad (21)$$


---

Theorem 1 establishes that the original game is entirely determined by the characteristic function  $c_\eta(\cdot)$ . Consequently, finding the optimal strategy reduces to deriving the explicit form of this curve. The following theorem provides the exact analytical characterization of  $c_\eta(\cdot)$  for any system dimension.

**Theorem 2.** *For any dimension  $N \geq 1$ , decoding threshold  $\eta \in \Lambda_{DC}$ , and  $\alpha \in (0, 1]$ , we have*

$$c_\eta(\alpha) = \frac{\tilde{\Psi}_N^*(\alpha)}{4\alpha}, \quad (22)$$

where  $\tilde{\Psi}_N^*(q)$  denotes the upper concave envelope of the function  $\tilde{\Psi}_N(q)$  over the domain  $q \in [0, 1]$ .

The function  $\tilde{\Psi}_N(q)$  is defined as

$$\tilde{\Psi}_N(q) \triangleq \Psi_N \left( \Phi_N^{-1}(q) \right), \quad (23)$$

where  $\Phi_N^{-1}(q)$  is the inverse of the function

$$\Phi_N(z) = \frac{\mathcal{V}_{lens}(\Delta, \eta\Delta, z)}{V_N(\Delta)}, \quad (24)$$

with

$$\mathcal{V}_{lens}(\Delta, \eta\Delta, z) = \mathcal{K}_N(\Delta, u_c(z)) + \mathcal{K}_N(\eta\Delta, z - u_c(z)), \quad (25)$$

$$\mathcal{K}_N(r, c) = \frac{\pi^{(N-1)/2} r^N}{\Gamma(\frac{N+1}{2})} \int_{c/r}^1 (1-t^2)^{\frac{N-1}{2}} dt, \quad (26)$$

$$u_c(z) = \frac{z^2 + \Delta^2(1 - \eta^2)}{2z}, \quad (27)$$

for  $z \in [(\eta - 1)\Delta, (\eta + 1)\Delta]$ . Moreover, for the same range of  $z$ , we have

$$\begin{aligned} \Psi_N(z) = \frac{1}{V_N(\Delta)} & \left( \left[ J_N(\Delta, u_c(z)) + z^2 \mathcal{V}_1 \right] \right. \\ & \left. + \left[ J_N(\eta\Delta, z - u_c(z)) + 4z^2 \mathcal{V}_2 - 2z Q_N(\eta\Delta, z - u_c(z)) \right] \right), \end{aligned} \quad (28)$$

where

$$\mathcal{V}_1 = \mathcal{K}_N(\Delta, u_c(z)), \quad (29)$$

$$\mathcal{V}_2 = \mathcal{K}_N(\eta\Delta, z - u_c(z)), \quad (30)$$

$$Q_N(r, d) = \frac{r^2 - d^2}{N+1} V_{N-1}(\sqrt{r^2 - d^2}), \quad (31)$$

$$J_N(r, d) = \frac{Nr^2}{N+2} \mathcal{K}_N(r, d) + \frac{2d}{N+2} Q_N(r, d). \quad (32)$$

Finally, the function  $\Gamma(\cdot)$  is defined in (1),  $V_N(\cdot)$  is defined in (3).

The detailed proof of Theorem 2 is provided in Section V; however, the following intuitive interpretation of the theorem would be helpful to better understand the proof. We consider a random variable  $Z$  representing the magnitude of the adversarial noise, we establish in Lemmas 2 and 3 that for both the probability of acceptance and the estimation error, we have

$$\text{PA}(g(\cdot), \eta) = \int_0^\infty \Phi_N(z) f_Z(z) dz, \quad (33)$$

$$\text{MSE}(g(\cdot), \eta) = \frac{1}{4\text{PA}(g(\cdot), \eta)} \int_0^\infty \Psi_N(z) f_Z(z) dz, \quad (34)$$

where  $\Phi_N(z)$  and  $\Psi_N(z)$  are the geometric kernels defined in (24) and (28). This scalar transformation allows us to reformulate  $c_\eta(\alpha)$  as an optimization over the density  $f_Z(z)$ , instead of the  $N$ -dimensional density  $g(\cdot)$ . Furthermore, Lemma 4 proves that we lose no optimality by restricting the support of  $Z$  to  $z \in [(\eta - 1)\Delta, (\eta + 1)\Delta]$ . Similarly, Lemma 5 establishes that simplifying the constraint from  $\text{PA}(g(\cdot), \eta) \geq \alpha$  in (19) to  $\text{PA}(g(\cdot), \eta) = \alpha$ , does not result in any loss of optimality. Following these simplifications, we define the random variable  $Q \triangleq \Phi_N(Z)$ . According to the lemmas above, the constraints and the objective function in (19) can be rewritten as

$$\text{PA}(g(\cdot), \eta) = \mathbb{E}[\Phi_N(Z)] = \mathbb{E}[Q] = \alpha, \quad (35)$$

$$\text{MSE}(g(\cdot), \eta) = \frac{1}{4\alpha} \mathbb{E}[\Psi_N(Z)] = \frac{1}{4\alpha} \mathbb{E}[\tilde{\Psi}_N(Q)], \quad (36)$$

where we define<sup>4</sup>  $\tilde{\Psi}_N(q) \triangleq \Psi_N(\Phi_N^{-1}(q))$ . Consequently, the optimization problem in (19) turns to a maximization over the distribution of the random variable  $Q$ :

$$\text{Maximize: } \frac{1}{4\alpha} \mathbb{E}[\tilde{\Psi}_N(Q)] \quad (37)$$

$$\text{Subject to: } \mathbb{E}[Q] = \alpha, \quad Q \in [0, 1]. \quad (38)$$

The intuition for why the solution is the upper concave envelope relies on the concept of linear over-estimators. Consider any straight line

$$L(q) = mq + b \quad (39)$$

that stays entirely above the error potential function, such that

$$mq + b \geq \tilde{\Psi}_N(q) \quad (40)$$

for all  $q \in [0, 1]$ . For any such line, the expected error is rigorously bounded:

$$\mathbb{E}[\tilde{\Psi}_N(Q)] \leq \mathbb{E}[mQ + b] = m\mathbb{E}[Q] + b = m\alpha + b. \quad (41)$$

This implies that every linear *ceiling* placed over the function  $\tilde{\Psi}_N(q)$  provides a valid upper bound  $m\alpha + b$  on the error at  $\alpha$ . The tightest possible bound is the infimum of all such linear ceilings, which is by definition the upper concave envelope  $\tilde{\Psi}_N^*(\alpha)$ . Geometrically, wherever  $\tilde{\Psi}_N(q)$  is concave, the tightest ceiling is the tangent line at  $q = \alpha$ . In regions where the function has a convex *dip*, the adversary *bridges* the gap using a linear chord (see Figure 6). This represents a mixed strategy between two optimal noise magnitudes that allows the adversary to reach the highest possible error ceiling allowed by the laws of linear averaging.

**Remark 1.** In Theorem 2, we characterized the function  $c_\eta(\alpha)$  defined in (19) for general dimensions  $N \geq 1$ . It is worth noting that if we choose  $N = 1$ , the characterization of  $c_\eta(\alpha)$  reduces to the one-dimensional case, which we have evaluated and analyzed previously in [18]. Specifically, the explicit functions for that specific case have been characterized in Appendix G of [18], and one can verify the consistency of the general result. In addition, for the sake of completeness and to provide a concrete example of the multidimensional setting, we explicitly evaluate this function for the case of  $N = 2$  in Appendix G.

<sup>4</sup>The function  $\Phi_N(z)$  is strictly decreasing over the domain  $[(\eta - 1)\Delta, (\eta + 1)\Delta]$ , making it a bijection and thus invertible over the range  $[0, 1]$ .

**Remark 2.** One might initially view the calculation of  $c_\eta(\alpha)$  in (22) as analytically intractable, particularly because the function  $\Phi_N(z)$  involves transcendental terms (e.g., for even  $N$ ) or high-order polynomials (for odd  $N$ ) that do not admit a closed-form inverse. Consequently, obtaining an explicit expression for the composite function  $\tilde{\Psi}_N(q)$  is generally not possible. However, numerically evaluating the concave envelope is straightforward and does not require explicit inversion. Instead, one can adopt a parametric approach: by sweeping the variable  $z$  across its domain  $[(\eta-1)\Delta, (\eta+1)\Delta]$ , we generate the locus of points  $(q_z, y_z) = (\Phi_N(z), \Psi_N(z))$ . The function  $\tilde{\Psi}_N^*(q)$  is then simply the upper boundary of the convex hull of this set of points, which can be efficiently computed using standard numerical libraries. We have used this technique to derive these functions for different settings and finally determined the equilibrium for different cases, as described in Section VI.

In the detailed proof of Theorem 2 provided in Section V, we not only derive the worst-case error bound but also explicitly characterize the adversarial noise distribution that achieves this bound. This optimal noise density, denoted as  $g_{\mathbf{N}_a}^*(\mathbf{x})$ , is constructed in Algorithm 2. The algorithm utilizes the geometric properties of  $\Psi_N$  defined in (28), and  $\Phi_N$  defined in (24), to determine whether a single spherical shell or a mixture of two spherical shells constitutes the optimal noise distribution.

**Remark 3.** It is worth emphasizing that the results established in Theorems 1 and 2, as well as the procedures in Algorithms 1 and 2, do not rely on specific functional forms for the utilities of the DC or the adversary. We only impose the intuitive conditions that the adversary's utility is strictly increasing with respect to both arguments, whereas the DC's utility is non-increasing in its first argument and non-decreasing in its second. These broad and common-sense assumptions ensure that our framework remains versatile enough to encompass a wide array of practical security and estimation scenarios without loss of generality.

#### IV. PROOF OF THEOREM 1

In this section, we establish the validity of Theorem 1. We begin by comparing the optimization performed in Algorithm 1 with the theoretical definition of  $\eta^*$  in (18). Algorithm 1 computes  $\hat{\eta}$  by solving the following optimization problem

$$\hat{\eta} = \arg \max_{\eta \in \Lambda_{\text{DC}}} \min_{\alpha \in \mathcal{L}_\eta} Q_{\text{DC}}(c_\eta(\alpha), \alpha), \quad (42)$$

where  $\mathcal{L}_\eta$  is defined in Algorithm 1 as

$$\mathcal{L}_\eta = \arg \max_{0 < \alpha \leq 1} Q_{\text{AD}}(c_\eta(\alpha), \alpha). \quad (43)$$

In contrast, based on (18), the value of  $\eta^*$  can be reformulated in terms of the set of realizable performance pairs. More precisely, let  $\mathcal{J}_\eta$  denote the set of operating points corresponding to the adversary's best responses

$$\mathcal{J}_\eta \triangleq \left\{ (\text{MSE}(g(\cdot), \eta), \text{PA}(g(\cdot), \eta)) \mid g(\cdot) \in \mathcal{B}_{\text{AD}}^\eta \right\}. \quad (44)$$

Using this set, based on (18), the value of  $\eta^*$  is given by

$$\eta^* = \arg \max_{\eta \in \Lambda_{\text{DC}}} \min_{(\beta, \alpha) \in \mathcal{J}_\eta} Q_{\text{DC}}(\beta, \alpha). \quad (45)$$

Comparing (42) and (45), it is evident that to prove  $\hat{\eta} = \eta^*$ , it suffices to demonstrate that the set of best-response points  $\mathcal{J}_\eta$  is identical to the set of points derived from the algorithm. More precisely, let us define the set  $\mathcal{K}_\eta$  as

$$\mathcal{K}_\eta \triangleq \{(c_\eta(\alpha), \alpha) \mid \alpha \in \mathcal{L}_\eta\}. \quad (46)$$

Thus, the proof of Theorem 1 reduces to showing that  $\mathcal{J}_\eta = \mathcal{K}_\eta$ . We establish this equality by proving mutual inclusion: first showing  $\mathcal{J}_\eta \subseteq \mathcal{K}_\eta$ , and subsequently  $\mathcal{K}_\eta \subseteq \mathcal{J}_\eta$ . The intermediate steps are formally shown the Sections IV-A and IV-B below.

Before proceeding with the main inclusion arguments, we first state and prove the following lemma.

**Lemma 1.** Let define the set  $\mathcal{C}_\eta$  as

$$\mathcal{C}_\eta \triangleq \{(c_\eta(\alpha), \alpha) \mid 0 < \alpha \leq 1\}. \quad (47)$$

Then, for any threshold  $\eta \in \Lambda_{\text{DC}}$ , the set of adversarial best responses  $\mathcal{J}_\eta$  satisfies  $\mathcal{J}_\eta \subseteq \mathcal{C}_\eta$ .

*Proof.* Consider an arbitrary operating point  $(\beta, \alpha) \in \mathcal{J}_\eta$  resulting from an adversarial best-response  $g^*(\cdot) \in \mathcal{B}_{\text{AD}}^\eta$ . By the definition in (44), we have  $\alpha = \text{PA}(g^*(\cdot), \eta)$  and  $\beta = \text{MSE}(g^*(\cdot), \eta)$ . That means  $g^*(\cdot)$  satisfies the constraint of the optimization problem in (19). Therefore, the value of the objective function in (19) at the feasible point  $g^*(\cdot)$ , i.e.,  $\text{MSE}(g^*(\cdot), \eta) = \beta$ , cannot exceed the maximum of the objective function, which is  $c_\eta(\alpha)$ . This immediately implies  $\beta \leq c_\eta(\alpha)$ .

We prove that equality must hold by contradiction. Suppose that  $\beta < c_\eta(\alpha)$ , represented by point  $A$  (red one) in Figure 3. By the definition of the characteristic function  $c_\eta(\alpha)$  in (19), there must exist an alternative distribution  $g'(\cdot)$ , corresponding to point  $B$  (black one) in Figure 3, such that

$$\text{MSE}(g'(\cdot), \eta) = c_\eta(\alpha), \quad (48)$$

$$\text{PA}(g'(\cdot), \eta) \geq \alpha. \quad (49)$$

Comparing the utilities, we observe that

$$\begin{aligned}
U_{AD}(g'(\cdot), \eta) &= Q_{AD}(\text{MSE}(g'(\cdot), \eta), \text{PA}(g'(\cdot), \eta)) \\
&\stackrel{(a)}{=} Q_{AD}(c_\eta(\alpha), \text{PA}(g'(\cdot), \eta)) \\
&\stackrel{(b)}{\geq} Q_{AD}(c_\eta(\alpha), \alpha) \\
&\stackrel{(c)}{>} Q_{AD}(\beta, \alpha) \\
&= U_{AD}(g^*(\cdot), \eta),
\end{aligned} \tag{50}$$

where (a) follows from (48); (b) follows from (49) and the fact that  $Q_{AD}$  is non-decreasing in its second argument; and (c) holds because  $Q_{AD}$  is strictly increasing in its first argument and  $c_\eta(\alpha) > \beta$ . This strictly higher utility for  $g'(\cdot)$  contradicts our initial assumption that  $g^*(\cdot)$  is a best response in  $\mathcal{B}_{AD}^\eta$ . Consequently, we must have  $\beta = c_\eta(\alpha)$ , which implies the point  $(\beta, \alpha)$  lies within  $\mathcal{C}_\eta$  defined in (47).  $\square$

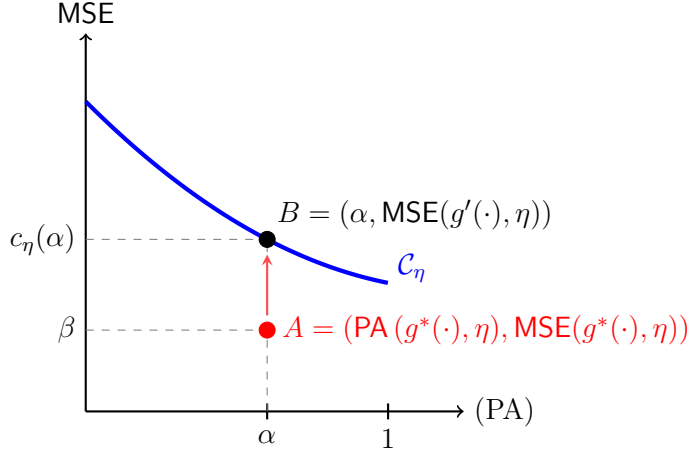


Fig. 3. Geometric proof of Lemma 1. Point A represents a suboptimal response where  $\beta < c_\eta(\alpha)$ . By choosing  $g'$  rather than  $g^*$  to move to Point B on the boundary  $\mathcal{C}_\eta$  (where the probability of acceptance is at least  $\alpha$ ), the adversary increases their MSE and potentially their probability of acceptance, leading to strictly higher utility.

We now prove  $\mathcal{J}_\eta = \mathcal{K}_\eta$  via double inclusion, in the following sections.

#### A. Proof of $\mathcal{J}_\eta \subseteq \mathcal{K}_\eta$

Consider an arbitrary pair  $(\beta, \alpha) \in \mathcal{J}_\eta$ , denoted as point A in Figure 4. We claim that  $(\beta, \alpha) \in \mathcal{K}_\eta$ , and we prove this by contradiction.

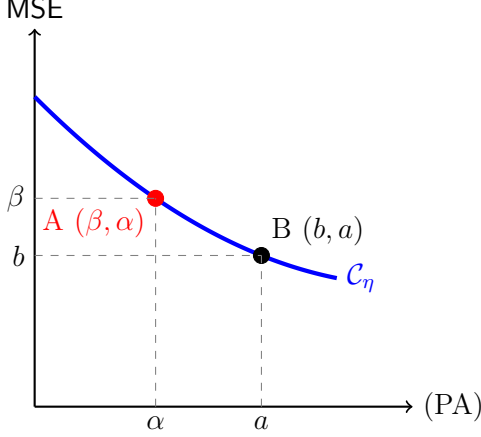


Fig. 4. Visual representation of the contradiction for  $\mathcal{J}_\eta \subseteq \mathcal{K}_\eta$ . Point A is a best response and thus lies on  $\mathcal{C}_\eta$  by Lemma 1. If A is not in  $\mathcal{K}_\eta$ , there must exist a point B on the same boundary  $\mathcal{C}_\eta$  that provides strictly higher utility, contradicting the optimality of A.

Assume, as a contradictory hypothesis, that  $A = (\beta, \alpha) \notin \mathcal{K}_\eta$ . By Lemma 1, we know that every adversarial best response lies on the boundary, so  $A \in \mathcal{C}_\eta$ , i.e.,  $\beta = c_\eta(\alpha)$ . Note that if  $\alpha \in \mathcal{L}_\eta$ , then from the definition of  $\mathcal{K}_\eta$  in (46), we would have  $A \in \mathcal{K}_\eta$ . Since we assumed  $A \notin \mathcal{K}_\eta$ , we can conclude that  $\alpha \notin \mathcal{L}_\eta$ . Then, from the definition of  $\mathcal{L}_\eta$  in (43), there must exist another  $a \in \mathcal{L}_\eta$  and another point  $B = (b, a) \in \mathcal{K}_\eta$  with  $b = c_\eta(a)$  that yields a strictly higher adversarial utility than A. That is,

$$Q_{\text{AD}}(b, a) > Q_{\text{AD}}(\beta, \alpha). \quad (51)$$

Since  $(\beta, \alpha) \in \mathcal{J}_\eta$ , based on the definition in (44), there exists a noise distribution  $g_\alpha(\cdot) \in \mathcal{B}_{\text{AD}}^\eta$  where

$$(\beta, \alpha) = (\text{MSE}(g_\alpha(\cdot), \eta), \text{PA}(g_\alpha(\cdot), \eta)). \quad (52)$$

Similarly, for the point  $(b, a) \in \mathcal{K}_\eta$ , since  $b = c_\eta(a)$ , from the optimization problem in (19), there exists a noise distribution  $g_b(\cdot) \in \Lambda_{\text{AD}}$  such that

$$b = \text{MSE}(g_b(\cdot), \eta), \quad (53)$$

and

$$\text{PA}(g_b(\cdot), \eta) \geq a. \quad (54)$$

Specifically,  $g_b(\cdot)$  is an optimal solution to the following maximization problem

$$\max_{g(\cdot) \in \Lambda_{\text{AD}}} \{ \text{MSE}(g(\cdot), \eta) \mid \text{PA}(g(\cdot), \eta) \geq a \}. \quad (55)$$

We can now evaluate the utility of the distribution  $g_b(\cdot)$  as follows

$$\begin{aligned}
U_{AD}(g_b(\cdot), \eta) &= Q_{AD}(\text{MSE}(g_b(\cdot), \eta), \text{PA}(g_b(\cdot), \eta)) \\
&\stackrel{(a)}{=} Q_{AD}(b, \text{PA}(g_b(\cdot), \eta)) \\
&\stackrel{(b)}{\geq} Q_{AD}(b, a) \\
&\stackrel{(c)}{>} Q_{AD}(\beta, \alpha) \\
&\stackrel{(d)}{=} Q_{AD}(\text{MSE}(g_\alpha(\cdot), \eta), \text{PA}(g_\alpha(\cdot), \eta)) \\
&= U_{AD}(g_\alpha(\cdot), \eta),
\end{aligned} \tag{56}$$

where (a) follows from (53); (b) follows from (54) and the non-decreasing property of  $Q_{AD}$ ; (c) follows from the contradictory assumption in (51); and (d) follows from (52).

The result of (56) implies  $U_{AD}(g_b(\cdot), \eta) > U_{AD}(g_\alpha(\cdot), \eta)$ . This is in contradiction with the fact that  $g_\alpha(\cdot) \in \mathcal{B}_{AD}^\eta$  is a best response strategy, meaning no other strategy including  $g_b(\cdot)$ , can yield strictly higher adversarial utility. Therefore, our initial assumption was incorrect, and we must have  $(\beta, \alpha) \in \mathcal{K}_\eta$ . Consequently,  $\mathcal{J}_\eta \subseteq \mathcal{K}_\eta$ .

### B. Proof of $\mathcal{K}_\eta \subseteq \mathcal{J}_\eta$

Consider an arbitrary point  $(b, a) \in \mathcal{K}_\eta$ . Let  $g_b(\cdot) \in \Lambda_{AD}$  be the noise distribution associated with  $(b, a)$ , where the relationships (53), (54), and (55) hold.

Now, consider a point  $(\beta, \alpha) \in \mathcal{J}_\eta$ , and let  $g_\alpha(\cdot) \in \mathcal{B}_{AD}^\eta$  be the corresponding noise distribution such that (52) holds. Note that based on Lemma 1, we have  $(\beta, \alpha) \in \mathcal{C}_\eta$ , i.e.,  $\beta = c_\eta(\alpha)$ .

Since  $(b, a) \in \mathcal{K}_\eta$ , by the definition (46), we should have  $b = c_\eta(a)$  and  $a \in \mathcal{L}_\eta$ , which together with (43) further implies,  $Q_{AD}(c_\eta(a), a) \geq Q_{AD}(c_\eta(a'), a')$  for any  $0 < a' \leq 1$ . In particular, for  $a' = \alpha$ , this implies

$$Q_{AD}(b, a) \geq Q_{AD}(\beta, \alpha). \tag{57}$$

Consider the following chain of inequalities regarding the utility of  $g_b(\cdot)$

$$\begin{aligned}
U_{AD}(g_b(\cdot), \eta) &= Q_{AD}(\text{MSE}(g_b(\cdot), \eta), \text{PA}(g_b(\cdot), \eta)) \\
&\stackrel{(a)}{=} Q_{AD}(b, \text{PA}(g_b(\cdot), \eta)) \\
&\stackrel{(b)}{\geq} Q_{AD}(b, a) \\
&\stackrel{(c)}{\geq} Q_{AD}(\beta, \alpha)
\end{aligned}$$

$$\begin{aligned}
&\stackrel{(d)}{=} Q_{\text{AD}}(\text{MSE}(g_\alpha(\cdot), \eta), \text{PA}(g_\alpha(\cdot), \eta)) \\
&= U_{\text{AD}}(g_\alpha(\cdot), \eta),
\end{aligned} \tag{58}$$

where (a) follows from (53); (b) follows from (54) and the fact that  $Q_{\text{AD}}(\cdot, \cdot)$  is a strictly increasing function with respect to its second argument; (c) follows from (57); and (d) follows from (52).

The result of (58) implies that  $U_{\text{AD}}(g_b(\cdot), \eta) \geq U_{\text{AD}}(g_\alpha(\cdot), \eta)$ . On the other hand, since  $g_\alpha(\cdot) \in \mathcal{B}_{\text{AD}}^\eta$  is a global best response, we must have  $U_{\text{AD}}(g_\alpha(\cdot), \eta) \geq U_{\text{AD}}(g(\cdot), \eta)$  for any  $g(\cdot)$ , and in particular  $g(\cdot) = g_b(\cdot)$ . Combining these two inequalities, we conclude that

$$U_{\text{AD}}(g_b(\cdot), \eta) = U_{\text{AD}}(g_\alpha(\cdot), \eta). \tag{59}$$

Consequently, all inequalities in the chain (58) must hold with equality. Specifically, looking at step (b) of (58), we must have

$$Q_{\text{AD}}(b, \text{PA}(g_b(\cdot), \eta)) = Q_{\text{AD}}(b, a). \tag{60}$$

Since  $Q_{\text{AD}}(\cdot, \cdot)$  is a strictly increasing function with respect to its second argument, this equality holds if and only if  $\text{PA}(g_b(\cdot), \eta) = a$ . This together with (53) implies

$$(b, a) = (\text{MSE}(g_b(\cdot), \eta), \text{PA}(g_b(\cdot), \eta)). \tag{61}$$

Finally, since  $g_\alpha(\cdot) \in \mathcal{B}_{\text{AD}}^\eta$  and we showed in (59) that  $U_{\text{AD}}(g_b(\cdot), \eta) = U_{\text{AD}}(g_\alpha(\cdot), \eta)$ , it implies that  $g_b(\cdot)$  achieves the global maximum utility. Therefore, we have  $g_b(\cdot) \in \mathcal{B}_{\text{AD}}^\eta$ , as defined in (15). By the definition in (44), this means  $(b, a) \in \mathcal{J}_\eta$ , which holds for every  $(b, a) \in \mathcal{K}_\eta$ . Therefore,  $\mathcal{K}_\eta \subseteq \mathcal{J}_\eta$ .

**Conclusion:** Having established both inclusions, we conclude that  $\mathcal{J}_\eta = \mathcal{K}_\eta$ . Substituting  $\mathcal{K}_\eta$  for  $\mathcal{J}_\eta$  in (45) completes the proof of Theorem 1.

## V. PROOF OF THEOREM 2

In this section, we provide the proof of the result stated in Theorem 2. Our first step is to derive a general expression for the probability of acceptance,  $\Pr(\mathcal{A}_\eta)$ , as a function of the magnitude of the adversarial noise. Specifically, let us define  $Z$  as the Euclidean norm of the adversarial noise

$$Z \triangleq \|\mathbf{n}_a\|_2. \tag{62}$$

We assume  $Z$  is distributed according to a general probability density function

$$f_Z(z) = \int_{\mathbf{n}_a: \|\mathbf{n}_a\|=z} g(\mathbf{n}_a) d\mathbf{n}_a, \tag{63}$$

supported on  $[0, \infty)$ . As established in (8), the DC accepts the computation if and only if the Euclidean distance between the two reports,  $\mathbf{Y}_1$  and  $\mathbf{Y}_2$ , does not exceed the threshold  $\eta\Delta$ . Recall

from the system model that the reports are given by  $\mathbf{Y}_h = \mathbf{U} + \mathbf{N}_h$  and  $\mathbf{Y}_a = \mathbf{U} + \mathbf{N}_a$ , where  $\mathbf{U}$  is the ground truth. When the DC computes the difference between the two reports, the common ground truth signal  $\mathbf{U}$  cancels out entirely

$$\begin{aligned} \|\mathbf{Y}_1 - \mathbf{Y}_2\|_2 &= \|(\mathbf{U} + \mathbf{N}_h) - (\mathbf{U} + \mathbf{N}_a)\|_2 \\ &= \|\mathbf{N}_h - \mathbf{N}_a\|_2. \end{aligned} \quad (64)$$

Consequently, the acceptance condition  $\|\mathbf{Y}_1 - \mathbf{Y}_2\|_2 \leq \eta\Delta$  reduces to a constraint on the relative distance between the noise vectors

$$\mathcal{A}_\eta : \quad \|\mathbf{N}_h - \mathbf{N}_a\|_2 \leq \eta\Delta. \quad (65)$$

In order to prove Theorem 2, we first show that the probability of acceptance,  $\text{PA}(g(\cdot), \eta)$ , only depends on the adversarial noise through the distribution of its magnitude distribution  $f_Z(z)$ , as shown in the following lemma.

**Lemma 2.** For any adversarial noise distribution characterized by the marginal magnitude PDF  $f_Z(z)$ , the probability of acceptance is given by

$$\text{Pr}(\mathcal{A}_\eta) = \int_0^\infty \Phi_N(z) f_Z(z) dz, \quad (66)$$

where  $\Phi_N(z)$  is defined piecewise as

$$\Phi_N(z) = \begin{cases} 1 & \text{if } 0 \leq z \leq (\eta-1)\Delta, \\ \frac{\mathcal{V}_{\text{lens}}(\Delta, \eta\Delta, z)}{V_N(\Delta)} & \text{if } (\eta-1)\Delta < z < (\eta+1)\Delta, \\ 0 & \text{if } z \geq (\eta+1)\Delta, \end{cases} \quad (67)$$

with

$$\begin{aligned} \mathcal{V}_{\text{lens}}(\Delta, \eta\Delta, z) &= \mathcal{K}_N(\Delta, u_c(z)) + \mathcal{K}_N(\eta\Delta, z - u_c(z)), \\ u_c(z) &= \frac{z^2 + \Delta^2(1 - \eta^2)}{2z}, \\ \mathcal{K}_N(r, c) &= \frac{\pi^{(N-1)/2} r^N}{\Gamma(\frac{N+1}{2})} \int_{c/r}^1 (1 - t^2)^{\frac{N-1}{2}} dt, \end{aligned} \quad (68)$$

and  $\Gamma(\cdot)$  is defined in (1), and  $V_N(\cdot)$  is defined in (3).

The detailed proof of this lemma can be found in Appendix A, but here we provide an intuitive geometric overview of the calculation. For any realization of the adversarial noise vector  $\mathbf{n}_a$  with a fixed magnitude  $\|\mathbf{n}_a\|_2 = z$ , the DC accepts the reports if the honest noise  $\mathbf{n}_h$  falls within an  $N$ -ball

of radius  $\eta\Delta$  centered at  $\mathbf{n}_a$ . While the conditional probability  $\Pr(\mathcal{A}_\eta \mid Z = z)$  formally requires averaging over all possible realizations of  $\mathbf{n}_a$  on the shell of radius  $z$ , the spherical *symmetry of the honest noise* distribution ensures that the intersection volume remains invariant, regardless of the specific direction of  $\mathbf{n}_a$ . Consequently, this probability is simply the volume of the intersection between the honest noise support (centered at the origin) and the acceptance ball (centered at  $\mathbf{n}_a$ ) divided by the total volume of the honest noise support. This geometry is illustrated in Figure 5, and in Appendix A, we evaluate the ratio of the two volumes for the different cases of  $z$ , as presented in (67).

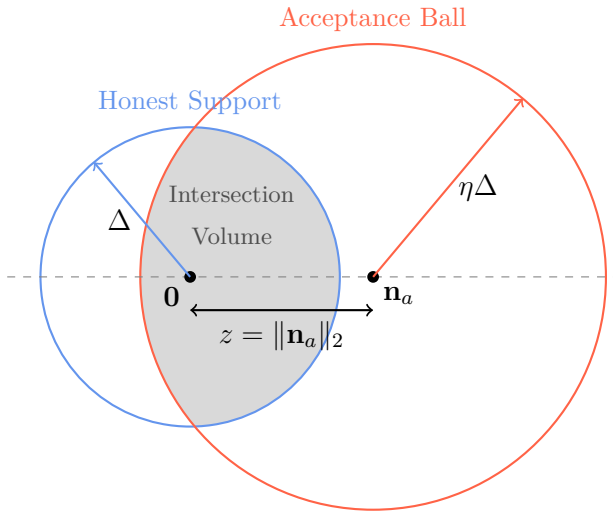


Fig. 5. The honest noise  $\mathbf{N}_h$  is uniformly distributed on the blue ball of radius  $\Delta$ . Given any adversarial noise  $\mathbf{n}_a$  with magnitude  $z$ , the condition  $\|\mathbf{N}_h - \mathbf{n}_a\|_2 \leq \eta\Delta$  is satisfied if  $\mathbf{N}_h$  falls within the red ball. Due to spherical symmetry, the conditional probability  $\Pr(\mathcal{A}_\eta \mid Z = z)$  depends only on the scalar distance  $z$ .

Having characterized the probability of acceptance in Lemma 2, the next step is to derive a corresponding analytical relationship for the estimation error. Specifically, we seek to express the Mean Squared Error (MSE) in terms of the adversarial noise distribution  $g_{\mathbf{N}_a}(\mathbf{n}_a)$ , and ideally show that it depends only on  $f_Z(z)$ . Recall that the DC estimates the ground truth  $\mathbf{U}$  by averaging the two reports,  $\hat{\mathbf{U}} = \frac{1}{2}(\mathbf{Y}_h + \mathbf{Y}_a)$ . The estimation error is therefore the magnitude of the average noise vector. More precisely, we have

$$\|\mathbf{U} - \hat{\mathbf{U}}\|_2^2 = \left\| \mathbf{U} - \left( \mathbf{U} + \frac{\mathbf{N}_h + \mathbf{N}_a}{2} \right) \right\|_2^2 = \left\| \frac{\mathbf{N}_h + \mathbf{N}_a}{2} \right\|_2^2 \quad (69)$$

The following lemma establishes the relationship between this error and the adversarial noise distribution, and shows that it is fully characterized by its marginal magnitude probability density function

$f_Z(z)$ . The lemma provides an analytical framework that characterizes the estimation performance through the density of the magnitude of the adversarial noise.

**Lemma 3.** For any adversarial noise distribution characterized by the marginal magnitude PDF  $f_Z(z)$ , the conditional MSE of the estimator is given by

$$\mathbb{E} \left[ \|\mathbf{U} - \hat{\mathbf{U}}\|_2^2 \mid \mathcal{A}_\eta \right] = \frac{1}{4 \Pr(\mathcal{A}_\eta)} \int_0^\infty \Psi_N(z) f_Z(z) dz. \quad (70)$$

Here,  $\Pr(\mathcal{A}_\eta)$  is the acceptance probability that is derived in Lemma 2, and

$$\Psi_N(z) = \begin{cases} z^2 + \frac{N}{N+2} \Delta^2 & \text{if } 0 \leq z \leq (\eta-1)\Delta, \\ \frac{1}{V_N(\Delta)} \Psi_N^{\text{lens}}(z) & \text{if } (\eta-1)\Delta < z < (\eta+1)\Delta, \\ 0 & \text{if } z \geq (\eta+1)\Delta, \end{cases} \quad (71)$$

where  $\Psi_N^{\text{lens}}(z)$  is given by

$$\Psi_N^{\text{lens}}(z) = \left[ J_N(\Delta, u_c) + z^2 \mathcal{V}_1 \right] + \left[ J_N(\eta\Delta, z - u_c) + 4z^2 \mathcal{V}_2 - 2z Q_N(\eta\Delta, z - u_c) \right], \quad (72)$$

with

$$\begin{aligned} u_c &= \frac{z^2 + \Delta^2(1 - \eta^2)}{2z} \\ \mathcal{K}_N(r, c) &= \frac{\pi^{(N-1)/2} r^N}{\Gamma(\frac{N+1}{2})} \int_{c/r}^1 (1 - t^2)^{\frac{N-1}{2}} dt, \\ \mathcal{V}_1 &= \mathcal{K}_N(\Delta, u_c), \\ \mathcal{V}_2 &= \mathcal{K}_N(\eta\Delta, z - u_c), \\ Q_N(r, d) &= \frac{r^2 - d^2}{N+1} V_{N-1}(\sqrt{r^2 - d^2}), \\ J_N(r, d) &= \frac{Nr^2}{N+2} \mathcal{K}_N(r, d) + \frac{2d}{N+2} Q_N(r, d), \end{aligned} \quad (73)$$

and  $\Gamma(\cdot)$  and  $V_N(\cdot)$  are defined in (1) and (3), respectively.

The proof of this lemma can be found in Appendix D.

Having established the general expressions for the probability of acceptance and the conditional MSE in Lemmas 2 and 3, the next step in the proof of Theorem 2 is to simplify the search space for the worst-case adversarial noise distribution. We show that without loss of optimality, we can restrict the support of the adversarial noise magnitude  $Z$  to the interval  $[(\eta-1)\Delta, (\eta+1)\Delta]$ . We formalize this reduction in the following lemma. For a given adversarial noise magnitude distribution  $f_Z(z)$ , we denote  $\Pr(\mathcal{A}_\eta; f_Z)$  as the probability of acceptance when the noise magnitude follows the

density  $f_Z(z)$ . Similarly,  $\mathbb{E} \left[ \|\mathbf{U} - \hat{\mathbf{U}}\|_2^2 \mid \mathcal{A}_\eta; f_Z \right]$  denotes the resulting estimation error for the case where the noise magnitude density is  $f_Z(z)$ .

**Lemma 4.** Let  $f_Z(z)$  be the probability density function of the adversarial noise magnitude, satisfying  $\Pr(\mathcal{A}_\eta; f_Z) > 0$ . There exists an alternative adversarial noise distribution with magnitude probability density function  $f_Z^*(z)$ , supported strictly on the interval  $[(\eta - 1)\Delta, (\eta + 1)\Delta]$ , such that

$$\Pr(\mathcal{A}_\eta; f_Z^*) \geq \Pr(\mathcal{A}_\eta; f_Z), \quad (74)$$

$$\mathbb{E} \left[ \|\mathbf{U} - \hat{\mathbf{U}}\|_2^2 \mid \mathcal{A}_\eta; f_Z^* \right] \geq \mathbb{E} \left[ \|\mathbf{U} - \hat{\mathbf{U}}\|_2^2 \mid \mathcal{A}_\eta; f_Z \right]. \quad (75)$$

The proof of this lemma is provided in Appendix E.

Lemma 4 implies that the search for the optimal adversarial noise can be restricted to noise magnitude PDFs supported on the interval  $[(\eta - 1)\Delta, (\eta + 1)\Delta]$ . We refer to the requirement that the noise magnitude is zero outside this interval as the *support condition*.

In the following lemma, we further simplify the analysis of the trade-off curve  $c_\eta(\alpha)$ . Specifically, we show that when solving the optimization problem formulated to characterize  $c_\eta(\alpha)$  in (19), the inequality constraint  $\text{PA}(g(\cdot), \eta) \geq \alpha$  can be replaced with the equality constraint  $\text{PA}(g(\cdot), \eta) = \alpha$  without affecting the optimal value.

**Lemma 5.** Let  $f_{Z,1}(z)$  be a PDF of the adversarial noise magnitude satisfying the support condition (i.e., supported on  $[(\eta - 1)\Delta, (\eta + 1)\Delta]$ ), with an acceptance probability  $\Pr(\mathcal{A}_\eta; f_{Z,1}) = \alpha_1 > \alpha$ . There exists another noise magnitude PDF  $f_{Z,2}(z)$  such that the probability of acceptance is exactly  $\alpha$ , i.e.,  $\Pr(\mathcal{A}_\eta; f_{Z,2}) = \alpha$ , and the conditional MSE is preserved. More precisely, we have

$$\mathbb{E} \left[ \|\mathbf{U} - \hat{\mathbf{U}}\|_2^2 \mid \mathcal{A}_\eta; f_{Z,2} \right] = \mathbb{E} \left[ \|\mathbf{U} - \hat{\mathbf{U}}\|_2^2 \mid \mathcal{A}_\eta; f_{Z,1} \right]. \quad (76)$$

The proof of this lemma is provided in Appendix F.

With Lemmas 2, 3, 4, and 5 established, we now proceed to prove the main result of Theorem 2. Lemma 4 restricts the search space to noise distributions supported on  $[(\eta - 1)\Delta, (\eta + 1)\Delta]$ , and Lemma 5 allows us to fix the acceptance probability constraint to equality. To prove (22), we proceed in two steps: first, we establish the upper bound by showing

$$c_\eta(\alpha) \leq \frac{\tilde{\Psi}_N^*(\alpha)}{4\alpha}, \quad (77)$$

and subsequently, we demonstrate that this bound is achievable.

### A. Derivation of the Upper Bound

Hereafter, without loss of generality, we assume that the noise magnitude satisfies the conditions of Lemma 4 and Lemma 5. Thus, the support of the noise magnitude PDF  $f_Z(z)$  is restricted to the interval  $[(\eta - 1)\Delta, (\eta + 1)\Delta]$ , and the probability of acceptance satisfies the equality constraint. Specifically, based on Lemma 5 and the definition of  $\Phi_N(z)$  in (67), the probability of acceptance is given by

$$\Pr(\mathcal{A}_\eta) = \int_{(\eta-1)\Delta}^{(\eta+1)\Delta} \Phi_N(z) f_Z(z) dz = \alpha. \quad (78)$$

Furthermore, using Lemma 3 restricted to this support, the conditional MSE is given by

$$\mathbb{E} \left[ \|\mathbf{U} - \hat{\mathbf{U}}\|_2^2 \mid \mathcal{A}_\eta \right] = \frac{1}{4\alpha} \int_{(\eta-1)\Delta}^{(\eta+1)\Delta} \Psi_N(z) f_Z(z) dz. \quad (79)$$

Let us define the variable  $q$  as the conditional probability of acceptance for a given noise magnitude  $z$ , i.e.,

$$q = \Phi_N(z). \quad (80)$$

Since the intersection volume (and thus  $\Phi_N(z)$ ) is a strictly decreasing function of  $z$  over the domain  $[(\eta - 1)\Delta, (\eta + 1)\Delta]$ , the mapping is invertible. Also, the range of  $q$  corresponds to  $[0, 1]$ . Based on this definition, we have the inverse relationship and the differential transformation

$$z = \Phi_N^{-1}(q), \quad \text{and} \quad dq = \Phi'_N(z) dz. \quad (81)$$

To facilitate the change of variables, we define the weight function  $w(q)$  as

$$w(q) = \frac{-f_Z(\Phi_N^{-1}(q))}{\Phi'_N(\Phi_N^{-1}(q))}. \quad (82)$$

Since  $f_Z(z)$  is a valid PDF satisfying the normalization condition  $\int_{(\eta-1)\Delta}^{(\eta+1)\Delta} f_Z(z) dz = 1$ , applying the change of variables using (81) and (82) yields the transformed normalization constraint

$$\int_0^1 w(q) dq = 1. \quad (83)$$

Similarly, substituting  $\Phi_N(z) = q$  into (78) transforms the acceptance probability constraint into

$$\int_0^1 q w(q) dq = \alpha. \quad (84)$$

We now express the error kernel  $\Psi_N(z)$  in terms of  $q$  by defining  $\tilde{\Psi}_N(q) \triangleq \Psi_N(\Phi_N^{-1}(q))$ . Substituting this into the conditional MSE formula (79) and applying the change of variables, we have

$$\mathbb{E} \left[ \|\mathbf{U} - \hat{\mathbf{U}}\|_2^2 \mid \mathcal{A}_\eta \right] = \frac{1}{4\alpha} \int_0^1 \tilde{\Psi}_N(q) w(q) dq. \quad (85)$$

To maximize this expectation, we define  $\tilde{\Psi}_N^*(q)$  as the upper concave envelope of the function  $\tilde{\Psi}_N(q)$  over the interval  $q \in [0, 1]$ . By definition,  $\tilde{\Psi}_N(q) \leq \tilde{\Psi}_N^*(q)$  for all  $q$ . Since  $\tilde{\Psi}_N^*(q)$  is concave, we can apply Jensen's inequality treating  $w(q)$  as a probability density function (justified by (83)). We proceed as follows

$$\begin{aligned} \int_0^1 \tilde{\Psi}_N(q) w(q) dq &\leq \int_0^1 \tilde{\Psi}_N^*(q) w(q) dq \\ &\leq \tilde{\Psi}_N^* \left( \frac{\int_0^1 q w(q) dq}{\int_0^1 w(q) dq} \right) \cdot \int_0^1 w(q) dq. \end{aligned} \quad (86)$$

Substituting the constraints (83) and (84) into the inequality above, we obtain

$$\int_0^1 \tilde{\Psi}_N(q) w(q) dq \leq \tilde{\Psi}_N^* \left( \frac{\alpha}{1} \right) \cdot 1 = \tilde{\Psi}_N^*(\alpha). \quad (87)$$

Finally, substituting this bound back into (85) yields the upper bound on the worst-case conditional expectation

$$c_\eta(\alpha) = \max_{f_Z} \mathbb{E} \left[ \|\mathbf{U} - \hat{\mathbf{U}}\|_2^2 \mid \mathcal{A}_\eta \right] \leq \frac{\tilde{\Psi}_N^*(\alpha)}{4\alpha}. \quad (88)$$

### B. Achievability of the Upper Bound

In the previous subsection, we established the upper bound on the worst-case error. Specifically, we showed that

$$c_\eta(\alpha) \leq \frac{\tilde{\Psi}_N^*(\alpha)}{4\alpha}. \quad (89)$$

In order to complete the proof of Theorem 2, we need to demonstrate the reverse inequality

$$c_\eta(\alpha) \geq \frac{\tilde{\Psi}_N^*(\alpha)}{4\alpha}. \quad (90)$$

Based on the definition of  $c_\eta(\alpha)$  in (19), proving (90) is equivalent to showing that there exists at least one admissible noise magnitude distribution  $f_Z(z)$  that satisfies the following two conditions simultaneously. First, the resulting probability of acceptance must equal the target  $\alpha$ , that is

$$\Pr(\mathcal{A}_\eta) = \int \Phi_N(z) f_Z(z) dz = \alpha. \quad (91)$$

Second, the resulting conditional MSE must equal the upper bound derived in (89)

$$\mathbb{E} \left[ \|\mathbf{U} - \hat{\mathbf{U}}\|_2^2 \mid \mathcal{A}_\eta \right] = \frac{1}{4\Pr(\mathcal{A}_\eta)} \int \Psi_N(z) f_Z(z) dz = \frac{\tilde{\Psi}_N^*(\alpha)}{4\alpha}. \quad (92)$$

We construct this specific noise distribution by considering the properties of the concave envelope  $\tilde{\Psi}_N^*(q)$ . Recall that  $\tilde{\Psi}_N^*(q)$  is the upper concave envelope of  $\tilde{\Psi}_N(q)$  over the interval  $q \in [0, 1]$ . We distinguish between two cases depending on whether the function  $\tilde{\Psi}_N(\alpha)$  coincides with its envelope at  $q = \alpha$  (illustrated by the point  $\alpha_1$  and  $\alpha_2$  in Figure 6). Consider following cases:

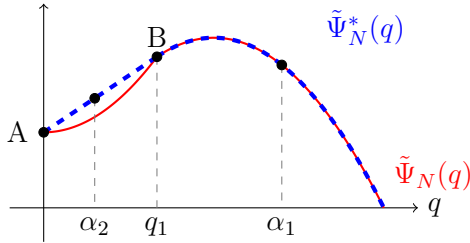


Fig. 6. A sample potential function  $\tilde{\Psi}_N(q)$  and its upper concave envelope  $\tilde{\Psi}_N^*(q)$ . Over the interval  $[0, q_1]$ , the concave envelope is defined by the linear chord connecting points A and B, while for  $q \in [q_1, 1]$ , the envelope coincides with the function itself. To achieve the upper bound in (89), for the case of  $\alpha_1$ , we use a noise distribution uniformly distributed over the surface of an  $N$ -sphere with radius  $z = \Phi_N^{-1}(\alpha_1)$  as derived in (94). For the case of  $\alpha_2$ , we use a mixed strategy where the noise is uniformly distributed over the surface of an  $N$ -sphere of radius  $z_1 = \Phi_N^{-1}(0)$  with probability  $\beta_1$ , and uniformly over the surface of an  $N$ -sphere of radius  $z_2 = \Phi_N^{-1}(q_1)$  with probability  $1 - \beta_1$ , as derived in (100).

1)  $\tilde{\Psi}_N^*(\alpha) = \tilde{\Psi}_N(\alpha)$ : This implies the function is already on the boundary of its concave hull at  $\alpha$  (see  $\alpha_1$  in Figure 6). We propose that the adversary employs a noise magnitude concentrated at a single value  $z^* = \Phi_N^{-1}(\alpha)$ . In the  $N$ -dimensional space, this corresponds to an adversarial noise vector  $\mathbf{N}_a$  that is uniformly distributed over the surface of the  $N$ -sphere with radius  $z^*$ . Mathematically, the probability density function of the vector  $\mathbf{N}_a$  is given by

$$f_{\mathbf{N}_a}(\mathbf{x}) = \frac{1}{S_N(z^*)} \delta(\|\mathbf{x}\|_2 - z^*), \quad (93)$$

where  $S_N(r) = \frac{2\pi^{N/2}}{\Gamma(N/2)} r^{N-1}$  denotes the surface area of an  $N$ -sphere of radius  $r$ . This vector distribution induces the magnitude PDF

$$f_Z(z) = \delta(z - z^*). \quad (94)$$

Substituting this distribution into the acceptance probability integral in (91), we obtain

$$\Pr(\mathcal{A}_\eta) = \int \Phi_N(z) \delta(z - z^*) dz = \Phi_N(z^*) = \Phi_N(\Phi_N^{-1}(\alpha)) = \alpha. \quad (95)$$

Thus, the first condition is satisfied. Next, we evaluate the conditional MSE for this distribution.

Substituting (94) into the MSE expression, we get

$$\begin{aligned} \mathbb{E} [\|\mathbf{U} - \hat{\mathbf{U}}\|_2^2 \mid \mathcal{A}_\eta] &= \frac{1}{4\alpha} \int \Psi_N(z) \delta(z - z^*) dz \\ &= \frac{1}{4\alpha} \Psi_N(z^*) \\ &= \frac{1}{4\alpha} \Psi_N(\Phi_N^{-1}(\alpha)). \end{aligned} \quad (96)$$

Using the definition  $\tilde{\Psi}_N(\alpha) = \Psi_N(\Phi_N^{-1}(\alpha))$  and the case assumption  $\tilde{\Psi}_N(\alpha) = \tilde{\Psi}_N^*(\alpha)$ , this becomes

$$\mathbb{E} \left[ \|\mathbf{U} - \hat{\mathbf{U}}\|_2^2 \mid \mathcal{A}_\eta \right] = \frac{\tilde{\Psi}_N^*(\alpha)}{4\alpha}. \quad (97)$$

This confirms that the single-point distribution defined in (94) achieves the upper bound when the function touches its envelope.

2)  $\tilde{\Psi}_N^*(\alpha) > \tilde{\Psi}_N(\alpha)$ : In this case (see  $\alpha_2$  in Figure 6), since  $\tilde{\Psi}_N^*(q)$  is the upper concave envelope, the point  $(\alpha, \tilde{\Psi}_N^*(\alpha))$  lies on a linear chord connecting two points on the original curve  $\tilde{\Psi}_N(q)$ . More precisely, there exist  $q_1$  and  $q_2$  such that  $0 \leq q_1 < \alpha < q_2 \leq 1$  where the envelope touches the function:

$$\tilde{\Psi}_N^*(q_1) = \tilde{\Psi}_N(q_1), \quad \text{and} \quad \tilde{\Psi}_N^*(q_2) = \tilde{\Psi}_N(q_2). \quad (98)$$

Furthermore, for all  $q \in [q_1, q_2]$ , we have

$$\tilde{\Psi}_N^*(q) = \frac{\tilde{\Psi}_N(q_2) - \tilde{\Psi}_N(q_1)}{q_2 - q_1}(q - q_1) + \tilde{\Psi}_N(q_1). \quad (99)$$

We propose that the adversary employs a mixed strategy. Let  $z_1 = \Phi_N^{-1}(q_1)$  and  $z_2 = \Phi_N^{-1}(q_2)$ . The adversary selects a noise vector  $\mathbf{N}_a$  uniformly distributed over the surface of an  $N$ -sphere of radius  $z_1$  with probability  $\beta_1$ , and uniformly over the surface of an  $N$ -sphere of radius  $z_2$  with probability  $\beta_2$ . The mixing weights are defined as  $\beta_1 = \frac{q_2 - \alpha}{q_2 - q_1}$  and  $\beta_2 = \frac{\alpha - q_1}{q_2 - q_1}$ . Mathematically, the probability density function of the adversarial noise vector is

$$f_{\mathbf{N}_a}(\mathbf{x}) = \beta_1 \frac{1}{S_N(z_1)} \delta(\|\mathbf{x}\|_2 - z_1) + \beta_2 \frac{1}{S_N(z_2)} \delta(\|\mathbf{x}\|_2 - z_2), \quad (100)$$

where  $S_N(r)$  is the surface area of the  $N$ -sphere of radius  $r$ . This vector distribution induces the following magnitude PDF

$$f_Z(z) = \beta_1 \delta(z - z_1) + \beta_2 \delta(z - z_2). \quad (101)$$

Note that by construction  $\beta_1 + \beta_2 = 1$  and  $\beta_1 q_1 + \beta_2 q_2 = \alpha$ . We first verify the acceptance probability condition (91) for this distribution, as follows

$$\begin{aligned} \Pr(\mathcal{A}_\eta) &= \int \Phi_N(z) [\beta_1 \delta(z - z_1) + \beta_2 \delta(z - z_2)] dz \\ &= \beta_1 \Phi_N(z_1) + \beta_2 \Phi_N(z_2) \\ &= \beta_1 q_1 + \beta_2 q_2 \\ &= \alpha. \end{aligned} \quad (102)$$

Thus, the distribution yields the required acceptance probability. Finally, we evaluate the conditional MSE. Substituting (101) into the MSE integral, we have

$$\begin{aligned}\mathbb{E} \left[ \|\mathbf{U} - \hat{\mathbf{U}}\|_2^2 \mid \mathcal{A}_\eta \right] &= \frac{1}{4\alpha} \int \Psi_N(z) [\beta_1 \delta(z - z_1) + \beta_2 \delta(z - z_2)] dz \\ &= \frac{1}{4\alpha} (\beta_1 \Psi_N(z_1) + \beta_2 \Psi_N(z_2)) \\ &= \frac{1}{4\alpha} (\beta_1 \tilde{\Psi}_N(q_1) + \beta_2 \tilde{\Psi}_N(q_2)).\end{aligned}\quad (103)$$

Using the boundary conditions (98), we replace  $\tilde{\Psi}_N$  with  $\tilde{\Psi}_N^*$ , and then exploit the linearity property (99) of the envelope:

$$\begin{aligned}\mathbb{E} \left[ \|\mathbf{U} - \hat{\mathbf{U}}\|_2^2 \mid \mathcal{A}_\eta \right] &= \frac{1}{4\alpha} (\beta_1 \tilde{\Psi}_N^*(q_1) + \beta_2 \tilde{\Psi}_N^*(q_2)) \\ &= \frac{1}{4\alpha} \tilde{\Psi}_N^*(\beta_1 q_1 + \beta_2 q_2) \\ &= \frac{\tilde{\Psi}_N^*(\alpha)}{4\alpha}.\end{aligned}\quad (104)$$

This confirms that the mixture distribution defined in (101) also achieves the upper bound.

Since we have constructed a valid noise distribution  $f_Z(z)$  for any  $\alpha \in [0, 1]$  that achieves the bound, the proof of Theorem 2 is complete.

## VI. ILLUSTRATIVE EXAMPLES

In this section, we present clarifying examples for Theorems 1 and 2 to demonstrate how these results can be utilized to derive the equilibrium, defined in (17), in various settings. For all the following examples, we assume that  $\Delta = 1$ . This implies that for any dimension  $N$ , the noise of the honest node is uniformly distributed within an  $N$ -dimensional ball of radius 1, denoted as  $\mathcal{B}_N(1)$ .

**Example 1.** Consider a 2-dimensional system ( $N = 2$ ). We assume the utility functions for the adversary and the DC are given by

$$U_{AD}(g(\cdot), \eta) = \log(\text{MSE}(g(\cdot), \eta)) + 0.85 \log(\text{PA}(g(\cdot), \eta)), \quad (105)$$

$$U_{DC}(g(\cdot), \eta) = -\text{MSE}(g(\cdot), \eta) + 25\text{PA}(g(\cdot), \eta). \quad (106)$$

To determine the equilibrium, we first analyze the game from the perspective of the DC's commitment. For a discrete set of thresholds  $\eta \in \{2.0, 2.2, \dots, 8.0\}$ , we derive the system's characteristic functions  $c_\eta(\alpha)$ , defined in (19), which represent the maximum MSE the adversary can strictly enforce for a given acceptance probability  $\alpha$ . These curves are computed using Theorem 2 (specifically using the closed-form evaluations for  $N = 2$  provided in Appendix G).

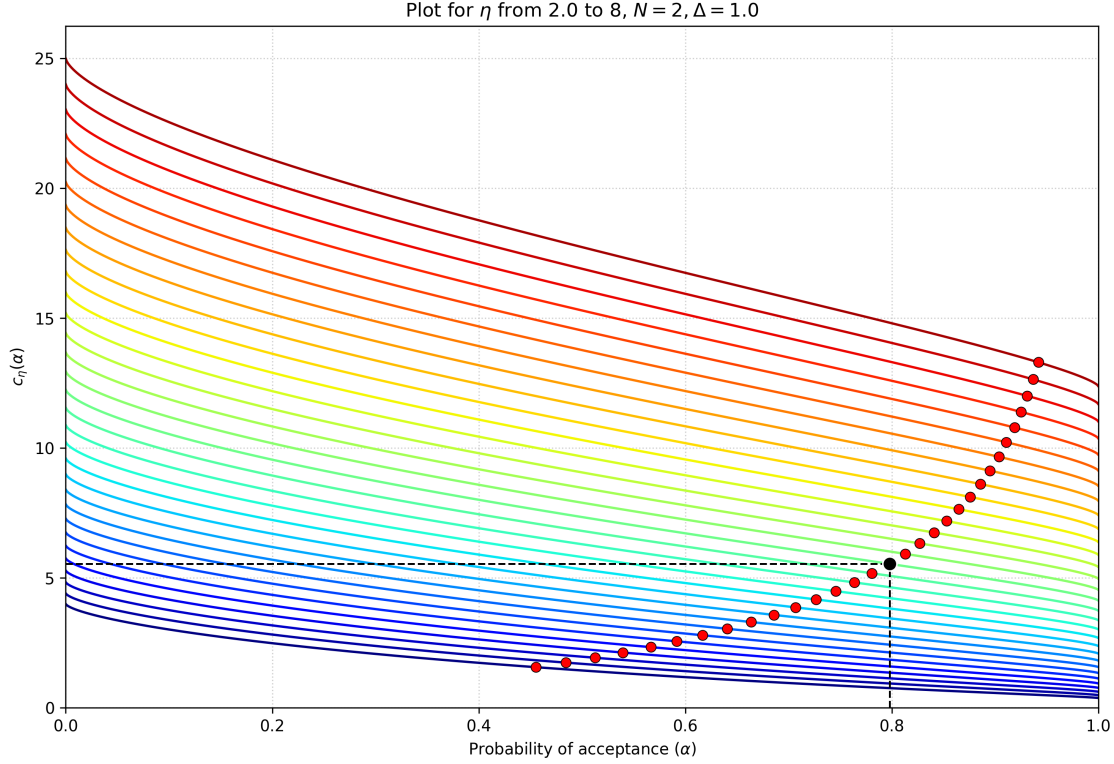


Fig. 7. Characteristic curves  $c_\eta(\alpha)$  defined in (19), for  $N = 2$  and  $\Delta = 1$  (Example 1). Each curve corresponds to a specific threshold  $\eta \in [2, 8]$ , mapping the acceptance probability  $\alpha$  (x-axis) to the maximum enforceable MSE (y-axis). The dots (red and black) on each curve represent the adversary's best response operating point  $(PA^*, MSE^*)$  for that specific  $\eta$ , and the utility function of the adversary defined in (105). The black dot highlights the global Stackelberg equilibrium of the game where the DC's utility, defined in (106), is maximized.

The resulting curves are illustrated in Figure 7. The curves range from the lowest blue curve, corresponding to the strictest threshold  $\eta = 2$ , to the uppermost red curve, corresponding to the loosest threshold  $\eta = 8$ . As expected, increasing  $\eta$  expands the adversary's feasible region, allowing for higher MSE at any given acceptance probability.

For any specific  $\eta$  committed to by the DC, the rational adversary selects the noise distribution  $g_\eta(\cdot)$  via Algorithm 2 that maximizes their utility defined in (105). Geometrically, this corresponds to finding the point on the curve  $c_\eta(\alpha)$  that maximizes the scalar function  $Q_{AD}$ . The adversary solves the optimization problem:

$$\alpha^*(\eta) = \arg \max_{0 < \alpha \leq 1} \{ \log(c_\eta(\alpha)) + 0.85 \log(\alpha) \}. \quad (107)$$

Once  $\alpha^*(\eta)$  is found, the resulting operating point of the system is given by the pair  $(\alpha^*(\eta), c_\eta(\alpha^*(\eta)))$ . These optimal operating points are depicted as solid dots on the curves in Figure 7.

Let us examine the adversary's response at the two extremes of our sweep:

- **Case  $\eta = 2$  (Strictest):**

$$\text{MSE} \approx 1.5622, \quad \text{PA} \approx 0.4555, \quad U_{\text{AD}} \approx -0.2224.$$

- **Case  $\eta = 8$  (Loosest):**

$$\text{MSE} \approx 13.2991, \quad \text{PA} \approx 0.9419, \quad U_{\text{AD}} \approx 2.5369.$$

It is evident that as the DC commits to a larger  $\eta$ , the adversary exploits the loosened constraint to achieve both higher liveness (PA) and higher error (MSE), strictly increasing their own utility. However, the DC's objective is more complex; it must find the "sweet spot" that balances the penalty of error against the reward of liveness.

Evaluating the DC's utility (106) at these extremes yields:

- At  $\eta = 2$ :  $U_{\text{DC}} \approx -1.5622 + 25(0.4555) \approx 9.8242$ .
- At  $\eta = 8$ :  $U_{\text{DC}} \approx -13.2991 + 25(0.9419) \approx 10.2495$ .

Interestingly, the DC prefers the loose threshold  $\eta = 8$  over the strict  $\eta = 2$ , as the gain in liveness outweighs the cost of increased error. However, neither is optimal. To find the Stackelberg equilibrium, the DC solves:

$$\eta^* = \arg \max_{\eta \in [2,8]} \{-c_\eta(\alpha^*(\eta)) + 25\alpha^*(\eta)\}. \quad (108)$$

Solving this optimization reveals that the optimal strategy is an intermediate value. The equilibrium is achieved at:

$$\text{Equilibrium } (\eta^* = 5.0) : \quad \left\{ \begin{array}{l} \text{MSE}^* \approx 5.5401 \\ \text{PA}^* \approx 0.7978 \\ U_{\text{AD}}^* \approx 1.5200 \\ U_{\text{DC}}^* \approx 14.4049 \end{array} \right.$$

**Interpretation:** Without the game of coding framework, a naive system designer might default to  $\eta = 2$ . Since the distance between two honest nodes is at most  $2\Delta$ , setting  $\eta = 2$  seems logical to reject any obvious attacks. However, our analysis shows this is suboptimal ( $U_{\text{DC}} \approx 9.8$  vs  $U_{\text{DC}}^* \approx 14.4$ ). At  $\eta = 2$ , the adversary is forced to attack aggressively to gain utility, resulting in a low probability of acceptance ( $\approx 45\%$ ) which harms the system's liveness.

By strategically relaxing the threshold to  $\eta^* = 5$ , the DC effectively *bribes* the adversary. The rational adversary, seeking to maximize their own utility (which includes log PA), shifts their strategy

to a noise distribution that is accepted much more frequently ( $\approx 80\%$ ). Although this allows for a higher MSE (5.54 vs 1.56), the substantial gain in system reliability and liveness leads to a strictly superior outcome for the DC.

**Example 2.** Consider a high-dimensional system with  $N = 25$ . We assume the utility function for the adversary is given by

$$U_{AD}(g(\cdot), \eta) = \log(MSE(g(\cdot), \eta)) + 0.20 \log(PA(g(\cdot), \eta)). \quad (109)$$

For the DC, we analyze the equilibrium under two distinct utility formulations to demonstrate how the choice of metric influences the optimal strategy:

$$\text{Case 1: } U_{DC}^{(1)}(g(\cdot), \eta) = \frac{PA(g(\cdot), \eta)}{\sqrt{MSE(g(\cdot), \eta)}}, \quad (110)$$

$$\text{Case 2: } U_{DC}^{(2)}(g(\cdot), \eta) = \frac{PA(g(\cdot), \eta)}{MSE(g(\cdot), \eta)}. \quad (111)$$

Similar to Example 1, we use Theorem 2 to compute the characteristic curves  $c_\eta(\alpha)$  for  $\eta \in [2.0, 8.0]$ . The resulting curves are illustrated in Figure 8. For each  $\eta$ , the adversary determines the optimal operating point  $(\alpha^*(\eta), c_\eta(\alpha^*(\eta)))$  by choosing the noise distribution via Algorithm 2 and solving

$$\alpha^*(\eta) = \arg \max_{0 < \alpha \leq 1} \{ \log(c_\eta(\alpha)) + 0.20 \log(\alpha) \}. \quad (112)$$

Since the adversary's utility (109) remains constant across both DC cases, the adversary's response points (marked as red dots in Figure 8) are identical for both scenarios. However, the DC's optimal commitment  $\eta^*$  changes depending on which utility function is maximized.

**Analysis of Case 1:** When the DC optimizes  $U_{DC}^{(1)}$ , the goal is to solve

$$\eta_1^* = \arg \max_{\eta} \frac{\alpha^*(\eta)}{\sqrt{c_\eta(\alpha^*(\eta))}}. \quad (113)$$

Solving this yields an intermediate equilibrium at  $\eta^* = 4.0$  (indicated by the black dot):

$$\text{Equilibrium 1 } (\eta^* = 4.0) : \quad \begin{cases} \text{MSE} \approx 4.2409 \\ \text{PA} \approx 0.5375 \\ U_{DC}^{(1)} \approx \mathbf{0.2610} \end{cases}$$

**Analysis of Case 2:** When the DC optimizes  $U_{DC}^{(2)}$ , the penalty for error is more severe (MSE vs.  $\sqrt{MSE}$ ). The optimization problem becomes

$$\eta_2^* = \arg \max_{\eta} \frac{\alpha^*(\eta)}{c_\eta(\alpha^*(\eta))}. \quad (114)$$

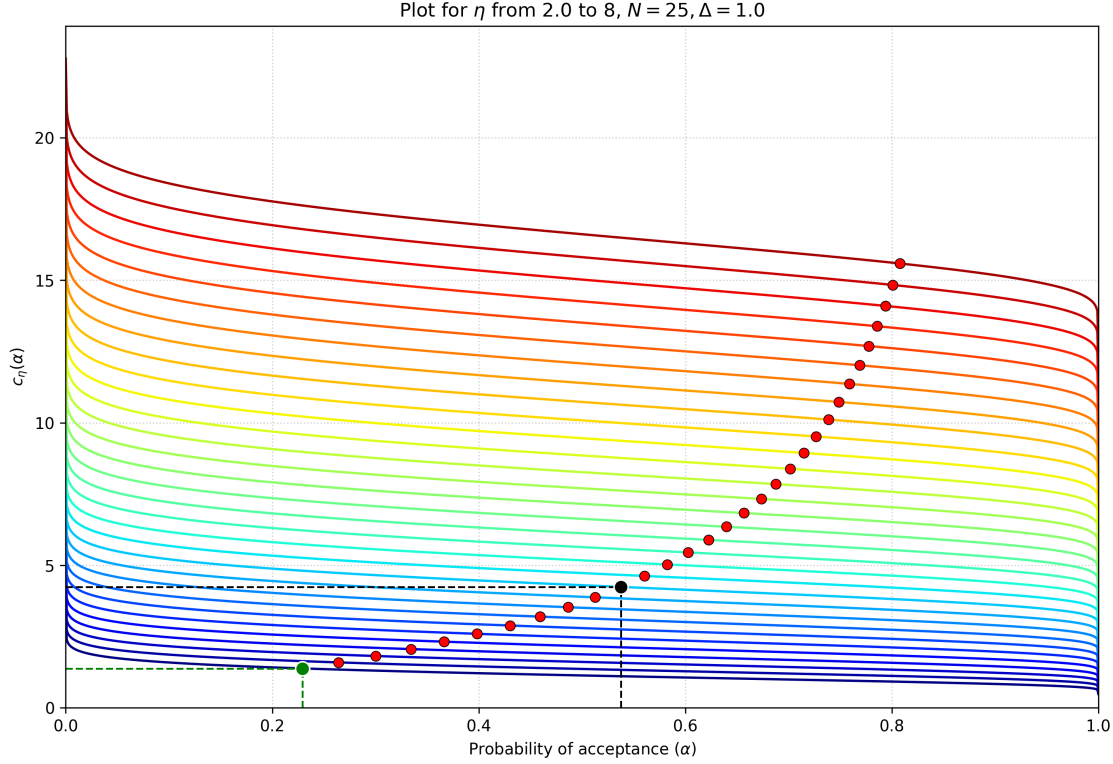


Fig. 8. Equilibrium analysis for  $N = 25$  with  $\eta \in [2.0, 8.0]$  (Example 2). The curves represent the characteristic functions  $c_\eta(\alpha)$ . The red dots indicate the adversary's best response for each  $\eta$ , with respect to the utility function of the adversary, defined in (109). The **black dot** marks the equilibrium for DC Case 1 (110), at  $\eta^* = 4.0$ . The **green dot** marks the equilibrium for DC Case 2 (111), at  $\eta^* = 2.0$ .

In this case, the equilibrium shifts to the strictest threshold  $\eta^* = 2.0$  (indicated by the green dot):

$$\text{Equilibrium 2 } (\eta^* = 2.0) : \begin{cases} \text{MSE} \approx 1.3808 \\ \text{PA} \approx 0.2292 \\ U_{\text{DC}}^{(2)} \approx 0.1660 \end{cases}$$

**Interpretation:** This example highlights how the DC's risk sensitivity dictates the optimal commitment strategy. In Case 1, where the penalty is sub-linear regarding the noise power ( $\sqrt{\text{MSE}}$ ), it is beneficial for the DC to relax the threshold to  $\eta = 4.0$ . This "bribes" the adversary into a significantly higher acceptance rate ( $\approx 54\%$  vs  $23\%$ ), which outweighs the cost of the increased error.

Conversely, in Case 2, the penalty is linear with noise power (MSE). Since the MSE grows rapidly as  $\eta$  increases (from 1.38 at  $\eta = 2$  to 15.59 at  $\eta = 8$ ), the gain in acceptance probability cannot

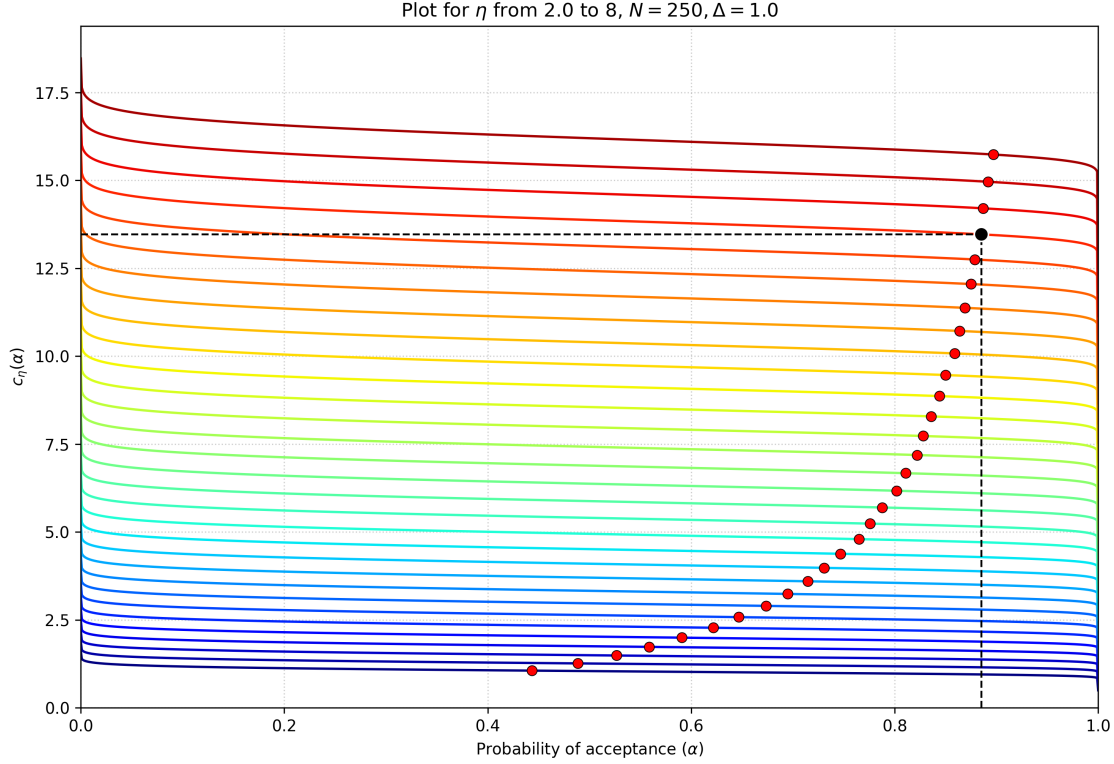


Fig. 9. Equilibrium analysis for  $N = 250$  with  $\eta \in [2.0, 8.0]$  (Example 3). The curves represent the characteristic functions  $c_\eta(\alpha)$ . The red dots indicate the adversary's best response for each  $\eta$  maximizing (115). The **black dot** highlights the global Stackelberg equilibrium where the DC's utility (116) is maximized.

compensate for the explosion in error. Thus, the DC is forced to adopt the strictest policy ( $\eta = 2.0$ ) to keep the error bounded, even at the cost of low system liveness.

**Example 3.** Consider a very high-dimensional system with  $N = 250$ . We assume the utility functions for the adversary and the DC are given by

$$U_{AD}(g(\cdot), \eta) = \log(MSE(g(\cdot), \eta)) + 0.10 \log(PA(g(\cdot), \eta)), \quad (115)$$

$$U_{DC}(g(\cdot), \eta) = -\log(MSE(g(\cdot), \eta)) + 10 \log(PA(g(\cdot), \eta)). \quad (116)$$

Following the same methodology described in Examples 1 and 2, we compute the characteristic curves  $c_\eta(\alpha)$  for  $\eta \in [2.0, 8.0]$ . For each committed  $\eta$ , the adversary calculates the best response using Algorithm 2 that maximizes (115). These optimal operating points are plotted as red dots in Figure 9.

To determine the equilibrium, the DC evaluates its utility (116) across the set of induced operating points. The results for the boundaries and the optimal point are:

- **Strictest** ( $\eta = 2.0$ ):

$$\text{MSE} \approx 1.0567, \quad \text{PA} \approx 0.4434, \quad \text{U}_{\text{DC}} \approx -8.1870.$$

- **Loosest** ( $\eta = 8.0$ ):

$$\text{MSE} \approx 15.7362, \quad \text{PA} \approx 0.8969, \quad \text{U}_{\text{DC}} \approx -3.8441.$$

The maximum utility for the DC is achieved at  $\eta^* = 7.4$ , marked by the black dot in Figure 9:

$$\text{Equilibrium } (\eta^* = 7.4) : \quad \left\{ \begin{array}{l} \text{MSE}^* \approx 13.4655 \\ \text{PA}^* \approx 0.8849 \\ \text{U}_{\text{AD}}^* \approx 2.5879 \\ \text{U}_{\text{DC}}^* \approx \mathbf{-3.8231} \end{array} \right.$$

## VII. CONCLUSION AND FUTURE WORKS

In this paper, we have significantly extended the game of coding framework to address vector-valued computations; moving beyond the scalar constraints of prior works. While previous research established the theoretical viability of the framework, its restriction to scalar values created a distinct gap with practical applications where vector operations are the norm, particularly in decentralized machine learning. We bridged this gap by providing a rigorous problem formulation for the  $N$ -dimensional Euclidean space, employing minimal and natural assumptions to ensure practical relevance. Furthermore, we fully characterized the equilibrium of the game, deriving the closed-form optimal strategies for both the DC and the adversary. Through illustrative examples, we demonstrated the dynamics of these strategies in various settings. Crucially, our analysis confirms that the resilience guarantees previously established for scalar settings, specifically the ability to maintain accuracy and liveness despite an adversarial majority, remain valid in the general high-dimensional case. Building on these established foundations, we propose to extend the game of coding framework in following key directions:

- 1) **Advanced Coding Techniques:** While previous works, including this study, relied on repetition coding (assigning the same task to multiple workers), we plan to explore advanced coding techniques to enhance computational efficiency; specifically, this requires deriving new acceptance policies and decoding rules that ensure reliability when using complex codes, such as MDS codes, in an adversarial environment.
- 2) **Resilience to Non-Myopic Adversaries:** Current models assume adversaries optimize for immediate rewards in a single-shot game. We plan to investigate non-myopic adversaries

who strategically sacrifice immediate gains to mislead learning algorithms over longer time horizons, with the objective of designing strategies that remain robust against such long-term manipulation.

3) **Unified Learning and Optimization:** We have analyzed the case where the adversary's strategy is unknown. We plan to develop a unified framework that performs distributed training while effectively managing the ambiguity of an unknown adversarial strategy simultaneously.

## REFERENCES

- [1] V. Guruswami, A. Rudra, and M. Sudan, *Essential Coding Theory*. Draft is Available, 2022.
- [2] Q. Yu, S. Li, N. Raviv, S. M. M. Kalan, M. Soltanolkotabi, and S. A. Avestimehr, "Lagrange coded computing: Optimal design for resiliency, security, and privacy," in *The 22nd International Conference on Artificial Intelligence and Statistics*, pp. 1215–1225, PMLR, 2019.
- [3] T. Jahani-Nezhad and M. A. Maddah-Ali, "Codedsketch: A coding scheme for distributed computation of approximated matrix multiplication," *IEEE Transactions on Information Theory*, vol. 67, no. 6, pp. 4185–4196, 2021.
- [4] R. Yosibash and R. Zamir, "Frame codes for distributed coded computation," in *2021 11th International Symposium on Topics in Coding (ISTC)*, pp. 1–5, 2021.
- [5] R. M. Roth, "Analog error-correcting codes," *IEEE Transactions on Information Theory*, vol. 66, no. 7, pp. 4075–4088, 2020.
- [6] T. Jahani-Nezhad and M. A. Maddah-Ali, "Berrut approximated coded computing: Straggler resistance beyond polynomial computing," *IEEE Transactions on Pattern Analysis and Machine Intelligence*, vol. 45, no. 1, pp. 111–122, 2023.
- [7] N. S. Bitcoin, "Bitcoin: A peer-to-peer electronic cash system," 2008.
- [8] V. Buterin *et al.*, "Ethereum white paper," *GitHub repository*, vol. 1, pp. 22–23, 2013.
- [9] S. Ruoti, B. Kaiser, A. Yerukhimovich, J. Clark, and R. Cunningham, "SoK: Blockchain technology and its potential use cases," *arXiv preprint arXiv:1909.12454*, 2019.
- [10] M. Shafay, R. W. Ahmad, K. Salah, I. Yaqoob, R. Jayaraman, and M. Omar, "Blockchain for deep learning: review and open challenges," *Cluster Computing*, vol. 26, no. 1, pp. 197–221, 2023.
- [11] S. Ding and C. Hu, "Survey on the convergence of machine learning and blockchain," in *Proceedings of SAI Intelligent Systems Conference*, pp. 170–189, Springer, 2022.
- [12] S. Kayikci and T. M. Khoshgoftaar, "Blockchain meets machine learning: a survey," *Journal of Big Data*, vol. 11, no. 1, pp. 1–29, 2024.
- [13] H. Taherdoost, "Blockchain and machine learning: A critical review on security," *Information*, vol. 14, no. 5, p. 295, 2023.
- [14] H. Taherdoost, "Blockchain technology and artificial intelligence together: a critical review on applications," *Applied Sciences*, vol. 12, no. 24, p. 12948, 2022.
- [15] R. Tian, L. Kong, X. Min, and Y. Qu, "Blockchain for ai: A disruptive integration," in *2022 IEEE 25th International Conference on Computer Supported Cooperative Work in Design (CSCWD)*, pp. 938–943, IEEE, 2022.

- [16] K. Salah, M. H. U. Rehman, N. Nizamuddin, and A. Al-Fuqaha, “Blockchain for ai: Review and open research challenges,” *IEEE Access*, vol. 7, pp. 10127–10149, 2019.
- [17] L. Zhao, Q. Wang, C. Wang, Q. Li, C. Shen, and B. Feng, “VeriML: Enabling integrity assurances and fair payments for machine learning as a service,” *IEEE Transactions on Parallel and Distributed Systems*, vol. 32, no. 10, pp. 2524–2540, 2021.
- [18] H. A. Nodehi, V. R. Cadambe, and M. A. Maddah-Ali, “Game of coding: Beyond honest-majority assumptions,” *IEEE Transactions on Information Theory (submitted)*, 2024.
- [19] H. A. Nodehi, V. R. Cadambe, and M. A. Maddah-Al, “Game of coding: Sybil resistant decentralized machine learning with minimal trust assumption,” *arXiv preprint*, 2024. <https://arxiv.org/abs/2410.05540>.
- [20] H. Akbari Nodehi, P. Moradi, and M. A. Maddah-Ali, “Game of coding with an unknown adversary,” in *2025 IEEE International Symposium on Information Theory (ISIT)*, (Ann Arbor, MI, USA), 2025.
- [21] H. A. Nodehi, V. R. Cadambe, and M. A. Maddah-Ali, “Game of coding: Coding theory in the presence of rational adversaries, motivated by decentralized machine learning,” *arXiv preprint arXiv:2601.02313*, 2026.
- [22] J. Thaler, “Proofs, arguments, and zero-knowledge,” *Foundations and Trends® in Privacy and Security*, vol. 4, no. 2–4, pp. 117–660, 2022.
- [23] B. Feng, L. Qin, Z. Zhang, Y. Ding, and S. Chu, “ZEN: An optimizing compiler for verifiable, zero-knowledge neural network inferences,” *Cryptology ePrint Archive*, 2021.
- [24] T. Liu, X. Xie, and Y. Zhang, “ZkCNN: Zero knowledge proofs for convolutional neural network predictions and accuracy,” in *Proceedings of the 2021 ACM SIGSAC Conference on Computer and Communications Security*, pp. 2968–2985, 2021.
- [25] Z. Xing, Z. Zhang, J. Liu, Z. Zhang, M. Li, L. Zhu, and G. Russello, “Zero-knowledge proof meets machine learning in verifiability: A survey,” *arXiv preprint arXiv:2310.14848*, 2023.
- [26] P. Mohassel and Y. Zhang, “SecureML: A system for scalable privacy-preserving machine learning,” in *2017 IEEE symposium on security and privacy (SP)*, pp. 19–38, IEEE, 2017.
- [27] S. Lee, H. Ko, J. Kim, and H. Oh, “vCNN: Verifiable convolutional neural network based on zk-snarks,” *IEEE Transactions on Dependable and Secure Computing*, 2024.
- [28] C. Weng, K. Yang, X. Xie, J. Katz, and X. Wang, “Mystique: Efficient conversions for {Zero-Knowledge} proofs with applications to machine learning,” in *30th USENIX Security Symposium (USENIX Security 21)*, pp. 501–518, 2021.
- [29] S. Chen, J. H. Cheon, D. Kim, and D. Park, “Interactive proofs for rounding arithmetic,” *IEEE Access*, vol. 10, pp. 122706–122725, 2022.
- [30] S. Garg, A. Jain, Z. Jin, and Y. Zhang, “Succinct zero knowledge for floating point computations,” in *Proceedings of the 2022 ACM SIGSAC Conference on Computer and Communications Security*, pp. 1203–1216, 2022.
- [31] S. Setty, V. Vu, N. Panpalia, B. Braun, A. J. Blumberg, and M. Walfish, “Taking {Proof-Based} verified computation a few steps closer to practicality,” in *21st USENIX Security Symposium (USENIX Security 12)*, pp. 253–268, 2012.
- [32] S. Bhat, C. Chen, Z. Cheng, Z. Fang, A. Hebbar, S. Kannan, R. Rana, P. Sheng, H. Tyagi, P. Viswanath, *et al.*, “Sakshi: Decentralized ai platforms,” *arXiv preprint arXiv:2307.16562*, 2023.
- [33] K. Conway, C. So, X. Yu, and K. Wong, “opml: Optimistic machine learning on blockchain,” *arXiv preprint arXiv:2401.17555*, 2024.

- [34] Q. Yu, M. Maddah-Ali, and S. Avestimehr, “Polynomial codes: an optimal design for high-dimensional coded matrix multiplication,” *Advances in Neural Information Processing Systems*, vol. 30, 2017.
- [35] S. Eskandari, M. Salehi, W. C. Gu, and J. Clark, “SoK: Oracles from the ground truth to market manipulation,” in *Proceedings of the 3rd ACM Conference on Advances in Financial Technologies*, pp. 127–141, 2021.
- [36] L. Breidenbach, C. Cachin, B. Chan, A. Coventry, S. Ellis, A. Juels, F. Koushanfar, A. Miller, B. Magauran, D. Moroz, *et al.*, “Chainlink 2.0: Next steps in the evolution of decentralized oracle networks,” *Chainlink Labs*, vol. 1, pp. 1–136, 2021.
- [37] B. Benligiray, S. Milic, and H. Vänttinen, “Decentralized APIs for web 3.0,” *API3 Foundation Whitepaper*, 2020.
- [38] H. Von Stackelberg, *Market structure and equilibrium*. Springer Science & Business Media, 2010.

## APPENDIX A PROOF OF LEMMA 2

To prove Lemma 2, we apply the law of total probability to express  $\Pr(\mathcal{A}_\eta)$  as

$$\Pr(\mathcal{A}_\eta) = \int_0^\infty \Pr(\mathcal{A}_\eta \mid Z = z) f_Z(z) dz. \quad (117)$$

Comparing (117) with (66), it is sufficient to derive the kernel function

$$\Phi_N(z) \triangleq \Pr(\mathcal{A}_\eta \mid Z = z). \quad (118)$$

Let  $\mathcal{S}_z$  denote the surface of the  $N$ -ball with radius  $z$  centered at the origin. Given a magnitude  $Z = z$ , the vector  $\mathbf{N}_a$  is distributed over this surface with a conditional probability density

$$f_{\mathbf{N}_a|Z}(\mathbf{n}_a|z) = \begin{cases} \frac{g(\mathbf{n}_a)}{f_Z(z)} & \mathbf{n}_a \in \mathcal{S}_z \\ 0 & \text{otherwise,} \end{cases}$$

where  $g(\cdot)$  is the adversarial noise distribution. Therefore, we can express the conditional acceptance probability as an integral over the surface  $\mathcal{S}_z$  as

$$\Pr(\mathcal{A}_\eta \mid Z = z) = \int_{\mathcal{S}_z} \Pr(\mathcal{A}_\eta \mid \mathbf{N}_a = \mathbf{n}_a) f_{\mathbf{N}_a|Z}(\mathbf{n}_a|z) d\mathbf{n}_a. \quad (119)$$

Now, let  $\mathcal{R}_{\text{honest}} = \{\mathbf{x} \in \mathbb{R}^N \mid \|\mathbf{x}\|_2 \leq \Delta\}$  be the support of the honest noise and

$$\mathcal{R}_{\text{acc}}(\mathbf{n}_a) = \{\mathbf{x} \in \mathbb{R}^N \mid \|\mathbf{x} - \mathbf{n}_a\|_2 \leq \eta\Delta\}, \quad (120)$$

be the acceptance region of the honest noise, for a fixed adversarial noise vector  $\mathbf{n}_a$ . Since  $\mathbf{N}_h$  is uniformly distributed over  $\mathcal{R}_{\text{honest}}$ , for any fixed  $\mathbf{n}_a$ , we have

$$\Pr(\mathcal{A}_\eta \mid \mathbf{N}_a = \mathbf{n}_a) = \frac{\text{Vol}(\mathcal{R}_{\text{honest}} \cap \mathcal{R}_{\text{acc}}(\mathbf{n}_a))}{\text{Vol}(\mathcal{R}_{\text{honest}})}. \quad (121)$$

Note that, due to the uniform distribution of  $\mathbf{N}_h$ , this probability only depends on the volume of the intersection. Furthermore, due to the spherical symmetry of the honest support  $\mathcal{R}_{\text{honest}}$ , this

volume only depends on the distance between the two centers, which in turn, depends only on the magnitude  $\|\mathbf{n}_a\|_2 = z$ , and remains invariant regardless of the direction of  $\mathbf{n}_a$ .

As discussed above, even though  $\mathcal{R}_{\text{acc}}(\mathbf{n}_a)$  depends on both magnitude and direction of  $\mathbf{n}_a$ , the quantity of interest, i.e.,  $\text{Vol}(\mathcal{R}_{\text{honest}} \cap \mathcal{R}_{\text{acc}}(\mathbf{n}_a))$  only depends on  $z = \|\mathbf{n}_a\|$ . Hence, with slight abuse of notation and for simplicity, we let  $\mathcal{R}_{\text{acc}}(z)$  denote the acceptance region for an arbitrary vector  $\mathbf{n}_a$  on the shell  $\mathcal{S}_z$ . Consequently, the ratio in (121) is constant for all  $\mathbf{n}_a \in \mathcal{S}_z$ . This allows us to move this constant term outside the integral in (119), and arrive at

$$\begin{aligned} \Pr(\mathcal{A}_\eta \mid Z = z) &= \frac{\text{Vol}(\mathcal{R}_{\text{honest}} \cap \mathcal{R}_{\text{acc}}(z))}{\text{Vol}(\mathcal{R}_{\text{honest}})} \int_{\mathcal{S}_z} f_{\mathbf{N}_a|Z}(\mathbf{n}_a|z) d\mathbf{n}_a \\ &\stackrel{(a)}{=} \frac{\mathcal{V}(\Delta, \eta\Delta, z)}{V_N(\Delta)} \cdot 1, \end{aligned} \quad (122)$$

where (a) follows from the fact that the conditional PDF  $f_{\mathbf{N}_a|Z}(\mathbf{n}_a|z)$  integrates to unity over its support  $\mathcal{S}_z$ , and  $\mathcal{V}(\Delta, \eta\Delta, z)$  represents the general intersection volume of two  $N$ -balls at distance  $z$  and radii  $\Delta$  and  $\eta\Delta$ . This volume is formally defined and evaluated in (125) of Appendix B.

Substituting the piecewise characterization of  $\mathcal{V}(\Delta, \eta\Delta, z)$  based on the geometric cases described in (141) into the volume ratio (121) and subsequently into the total probability integral (117) yields the three cases for  $\Phi_N(z)$  specified in (67). This completes the proof of Lemma 2.

## APPENDIX B GENERAL INTERSECTION VOLUME OF TWO HYPERSPHERES

In this section, we derive the general formula for the intersection volume between two  $N$ -dimensional balls in  $\mathbb{R}^N$ . Let the two balls be defined as the sets

$$\mathcal{B}_N(r_1, \mathbf{o}_1) = \{\mathbf{x} \in \mathbb{R}^N : \|\mathbf{x} - \mathbf{o}_1\|_2 \leq r_1\}, \quad (123)$$

$$\mathcal{B}_N(r_2, \mathbf{o}_2) = \{\mathbf{x} \in \mathbb{R}^N : \|\mathbf{x} - \mathbf{o}_2\|_2 \leq r_2\}, \quad (124)$$

where  $\mathbf{o}_1$  and  $\mathbf{o}_2$  are the center vectors in  $\mathbb{R}^N$ . Because the intersection volume is invariant under rotation and translation, and both balls are spherically symmetric, the intersection volume is a function of only the radii  $r_1, r_2$  and the Euclidean distance between the centers  $d = \|\mathbf{o}_1 - \mathbf{o}_2\|_2$ . Hence, we are interested in

$$\mathcal{V}(r_1, r_2, d) \triangleq \text{Vol}(\mathcal{B}_N(r_1, \mathbf{o}_1) \cap \mathcal{B}_N(r_2, \mathbf{o}_2)). \quad (125)$$

Recall that the volume of an  $N$ -ball of radius  $r$  is given by

$$V_N(r) = \frac{\pi^{N/2}}{\Gamma(\frac{N}{2} + 1)} r^N, \quad (126)$$

where  $\Gamma(\cdot)$  is the Euler Gamma function defined in (1). We consider the three distinct cases below.

### A. Case 1: No Intersection

If the distance between the centers is greater than or equal to the sum of the radii, i.e.,  $d \geq r_1 + r_2$ , the balls are disjoint or touch at a single point. Thus, the intersection volume is

$$\mathcal{V}(r_1, r_2, d) = 0. \quad (127)$$

### B. Case 2: Complete Containment

If the distance is sufficiently small such that one ball is entirely contained within the other, which occurs when  $d \leq |r_1 - r_2|$ , the intersection set is simply the smaller ball. More precisely, we have

$$\mathcal{V}(r_1, r_2, d) = V_N(\min(r_1, r_2)). \quad (128)$$

### C. Case 3: Partial Overlap

Partial overlap occurs when the boundaries of the two  $N$ -balls intersect, a condition satisfied when  $|r_1 - r_2| < d < r_1 + r_2$ . In this scenario, the overlap between the balls will be the union of two *hyperspherical caps* (see Figure 12). The volume of a general hyperspherical cap depends on the radius of its ball and the distance between the cutting hyper plane and the center of the ball, and is evaluated in Appendix C. However, depending on the configuration of the balls, two sub-cases can be identified. These cases are illustrated in Figure 10 and Figure 11. In the following, we first characterize the conditions for these two cases, and then formalize the parameters of the cap, and finally use the result of Appendix C to compute the volume of the intersection.

We denote the boundary of a set  $\mathcal{S}$  by  $\partial\mathcal{S}$ . In this scenario, the set of all points belonging to the boundaries of both balls, denoted by the intersection  $\partial\mathcal{B}_N(r_1, \mathbf{o}_1) \cap \partial\mathcal{B}_N(r_2, \mathbf{o}_2)$ , lies entirely within a flat  $(N - 1)$ -dimensional surface known as the **radical hyperplane** (see Figure 10).

Formally, the radical hyperplane is defined by the locus of points having equal distance with respect to both spheres. A point  $\mathbf{x}$  lies on this hyperplane if and only if

$$\|\mathbf{x} - \mathbf{o}_1\|_2^2 - r_1^2 = \|\mathbf{x} - \mathbf{o}_2\|_2^2 - r_2^2. \quad (129)$$

It is worth noting that the condition above can be rephrased as

$$2\mathbf{x}^T(\mathbf{o}_2 - \mathbf{o}_1) = (\|\mathbf{o}_2\|_2^2 - \|\mathbf{o}_1\|_2^2) - (r_2^2 - r_1^2), \quad (130)$$

which is a linear constraint, and clearly characterizes an  $(N - 1)$ -dimensional hyperplane. Moreover, from (130), it can be seen that the radical hyperplane is perpendicular to the direction  $\mathbf{o}_2 - \mathbf{o}_1$ . Furthermore, for any point  $\mathbf{x}$  on the intersection of the boundaries of two balls, we have  $\|\mathbf{x} - \mathbf{o}_1\|_2^2 = r_1^2$

and  $\|\mathbf{x} - \mathbf{o}_2\|_2^2 = r_2^2$ , which make both sides of (129) equal zero, and hence lie on the radical hyperplane.

The geometry of the intersection depends on the position of the radical hyperplane relative to the centers: Sub-cases 3a happens if two centers lie on opposite sides of the radical hyperplane, and Sub-case 3b indicates the both centers are on one side of the radical hyperplane. In order to formally characterize this distinction, without loss of generality, we assume  $\mathbf{o}_1$  is at the origin and  $\mathbf{o}_2$  is at  $(d, 0, \dots, 0)$  on the  $x_1$ -axis. Then, the radical hyperplane is perpendicular to the  $x_1$ -axis. Let  $\mathbf{y}$  be the intersection of the radical hyperplane at  $x_1$ -axis, and assume  $c_1 = \|\mathbf{o}_1 - \mathbf{y}\|_2$  and  $c_2 = \|\mathbf{o}_2 - \mathbf{y}\|_2$  are the geometric distances between the radical hyperplane and the centers  $\mathbf{o}_1$  and  $\mathbf{o}_2$ , respectively. Comparing Figure 10 and Figure 11, it turns out that transition from Sub-case 3a to 3b happens right at  $c_2 = 0$ , i.e., when  $\mathbf{y} = \mathbf{o}_2$ . Plugging  $\mathbf{x} = \mathbf{y} = \mathbf{o}_2$  in (129), we get  $\|\mathbf{o}_2 - \mathbf{o}_1\|_2^2 - r_1^2 = \|\mathbf{o}_2 - \mathbf{o}_2\|_2^2 - r_2^2$ , or equivalently,  $d^2 = r_1^2 - r_2^2$ . Then, we can characterize the two Sub-cases as follows.

1) *Sub-case 3a: Centers on opposite sides of the hyperplane:* When  $d^2 \geq r_1^2 - r_2^2$ , the radical hyperplane lies between the centers. Our goal is to determine  $c_1$  and  $c_2$ . In this configuration, we have

$$c_1 + c_2 = d. \quad (131)$$

Moreover, plugging  $\mathbf{y}$  in (129), we get

$$c_1^2 - r_1^2 = c_2^2 - r_2^2. \quad (132)$$

Solving (131) and (132) for  $c_1$  and  $c_2$ , we arrive at

$$c_1^{(1)} = \frac{d^2 + r_1^2 - r_2^2}{2d}, \quad c_2^{(1)} = \frac{d^2 + r_2^2 - r_1^2}{2d}. \quad (133)$$

Then, the volume of the intersection can be found from

$$\mathcal{V}(r_1, r_2, d) = \mathcal{K}_N(r_1, c_1^{(1)}) + \mathcal{K}_N(r_2, c_2^{(1)}), \quad (134)$$

where  $\mathcal{K}_N(r, c)$  is the volume of a hyperspherical cap in an  $N$ -ball of radius  $r$  with a cutting hyperplane at distance  $c$  from the center. This volume is evaluated in (143).

2) *Sub-case 3b: Centers on the same side of the hyperplane:* When  $d^2 < r_1^2 - r_2^2$ , the radical hyperplane lies to the right of both centers. Therefore, we have

$$c_1 - c_2 = d. \quad (135)$$

Solving this equation together with (132) for  $c_1$  and  $c_2$ , leads to

$$c_1^{(2)} = \frac{d^2 + r_1^2 - r_2^2}{2d}, \quad c_2^{(2)} = \frac{r_1^2 - r_2^2 - d^2}{2d}. \quad (136)$$

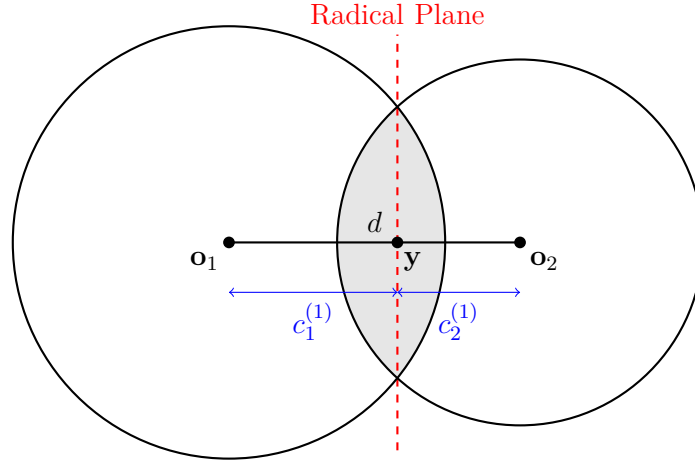


Fig. 10. Sub-case 3a: Both centers are outside the intersection, resulting in  $c_1^{(1)} + c_2^{(1)} = d$ .

As illustrated in Figure 11, in this case, for the intersection volume, we have

$$\begin{aligned} \mathcal{V}(r_1, r_2, d) &= \mathcal{K}_N(r_1, c_1^{(2)}) + (V_N(r_2) - \mathcal{K}_N(r_2, c_2^{(2)})) \\ &\stackrel{(a)}{=} \mathcal{K}_N(r_1, c_1^{(2)}) + \mathcal{K}_N(r_2, -c_2^{(2)}), \end{aligned} \quad (137)$$

where (a) follows from the fact that based on the definition of a hyperspherical cap in (142) and its volume in (143), for any  $c \in [0, r]$ , we have  $V_N(r) = \mathcal{K}_N(r, c) + \mathcal{K}_N(r, -c)$ . This identity reflects that a hyperplane divides a ball into two caps whose volumes sum to the total volume  $V_N(r)$ .

3) *Aggregation of Cases:* We observe that (134) and (137) can be unified into a single expression by allowing  $c_2$  to be a signed distance. If we define  $c_2 = \frac{d^2 + r_2^2 - r_1^2}{2d}$  as in (133), then in Case 3b,  $c_2$  becomes naturally negative ( $c_2 = -c_2^{(2)}$ ). Thus, for all configurations of partial overlap, we have

$$\mathcal{V}(r_1, r_2, d) = \mathcal{K}_N(r_1, c_1) + \mathcal{K}_N(r_2, c_2), \quad (138)$$

where

$$c_1 = \frac{d^2 + r_1^2 - r_2^2}{2d} \quad (139)$$

and

$$c_2 = \frac{d^2 + r_2^2 - r_1^2}{2d}. \quad (140)$$

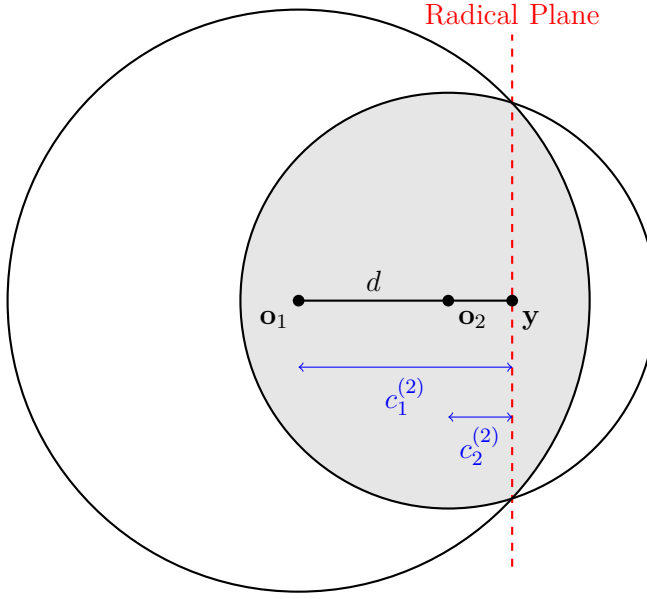


Fig. 11. Sub-case 3b: Center  $\mathbf{o}_2$  is inside the intersection, resulting in  $c_1^{(2)} - c_2^{(2)} = d$ .

#### D. General Expression for the Intersection Volume

By aggregating the results from Case 1 (127), Case 2 (128), and Case 3 (138), we obtain a comprehensive expression for the intersection volume of two  $N$ -balls. The general formula  $\mathcal{V}(r_1, r_2, d)$  is defined as the following piecewise function

$$\mathcal{V}(r_1, r_2, d) = \begin{cases} 0 & \text{if } d \geq r_1 + r_2 \quad (\text{No Intersection}), \\ V_N(\min(r_1, r_2)) & \text{if } d \leq |r_1 - r_2| \quad (\text{Complete Containment}), \\ \mathcal{V}_{\text{lens}}(r_1, r_2, d) & \text{if } |r_1 - r_2| < d < r_1 + r_2 \quad (\text{Partial Overlap}), \end{cases} \quad (141)$$

where  $V_N(r)$  is the volume of an  $N$ -ball of radius  $r$ , as defined in (3), and  $\mathcal{V}_{\text{lens}}$  is defined in (138)–(140).

## APPENDIX C

### DERIVATION OF THE HYPERSPHERICAL CAP VOLUME

A hyperspherical cap is defined as the portion of an  $N$ -ball cut off by a hyperplane. Without loss of generality, we can assume that the ball is at the origin. More precisely, consider an  $N$ -ball of radius  $r$  centered at the origin, which we denote as the set  $\mathcal{B}_N(r) = \{\mathbf{x} \in \mathbb{R}^N : \|\mathbf{x}\|_2 \leq r\}$ . If we cut this ball with a hyperplane perpendicular to the  $x$ -axis at the location  $c$ , where  $-r \leq c \leq r$ , the

resulting hyperspherical cap consists of all points in the ball with an  $x$ -coordinate greater than or equal to  $c$ . We formally define this region as

$$\mathcal{C}_N(r, c) \triangleq \{(x, x_2, \dots, x_N) \in \mathbb{R}^N : x^2 + x_2^2 + \dots + x_N^2 \leq r^2, x \geq c\}. \quad (142)$$

This geometric concept is illustrated for the 2D case in Figure 12. We denote the volume of this cap by

$$\mathcal{K}_N(r, c) \triangleq \text{Vol}(\mathcal{C}_N(r, c)). \quad (143)$$

To compute the volume  $\mathcal{K}_N(r, c)$ , we integrate the volumes of its cross-sections along the axis of symmetry, which in this coordinate system is the  $x$ -axis. More precisely, consider a slice of the cap at a position  $x$ , for some  $c \leq x \leq r$ , as shown in Figure 12. This cross-section is an  $(N - 1)$ -dimensional ball lying in the hyperplane perpendicular to the  $x$ -axis. By the Pythagorean theorem, the radius  $\rho(x)$  of this  $(N - 1)$ -ball is given by

$$\rho(x) = \sqrt{r^2 - x^2}. \quad (144)$$

The volume of this cross-sectional slice is  $V_{N-1}(\rho(x))$ . To find the total volume of the cap, we integrate this quantity from the cutting location  $c$  to the edge of the ball  $r$ . That is,

$$\mathcal{K}_N(r, c) = \int_c^r V_{N-1}(\sqrt{r^2 - x^2}) dx. \quad (145)$$

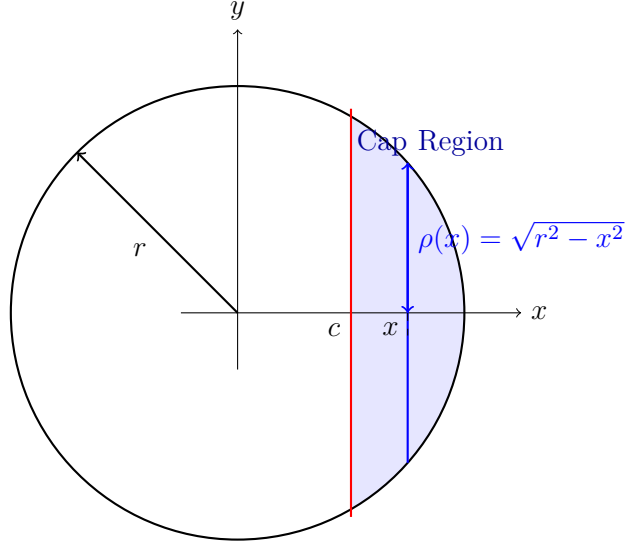


Fig. 12. Illustration of a hyperspherical cap (shown in 2D). The volume is calculated by integrating the area of the cross-sectional slices (blue vertical line) from  $x = c$  to  $x = r$ . In  $\mathbb{R}^N$ , each slice is an  $(N - 1)$ -ball.

Recall that the volume of an  $(N - 1)$ -ball of radius  $\rho$  is given by  $V_{N-1}(\rho) = \frac{\pi^{(N-1)/2}}{\Gamma(\frac{N+1}{2})} \rho^{N-1}$ .

Substituting this formula into (145) leads to

$$\mathcal{K}_N(r, c) = \frac{\pi^{(N-1)/2}}{\Gamma(\frac{1}{2}(N+1))} \int_c^r (r^2 - x^2)^{\frac{N-1}{2}} dx. \quad (146)$$

By performing the substitution  $t = x/r$ , which implies  $dx = rdt$ , the limits of integration in (146) change from  $[c, r]$  to  $[c/r, 1]$ . We thus obtain

$$\begin{aligned} \int_c^r (r^2 - x^2)^{\frac{N-1}{2}} dx &= \int_{c/r}^1 (r^2 - r^2 t^2)^{\frac{N-1}{2}} (r dt) \\ &= r^N \int_{c/r}^1 (1 - t^2)^{\frac{N-1}{2}} dt. \end{aligned} \quad (147)$$

Substituting (147) into (146), the final expression for the volume of the hyperspherical cap is given by

$$\mathcal{K}_N(r, c) = \frac{\pi^{(N-1)/2} r^N}{\Gamma(\frac{N+1}{2})} \int_{c/r}^1 (1 - t^2)^{\frac{N-1}{2}} dt. \quad (148)$$

## APPENDIX D

### PROOF OF LEMMA 3

To prove Lemma 3, recall that the conditional expected error is defined as  $\mathbb{E}[\|\mathbf{U} - \hat{\mathbf{U}}\|_2^2 \mid \mathcal{A}_\eta]$ .

Using the law of total expectation conditioned on the adversarial noise  $\mathbf{N}_a$ , we write

$$\mathbb{E}[\|\mathbf{U} - \hat{\mathbf{U}}\|_2^2 \mid \mathcal{A}_\eta] = \int_{\mathbf{n}_a} \mathbb{E}[\|\mathbf{U} - \hat{\mathbf{U}}\|_2^2 \mid \mathcal{A}_\eta, \mathbf{N}_a = \mathbf{n}_a] g_{\mathbf{N}_a \mid \mathcal{A}_\eta}(\mathbf{n}_a) d\mathbf{n}_a. \quad (149)$$

Using Bayes' theorem, the posterior density  $g_{\mathbf{N}_a \mid \mathcal{A}_\eta}(\mathbf{n}_a)$  is

$$g_{\mathbf{N}_a \mid \mathcal{A}_\eta}(\mathbf{n}_a) = \frac{\Pr(\mathcal{A}_\eta \mid \mathbf{N}_a = \mathbf{n}_a) g_{\mathbf{N}_a}(\mathbf{n}_a)}{\Pr(\mathcal{A}_\eta)} = \frac{\Pr(\mathcal{A}_\eta \mid \mathbf{N}_a = \mathbf{n}_a) \int_0^\infty f_{\mathbf{N}_a \mid Z}(\mathbf{n}_a \mid z) f_Z(z) dz}{\Pr(\mathcal{A}_\eta)}. \quad (150)$$

Note that, here we have

$$f_{\mathbf{N}_a \mid Z}(\mathbf{n}_a \mid z) = \begin{cases} \frac{g(\mathbf{n}_a)}{f_Z(z)} & \mathbf{n}_a \in \mathcal{S}_z \\ 0 & \text{otherwise,} \end{cases}$$

and  $\mathcal{S}_z \triangleq \{\mathbf{x} \in \mathbb{R}^N : \|\mathbf{x}\|_2 = z\}$  denotes the surface of the  $N$ -ball with radius  $z$ . Substituting (150) back into (149) yields

$$\begin{aligned} \mathbb{E}[\|\mathbf{U} - \hat{\mathbf{U}}\|_2^2 \mid \mathcal{A}_\eta] &= \int_{\mathbf{n}_a} \mathbb{E}[\|\mathbf{U} - \hat{\mathbf{U}}\|_2^2 \mid \mathcal{A}_\eta, \mathbf{N}_a = \mathbf{n}_a] \frac{\Pr(\mathcal{A}_\eta \mid \mathbf{N}_a = \mathbf{n}_a) \int_0^\infty f_{\mathbf{N}_a \mid Z}(\mathbf{n}_a \mid z) f_Z(z) dz}{\Pr(\mathcal{A}_\eta)} d\mathbf{n}_a \\ &= \frac{1}{\Pr(\mathcal{A}_\eta)} \int_0^\infty \int_{\mathcal{S}_z} \mathbb{E}[\|\mathbf{U} - \hat{\mathbf{U}}\|_2^2 \mid \mathcal{A}_\eta, \mathbf{N}_a = \mathbf{n}_a] \Pr(\mathcal{A}_\eta \mid \mathbf{N}_a = \mathbf{n}_a) f_{\mathbf{N}_a \mid Z}(\mathbf{n}_a \mid z) d\mathbf{n}_a f_Z(z) dz. \end{aligned} \quad (151)$$

Let us define

$$\mathcal{I}(z) \triangleq \int_{\mathcal{S}_z} \mathbb{E}[\|\mathbf{U} - \hat{\mathbf{U}}\|_2^2 \mid \mathcal{A}_\eta, \mathbf{N}_a = \mathbf{n}_a] \Pr(\mathcal{A}_\eta \mid \mathbf{N}_a = \mathbf{n}_a) f_{\mathbf{N}_a \mid Z}(\mathbf{n}_a \mid z) d\mathbf{n}_a. \quad (152)$$

Comparing (151) with (70), to prove Lemma 3, it is sufficient to derive the kernel function

$$\Psi_N(z) \triangleq 4\mathcal{I}(z). \quad (153)$$

Expanding the quadratic form of the estimation error for a fixed vector  $\mathbf{n}_a \in \mathcal{S}_z$ , we obtain

$$\mathbb{E}[\|\mathbf{U} - \hat{\mathbf{U}}\|_2^2 | \mathcal{A}_\eta, \mathbf{N}_a = \mathbf{n}_a] = \frac{1}{4} \left( \|\mathbf{n}_a\|_2^2 + 2\mathbf{n}_a^\top \mathbb{E}[\mathbf{N}_h | \mathcal{A}_\eta, \mathbf{N}_a = \mathbf{n}_a] + \mathbb{E}[\|\mathbf{N}_h\|_2^2 | \mathcal{A}_\eta, \mathbf{N}_a = \mathbf{n}_a] \right). \quad (154)$$

Note that  $\|\mathbf{n}_a\|_2^2 = z^2$  for every  $\mathbf{n}_a \in \mathcal{S}_z$ . However, we need to find  $f_{\mathbf{N}_h | \mathcal{A}_\eta, \mathbf{n}_a}(\mathbf{n}_h | \mathbf{n}_a)$  to further simplify  $\mathcal{I}(z)$ . In the following, we evaluate the term  $\mathcal{I}(z)$  for the following three cases, which are defined based on the overlap between honest noise ball  $\mathcal{R}_{\text{honest}} = \mathcal{B}_N(\Delta)$  and the acceptance region  $\mathcal{R}_{\text{acc}}(\mathbf{n}_a) = \mathcal{B}_N(\eta\Delta, \mathbf{n}_a)$ .

#### A. Case 1: Complete Containment ( $0 \leq z \leq (\eta - 1)\Delta$ )

In this regime, the magnitude of the adversarial noise  $z$  is sufficiently small that the support of the honest noise is entirely contained within the acceptance region, i.e.,  $\mathcal{R}_{\text{honest}} \subseteq \mathcal{R}_{\text{acc}}(\mathbf{n}_a)$ , for any adversarial vector  $\mathbf{n}_a$  with magnitude  $z$ . This implies that for any fixed  $\mathbf{n}_a$  with  $\|\mathbf{n}_a\|_2 = z \in [0, (\eta - 1)\Delta]$  we have

$$\Pr(\mathcal{A}_\eta | \mathbf{N}_a = \mathbf{n}_a) = \Pr(\mathcal{A}_\eta | \mathbf{N}_a = \mathbf{n}_a, \mathbf{N}_h = \mathbf{n}_h) = 1, \quad \forall \mathbf{n}_h \in \mathcal{B}_N(\Delta). \quad (155)$$

Therefore, we have

$$\begin{aligned} f_{\mathbf{N}_h | \mathcal{A}_\eta, \mathbf{N}_a}(\mathbf{n}_h | \mathbf{n}_a) &= \frac{\Pr(\mathcal{A}_\eta | \mathbf{N}_a = \mathbf{n}_a, \mathbf{N}_h = \mathbf{n}_h) f_{\mathbf{N}_h | \mathbf{N}_a}(\mathbf{n}_h | \mathbf{n}_a)}{\Pr(\mathcal{A}_\eta | \mathbf{N}_a = \mathbf{n}_a)} \\ &\stackrel{(a)}{=} \frac{\Pr(\mathcal{A}_\eta | \mathbf{N}_a = \mathbf{n}_a, \mathbf{N}_h = \mathbf{n}_h) f_{\mathbf{N}_h}(\mathbf{n}_h)}{\Pr(\mathcal{A}_\eta | \mathbf{N}_a = \mathbf{n}_a)} \\ &\stackrel{(b)}{=} \frac{1 \cdot f_{\mathbf{N}_h}(\mathbf{n}_h)}{1} = f_{\mathbf{N}_h}(\mathbf{n}_h), \end{aligned} \quad (156)$$

where (a) follows from the fact that the honest noise  $\mathbf{N}_h$  is generated independently of the adversarial noise  $\mathbf{N}_a$ , and (b) follows from the containment condition in (155). The identity in (156) demonstrates that the posterior distribution of  $\mathbf{N}_h$  remains a uniform distribution over the ball  $\mathcal{B}_N(\Delta)$ , i.e., conditioning on the acceptance event  $\mathcal{A}_\eta$  and the realization  $\mathbf{n}_a$  with  $\|\mathbf{n}_a\|_2 = z$  provides no additional information about the honest noise in this regime. Therefore, we can evaluate the terms in (154) as follows.

- **Second Moment of Honest Noise:** The expectation of the squared magnitude is calculated by integrating over the uniform ball  $\mathcal{B}_N(\Delta)$ . Using the result from Equation (263), we have

$$\mathbb{E}[\|\mathbf{N}_h\|_2^2 | \mathcal{A}_\eta, \mathbf{N}_a = \mathbf{n}_a] = \mathbb{E}[\|\mathbf{N}_h\|_2^2] = \frac{N}{N+2} \Delta^2. \quad (157)$$

- **Adversarial Magnitude:** For any point  $\mathbf{n}_a$  residing on the surface  $\mathcal{S}_z$ , the squared magnitude is constant by definition

$$\|\mathbf{n}_a\|_2^2 = z^2. \quad (158)$$

- **Cross Term (First Moment):** Since  $\mathbf{N}_h$  is uniformly distributed over the ball  $\mathcal{B}_N(\Delta)$ , which is centered at the origin, its expected value is the zero vector. Thus, the cross term vanishes

$$2\mathbf{n}_a^\top \mathbb{E}[\mathbf{N}_h \mid \mathcal{A}_\eta, \mathbf{N}_a = \mathbf{n}_a] = 2\mathbf{n}_a^\top \mathbb{E}[\mathbf{N}_h] = 2\mathbf{n}_a^\top \mathbf{0} = 0. \quad (159)$$

Substituting the results from (157), (158), and (159) back into (154), we find that for any  $\mathbf{n}_a \in \mathcal{S}_z$

$$\mathbb{E}[\|\mathbf{U} - \hat{\mathbf{U}}\|_2^2 \mid \mathcal{A}_\eta, \mathbf{N}_a = \mathbf{n}_a] = \frac{1}{4} \left( \frac{N}{N+2} \Delta^2 + z^2 \right). \quad (160)$$

Crucially, the expression in (160) depends only on the magnitude  $z$  and is invariant to the direction of  $\mathbf{n}_a$ . Hence, it can be moved out of the integral in the definition of  $\mathcal{I}(z)$ . Plugging (155) and (160) into the integral in (152)(151) we arrive at

$$\begin{aligned} \mathcal{I}(z) &= \frac{1}{4} \left( z^2 + \frac{N}{N+2} \Delta^2 \right) \int_{\mathcal{S}_z} f_{\mathbf{N}_a|Z}(\mathbf{n}_a|z) d\mathbf{n}_a \\ &\stackrel{(c)}{=} \frac{1}{4} \left( z^2 + \frac{N}{N+2} \Delta^2 \right), \end{aligned} \quad (161)$$

where (c) follows from the fact that the conditional PDF  $f_{\mathbf{N}_a|Z}(\mathbf{n}_a|z)$  must integrate to unity over its support  $\mathcal{S}_z$ . By substituting (161) into (153) and comparing the result to (71), we find that it matches the first branch of the piecewise function  $\Psi_N(z)$ .

### B. Case 2: Partial Overlap $((\eta - 1)\Delta < z < (\eta + 1)\Delta)$

In this regime, the magnitude of the adversarial noise  $z$  results in a partial intersection between the support of the honest noise and the acceptance region. Conditioned on  $\mathcal{A}_\eta$  and any fixed realization  $\mathbf{n}_a \in \mathcal{S}_z$  of the adversarial noise, the honest noise vector  $\mathbf{N}_h$  is constrained by two distinct geometric requirements: its prior support  $\mathcal{R}_{\text{honest}} = \mathcal{B}_N(\Delta)$  and the acceptance region  $\mathcal{R}_{\text{acc}}(\mathbf{n}_a) = \mathcal{B}_N(\eta\Delta, \mathbf{n}_a)$ . Hence, the posterior support of  $\mathbf{N}_h$  is determined by  $\mathcal{R}_{\text{lens}}(\mathbf{n}_a)$  (See Figure 13), where

$$\mathcal{R}_{\text{lens}}(\mathbf{n}_a) \triangleq \mathcal{R}_{\text{honest}} \cap \mathcal{R}_{\text{acc}}(\mathbf{n}_a) = \{\mathbf{n} \in \mathbb{R}^N \mid \|\mathbf{n}\|_2 \leq \Delta \text{ and } \|\mathbf{n} - \mathbf{n}_a\|_2 \leq \eta\Delta\}. \quad (162)$$

Based on the general formula for the intersection of two  $N$ -balls, the volume of this region is  $\mathcal{V}_{\text{lens}}(\Delta, \eta\Delta, z)$ , as defined in (141). Recall from (121) in the proof of Lemma 2, that

$$\Pr(\mathcal{A}_\eta \mid \mathbf{N}_a = \mathbf{n}_a) = \frac{\mathcal{V}_{\text{lens}}(\Delta, \eta\Delta, z)}{V_N(\Delta)}. \quad (163)$$

We now determine the posterior distribution of the honest noise  $\mathbf{N}_h$  conditioned on both the acceptance event  $\mathcal{A}_\eta$  and the fixed vector  $\mathbf{n}_a$ . Applying Bayes' theorem, we have

$$\begin{aligned}
f_{\mathbf{N}_h|\mathcal{A}_\eta, \mathbf{N}_a}(\mathbf{n}_h|\mathbf{n}_a) &= \frac{\Pr(\mathcal{A}_\eta | \mathbf{N}_h = \mathbf{n}_h, \mathbf{N}_a = \mathbf{n}_a) f_{\mathbf{N}_h|\mathbf{N}_a}(\mathbf{n}_h|\mathbf{n}_a)}{\Pr(\mathcal{A}_\eta | \mathbf{N}_a = \mathbf{n}_a)} \\
&\stackrel{(a)}{=} \frac{\Pr(\mathcal{A}_\eta | \mathbf{N}_h = \mathbf{n}_h, \mathbf{N}_a = \mathbf{n}_a) f_{\mathbf{N}_h}(\mathbf{n}_h)}{\Pr(\mathcal{A}_\eta | \mathbf{N}_a = \mathbf{n}_a)} \\
&\stackrel{(b)}{=} \frac{\mathbb{I}(\mathbf{n}_h \in \mathcal{R}_{\text{lens}}(\mathbf{n}_a)) \cdot \frac{1}{V_N(\Delta)}}{\mathcal{V}_{\text{lens}}(\Delta, \eta\Delta, z)/V_N(\Delta)} \\
&= \frac{1}{\mathcal{V}_{\text{lens}}(\Delta, \eta\Delta, z)} \mathbb{I}(\mathbf{n}_h \in \mathcal{R}_{\text{lens}}(\mathbf{n}_a)),
\end{aligned} \tag{164}$$

where (a) follows from the independence of  $\mathbf{N}_h$  and  $\mathbf{N}_a$ , and (b) follows from substituting (163), applying the uniform prior of  $\mathbf{N}_h$  over  $\mathcal{B}_N(\Delta)$ , and utilizing the geometric definition of the acceptance event for a fixed  $\mathbf{n}_a$ . This confirms that  $\mathbf{N}_h$  is uniformly distributed over the intersection region  $\mathcal{R}_{\text{lens}}(\mathbf{n}_a)$ .

Now, we are ready to evaluate the terms in (154). To this end, without loss of generality, we align  $\mathbf{n}_a$  with the first axis, i.e., we assume  $\mathbf{n}_a = [z, 0, \dots, 0]^\top$ . In this alignment, we have  $\mathbf{n}_a^\top \mathbf{N}_h = z n_{h,1}$ , where  $n_{h,1}$  is the first component of the honest noise vector. Substituting this into (154) leads to

$$\begin{aligned}
\mathbb{E}\left[\|\mathbf{U} - \hat{\mathbf{U}}\|_2^2 | \mathcal{A}_\eta, \mathbf{N}_a = \mathbf{n}_a\right] &= \frac{1}{4} \left( z^2 + 2z\mathbb{E}[n_{h,1} | \mathcal{A}_\eta, \mathbf{N}_a = \mathbf{n}_a] + \mathbb{E}\left[\|\mathbf{N}_h\|_2^2 | \mathcal{A}_\eta, \mathbf{N}_a = \mathbf{n}_a\right] \right) \\
&= \frac{1}{4} \left( z^2 + 2z \int_{\mathcal{B}_N(\Delta)} n_{h,1} f_{\mathbf{N}_h|\mathcal{A}_\eta, \mathbf{N}_a}(\mathbf{n}_h) d\mathbf{n}_h + \int_{\mathcal{B}_N(\Delta)} \|\mathbf{n}_h\|_2^2 f_{\mathbf{N}_h|\mathcal{A}_\eta, \mathbf{N}_a}(\mathbf{n}_h) d\mathbf{n}_h \right) \\
&\stackrel{(c)}{=} \frac{1}{4} \left( z^2 + 2z \int_{\mathcal{R}_{\text{lens}}(\mathbf{n}_a)} n_{h,1} \frac{1}{\mathcal{V}} d\mathbf{n}_h + \int_{\mathcal{R}_{\text{lens}}(\mathbf{n}_a)} \|\mathbf{n}_h\|_2^2 \frac{1}{\mathcal{V}} d\mathbf{n}_h \right) \\
&= \frac{1}{4\mathcal{V}} (z^2 \mathcal{V} + 2z I_1 + I_2),
\end{aligned} \tag{165}$$

where  $\mathcal{V} = \mathcal{V}_{\text{lens}}(\Delta, \eta\Delta, z)$ , and

$$I_1 = \int_{\mathcal{R}_{\text{lens}}(\mathbf{n}_a)} n_{h,1} d\mathbf{n}_h, \tag{166}$$

$$I_2 = \int_{\mathcal{R}_{\text{lens}}(\mathbf{n}_a)} \|\mathbf{n}_h\|_2^2 d\mathbf{n}_h. \tag{167}$$

Moreover, in (c) we replaced the conditional PDF of  $\mathbf{N}_h$  from (164).

Before calculating  $I_1$  and  $I_2$ , we analyze the geometry of the integration domain. As discussed in Appendix B-C, the integration domain  $\mathcal{R}_{\text{lens}}(\mathbf{n}_a)$  comprises of two hyperspherical caps, obtained by cutting the balls by the radical plane. More precisely, we have  $\mathcal{R}_{\text{lens}}(\mathbf{n}_a) = \mathcal{R}_1 \cup \mathcal{R}_2$ , where

$$\mathcal{R}_1 = \{\mathbf{r} \in \mathbb{R}^N \mid \|\mathbf{r}\|_2 \leq \Delta \text{ and } r_1 \geq u_c\}, \tag{168}$$

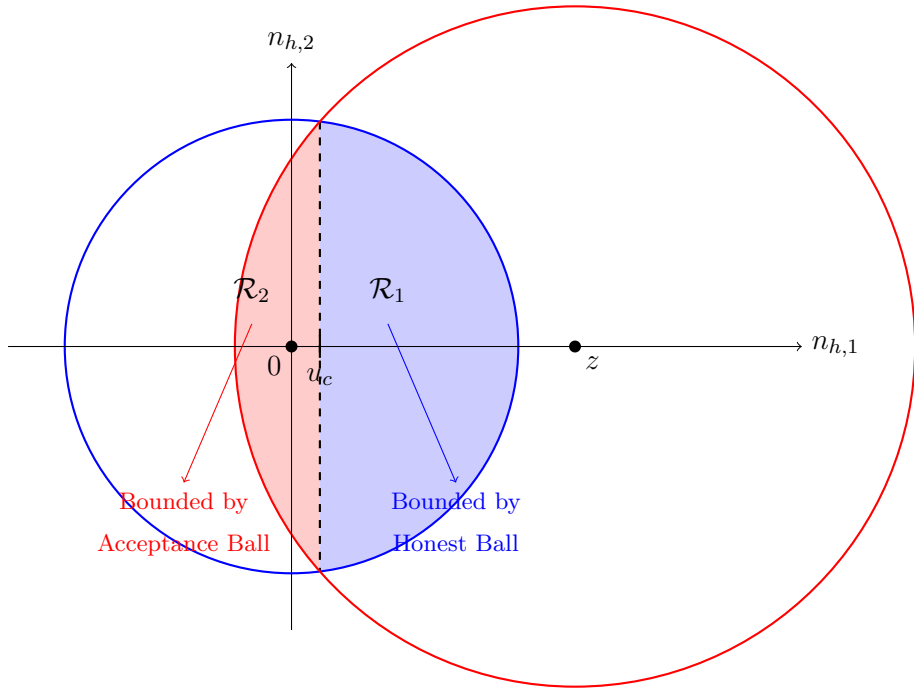


Fig. 13. Cross-sectional decomposition of the  $N$ -dimensional intersection region  $\mathcal{R}_{\text{lens}}(\mathbf{n}_a)$ . The vertical line at  $n_{h,1} = u_c$  represents the radical hyperplane, which divides the volume into standard cap  $\mathcal{R}_1$  and shifted cap  $\mathcal{R}_2$ .

and

$$\mathcal{R}_2 = \{\mathbf{r} \in \mathbb{R}^N \mid \|\mathbf{r} - \mathbf{n}_a\|_2 \leq \eta\Delta \text{ and } r_1 \leq u_c\}, \quad (169)$$

and the cutting point  $u_c$  is given by

$$u_c = \frac{z^2 + \Delta^2(1 - \eta^2)}{2z}. \quad (170)$$

Based on the definition of the hyperspherical cap volume in (146), the volume of  $\mathcal{R}_1$  is given by  $\mathcal{V}_1 = \mathcal{K}_N(\Delta, u_c)$ . Moreover,  $\mathcal{R}_2$  corresponds to a shifted, left-oriented cap. As established in the geometric analysis of Figure 20, the volume of  $\mathcal{R}_2$  is determined by the radius  $\eta\Delta$  and the distance from the center  $z - u_c$ . Thus, based on (146), the volume of  $\mathcal{R}_2$  is  $\mathcal{V}_2 = \mathcal{K}_N(\eta\Delta, z - u_c)$ .

Using this decomposition, we can rewrite the moment integrals  $I_1$  in (166) and  $I_2$  in (167) as follows

$$I_1 = \int_{\mathcal{R}_1} n_{h,1} d\mathbf{n}_h + \int_{\mathcal{R}_2} n_{h,1} d\mathbf{n}_h, \quad (171)$$

$$I_2 = \int_{\mathcal{R}_1} \|\mathbf{n}_h\|_2^2 d\mathbf{n}_h + \int_{\mathcal{R}_2} \|\mathbf{n}_h\|_2^2 d\mathbf{n}_h. \quad (172)$$

1) Calculation of  $I_1$ :

- For **Cap 1**, based on definition (216), we have

$$\int_{\mathcal{R}_1} n_{h,1} d\mathbf{n}_h = Q_N(\Delta, u_c). \quad (173)$$

- For **Cap 2**, based on (250), we have

$$\int_{\mathcal{R}_2} n_{h,1} d\mathbf{n}_h = -Q_N(\eta\Delta, z - u_c) + z\mathcal{V}_2. \quad (174)$$

It is important to note from (223) that  $Q_N(r, d)$  depends only on the intersection height  $h = \sqrt{r^2 - d^2}$ . Since both caps share the same intersection boundary (the  $(N - 1)$ -sphere of radius  $h$ ), we have  $Q_N(\Delta, u_c) = Q_N(\eta\Delta, z - u_c)$ . Thus, based on (171), (173), and (174), we have

$$I_1 = Q_N(\Delta, u_c) - Q_N(\eta\Delta, z - u_c) + z\mathcal{V}_2 = z\mathcal{V}_2. \quad (175)$$

2) *Calculation of  $I_2$ :*

- For **Cap 1**, based on definition (217), we have

$$\int_{\mathcal{R}_1} \|\mathbf{n}_h\|_2^2 d\mathbf{n}_h = J_N(\Delta, u_c). \quad (176)$$

- For **Cap 2**, based on (254), we have

$$\int_{\mathcal{R}_2} \|\mathbf{n}_h\|_2^2 d\mathbf{n}_h = J_N(\eta\Delta, z - u_c) - 2zQ_N(\eta\Delta, z - u_c) + z^2\mathcal{V}_2. \quad (177)$$

Thus, based on (172), (176), and (177), we have

$$I_2 = J_N(\Delta, u_c) + J_N(\eta\Delta, z - u_c) - 2zQ_N(\eta\Delta, z - u_c) + z^2\mathcal{V}_2. \quad (178)$$

Now based on (175), and (178), we evaluate the numerator of (165). Recall that  $I_1 = z\mathcal{V}_2$ , so the term  $2zI_1$  becomes  $2z^2\mathcal{V}_2$ . Expanding the total volume term as  $z^2\mathcal{V} = z^2\mathcal{V}_1 + z^2\mathcal{V}_2$ , the numerator of (165) becomes

$$\begin{aligned} \text{Numerator} &= (z^2\mathcal{V}_1 + z^2\mathcal{V}_2) + I_2 + 2z^2\mathcal{V}_2 \\ &= z^2\mathcal{V}_1 + 3z^2\mathcal{V}_2 + I_2. \end{aligned} \quad (179)$$

By substituting the explicit expression for  $I_2$  from (178), we have

$$\begin{aligned} \text{Numerator} &= z^2\mathcal{V}_1 + 3z^2\mathcal{V}_2 + \left[ J_N(\Delta, u_c) + J_N(\eta\Delta, z - u_c) - 2zQ_N(\eta\Delta, z - u_c) + z^2\mathcal{V}_2 \right] \\ &= \left[ J_N(\Delta, u_c) + z^2\mathcal{V}_1 \right] + \left[ J_N(\eta\Delta, z - u_c) + 4z^2\mathcal{V}_2 - 2zQ_N(\eta\Delta, z - u_c) \right]. \end{aligned} \quad (180)$$

We recognize this expression as the geometric kernel function for the lens intersection, denoted as

$$\Psi_N^{\text{lens}}(z) \triangleq \left[ J_N(\Delta, u_c) + z^2\mathcal{V}_1 \right] + \left[ J_N(\eta\Delta, z - u_c) + 4z^2\mathcal{V}_2 - 2zQ_N(\eta\Delta, z - u_c) \right]. \quad (181)$$

Thus, based on (165), we have

$$\mathbb{E} \left[ \|\mathbf{U} - \hat{\mathbf{U}}\|_2^2 \mid \mathcal{A}_\eta, \mathbf{N}_a = \mathbf{n}_a \right] = \frac{\Psi_N^{\text{lens}}(z)}{4\mathcal{V}_{\text{lens}}(\Delta, \eta\Delta, z)}. \quad (182)$$

We now return to the kernel term  $\mathcal{I}(z)$  defined in (152). By substituting (182) and (163) into (152), we obtain

$$\begin{aligned} \mathcal{I}(z) &= \int_{\mathcal{S}_z} \left( \frac{\Psi_N^{\text{lens}}(z)}{4\mathcal{V}_{\text{lens}}(\Delta, \eta\Delta, z)} \right) \left( \frac{\mathcal{V}_{\text{lens}}(\Delta, \eta\Delta, z)}{V_N(\Delta)} \right) f_{\mathbf{N}_a|Z}(\mathbf{n}_a|z) d\mathbf{n}_a \\ &= \frac{\Psi_N^{\text{lens}}(z)}{4V_N(\Delta)} \int_{\mathcal{S}_z} f_{\mathbf{N}_a|Z}(\mathbf{n}_a|z) d\mathbf{n}_a \\ &= \frac{\Psi_N^{\text{lens}}(z)}{4V_N(\Delta)}, \end{aligned} \quad (183)$$

where the last equality follows from the fact that the conditional density  $f_{\mathbf{N}_a|Z}(\mathbf{n}_a|z)$  integrates to unity over its support  $\mathcal{S}_z$ .

By substituting (183) into (153) and comparing the result to (71), we find that it matches the second branch of the piecewise function  $\Psi_N(z)$ .

### C. Case 3: No Intersection ( $z \geq (\eta + 1)\Delta$ )

In this final regime, based on (67), and given the condition for this case that  $z \geq (\eta + 1)\Delta$ , it follows that

$$\Pr(\mathcal{A}_\eta \mid Z = z) = 0. \quad (184)$$

Substituting this into the definition of the integral term  $\mathcal{I}(z)$  from (151), we obtain

$$\mathcal{I}(z) = \mathbb{E}[\|\mathbf{U} - \hat{\mathbf{U}}\|_2^2 \mid \mathcal{A}_\eta, Z = z] \cdot 0 = 0. \quad (185)$$

Based on the definition of (118), the result of (185) corresponds exactly to the third branch of the piecewise function  $\Psi_N(z)$  defined in (71). This completes the proof of Lemma 3.

## APPENDIX E PROOF OF LEMMA 4

To prove Lemma 4, we proceed in two steps. First, we show that any probability mass located in the region  $z > (\eta + 1)\Delta$  can be removed and redistributed to the other region, thereby increasing the probability of acceptance while maintaining the conditional MSE. Second, we show that any probability mass located in the region  $z < (\eta - 1)\Delta$  can be shifted to the point  $z = (\eta - 1)\Delta$  to increase the conditional MSE without affecting the probability of acceptance.

*Step 1: Removing mass from  $z > (\eta + 1)\Delta$*

Consider an initial noise distribution  $f_Z(z)$  and let

$$P_{\text{tail}} \triangleq \int_{(\eta+1)\Delta}^{\infty} f_Z(z) dz. \quad (186)$$

If  $P_{\text{tail}} = 0$ , the support is already bounded from above. Otherwise, as illustrated in Figure 14, assume that some mass exists beyond the acceptance boundary  $(\eta + 1)\Delta$ . According to (67) and (71), we have  $\Phi_N(z) = 0$  and  $\Psi_N(z) = 0$  for  $z \geq (\eta + 1)\Delta$ .

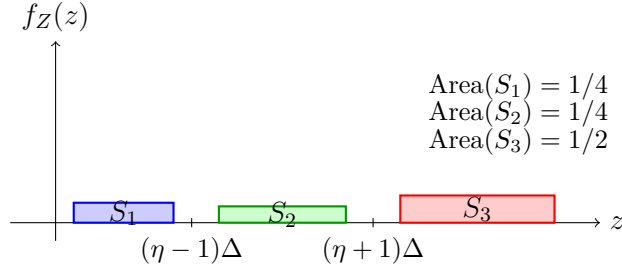


Fig. 14. Visualization of an initial adversarial noise density  $f_Z(z)$ . The total probability mass is partitioned into three regions:  $S_1$  (head),  $S_2$  (support), and  $S_3$  (tail), where the mass  $P_{\text{tail}} = \text{Area}(S_3)$  lies in the zero-acceptance region  $z > (\eta + 1)\Delta$ .

We define an intermediate distribution  $f_1(z)$  by truncating and normalizing  $f_Z(z)$ , as shown in Figure 15, where the remaining mass is scaled up to maintain a valid PDF:

$$f_1(z) = \begin{cases} \frac{f_Z(z)}{1-P_{\text{tail}}} & \text{if } z \leq (\eta + 1)\Delta, \\ 0 & \text{if } z > (\eta + 1)\Delta. \end{cases} \quad (187)$$

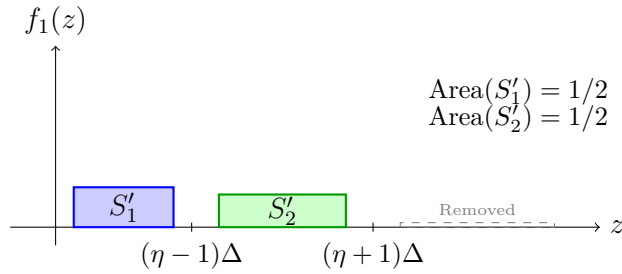


Fig. 15. Intermediate distribution  $f_1(z)$  following the truncation and renormalization process defined in (187). By removing the tail mass  $P_{\text{tail}}$  and scaling the remaining density, the probability of acceptance is increased according to (188) while the conditional MSE remains constant.

Using Lemma 2, the acceptance probability for  $f_1(z)$  is

$$\begin{aligned} \Pr(\mathcal{A}_\eta; f_1) &= \int_0^\infty \Phi_N(z) f_1(z) dz \\ &\stackrel{(a)}{=} \frac{1}{1 - P_{\text{tail}}} \int_0^{(\eta+1)\Delta} \Phi_N(z) f_Z(z) dz \\ &\stackrel{(b)}{=} \frac{1}{1 - P_{\text{tail}}} \int_0^\infty \Phi_N(z) f_Z(z) dz \\ &\stackrel{(c)}{=} \frac{1}{1 - P_{\text{tail}}} \Pr(\mathcal{A}_\eta; f_Z) \end{aligned} \quad (188)$$

$$\geq \Pr(\mathcal{A}_\eta; f_Z), \quad (189)$$

where (a) and (b) follows from (187) and the fact that  $\Phi_N(z) = 0$  for  $z > (\eta+1)\Delta$ , and (c) follows from Lemma 2. Thus, the acceptance probability increases (or stays the same if  $P_{\text{tail}} = 0$ ), satisfying the constraint more loosely.

Next, we check the conditional MSE, i.e.,  $\mathbb{E} [\|\mathbf{U} - \hat{\mathbf{U}}\|_2^2 | \mathcal{A}_\eta; f_1]$ , using Lemma 3. More precisely, we have

$$\begin{aligned} \mathbb{E} [\|\mathbf{U} - \hat{\mathbf{U}}\|_2^2 | \mathcal{A}_\eta; f_1] &= \frac{1}{4 \Pr(\mathcal{A}_\eta; f_1)} \int_0^\infty \Psi_N(z) f_1(z) dz \\ &\stackrel{(a)}{=} \frac{1 - P_{\text{tail}}}{4 \Pr(\mathcal{A}_\eta; f_Z)} \cdot \frac{1}{1 - P_{\text{tail}}} \int_0^{(\eta+1)\Delta} \Psi_N(z) f_Z(z) dz \\ &\stackrel{(b)}{=} \frac{1}{4 \Pr(\mathcal{A}_\eta; f_Z)} \int_0^\infty \Psi_N(z) f_Z(z) dz \\ &\stackrel{(c)}{=} \mathbb{E} [\|\mathbf{U} - \hat{\mathbf{U}}\|_2^2 | \mathcal{A}_\eta; f_Z], \end{aligned} \quad (190)$$

where (a) follows from (187), (188) and the fact that  $\Psi_N(z) = 0$  for  $z > (\eta+1)\Delta$ , (b) follows from fact that  $\Psi_N(z) = 0$  for  $z > (\eta+1)\Delta$ , and (c) follows from Lemma 2. Thus, removing the tail does not change the conditional MSE.

### Step 2: Shifting mass from $z < (\eta-1)\Delta$

Now consider the distribution  $f_1(z)$  from Step 1, which is supported on  $[0, (\eta+1)\Delta]$ . We construct the final distribution  $f_Z^*(z)$  by shifting all mass from  $[0, (\eta-1)\Delta]$  to a Dirac delta function at  $z = (\eta-1)\Delta$ , as illustrated in Figure 16. Let

$$P_{\text{head}} \triangleq \int_0^{(\eta-1)\Delta} f_1(z) dz. \quad (191)$$

We define

$$f_Z^*(z) = P_{\text{head}} \delta(z - (\eta-1)\Delta) + f_1(z) \mathbb{I}((\eta-1)\Delta \leq z \leq (\eta+1)\Delta). \quad (192)$$

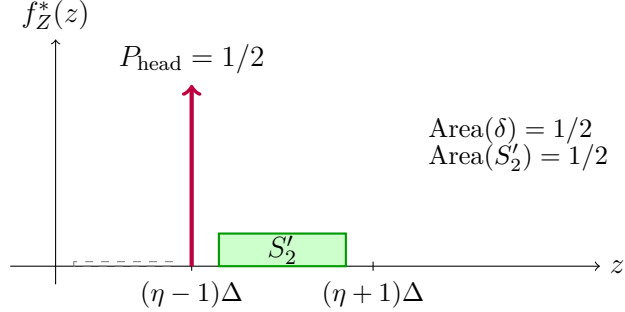


Fig. 16. Final optimal distribution  $f_Z^*(z)$  (illustrating the construction in (192)). All mass from the region  $z < (\eta-1)\Delta$  is concentrated at the boundary point  $(\eta-1)\Delta$ . This shift maximizes the conditional MSE, without decreasing the probability of acceptance.

First, we analyze the acceptance probability. We have

$$\begin{aligned}
 \Pr(\mathcal{A}_\eta; f_Z^*) &= \int_0^\infty \Phi_N(z) f_Z^*(z) dz \\
 &\stackrel{(a)}{=} P_{\text{head}} \Phi_N((\eta-1)\Delta) + \int_{(\eta-1)\Delta}^{(\eta+1)\Delta} \Phi_N(z) f_1(z) dz \\
 &\stackrel{(b)}{=} P_{\text{head}} \cdot 1 + \int_{(\eta-1)\Delta}^{(\eta+1)\Delta} \Phi_N(z) f_1(z) dz \\
 &\stackrel{(c)}{=} \int_0^{(\eta-1)\Delta} 1 \cdot f_1(z) dz + \int_{(\eta-1)\Delta}^{(\eta+1)\Delta} \Phi_N(z) f_1(z) dz \\
 &\stackrel{(d)}{=} \int_0^\infty \Phi_N(z) f_1(z) dz \\
 &= \Pr(\mathcal{A}_\eta; f_1),
 \end{aligned} \tag{193}$$

where (a) follows from the sifting property of the Dirac delta function,  $\int_0^\infty h(z) \delta(z - z_0) dz = h(z_0)$  for  $z_0 \geq 0$ , and the definition of  $f_Z^*(z)$  in (192); (b) follows from (67), which implies  $\Phi_N((\eta-1)\Delta) = 1$ ; (c) follows from the definition  $P_{\text{head}}$  in (191); and (d) follows from the fact that  $\Phi_N(z) = 1$  for  $0 \leq z \leq (\eta-1)\Delta$ , and  $\Phi_N(z) = 0$  for  $z > (\eta+1)\Delta$ , allowing us to combine the integration domains  $[0, (\eta-1)\Delta]$  and  $[(\eta-1)\Delta, \infty)$  back into  $[0, \infty)$ . Thus, the acceptance probability remains unchanged.

Next, we examine the conditional MSE. Note that based on Lemma 3, we have

$$\mathbb{E} \left[ \|\mathbf{U} - \hat{\mathbf{U}}\|_2^2 \mid \mathcal{A}_\eta; f_Z^* \right] = \frac{\int_0^\infty \Psi_N(z) f_Z^*(z) dz}{4 \Pr(\mathcal{A}_\eta; f_Z^*)}. \tag{194}$$

From the previous step, we established that the probability of acceptance remains unchanged, i.e.,  $\Pr(\mathcal{A}_\eta; f_Z^*) = \Pr(\mathcal{A}_\eta; f_1)$ . Thus, comparing the MSEs reduces to comparing the numerators. We

analyze the numerator for  $f_Z^*$ , as follows

$$\begin{aligned}
\int_0^\infty \Psi_N(z) f_Z^*(z) dz &\stackrel{(a)}{=} P_{\text{head}} \Psi_N((\eta-1)\Delta) + \int_{(\eta-1)\Delta}^{(\eta+1)\Delta} \Psi_N(z) f_1(z) dz \\
&\stackrel{(b)}{=} \Psi_N((\eta-1)\Delta) \left( \int_0^{(\eta-1)\Delta} f_1(z) dz \right) + \int_{(\eta-1)\Delta}^{(\eta+1)\Delta} \Psi_N(z) f_1(z) dz \\
&\stackrel{(c)}{\geq} \int_0^{(\eta-1)\Delta} \Psi_N(z) f_1(z) dz + \int_{(\eta-1)\Delta}^{(\eta+1)\Delta} \Psi_N(z) f_1(z) dz \\
&\stackrel{(d)}{=} \int_0^\infty \Psi_N(z) f_1(z) dz,
\end{aligned} \tag{195}$$

where (a) follows from the definition of  $f_Z^*$  and the sifting property of the Dirac delta,  $\int_0^\infty h(z) \delta(z - z_0) dz = h(z_0)$  for  $z_0 \geq 0$ ; (b) substitutes the definition of  $P_{\text{head}}$ ; (c) follows from the fact that  $\Psi_N(z) = z^2 + \frac{N}{N+2} \Delta^2$  is strictly increasing for  $z \geq 0$ , which implies  $\Psi_N((\eta-1)\Delta) \geq \Psi_N(z)$  for all  $z \in [0, (\eta-1)\Delta]$ ; and (d) follows from combining the integrals over  $[0, (\eta+1)\Delta]$  and the fact that, based on Lemma 3 (specifically Eq. (71)),  $\Psi_N(z) = 0$  for  $z > (\eta+1)\Delta$ , which allows extending the upper limit of integration to  $\infty$ .

Now based on Lemma 3, we have

$$\begin{aligned}
\mathbb{E} \left[ \|\mathbf{U} - \hat{\mathbf{U}}\|_2^2 \mid \mathcal{A}_\eta; f_Z^* \right] &= \frac{\int_0^\infty \Psi_N(z) f_Z^*(z) dz}{4 \Pr(\mathcal{A}_\eta; f_Z^*)} \\
&\stackrel{(a)}{\geq} \frac{\int_0^\infty \Psi_N(z) f_1(z) dz}{4 \Pr(\mathcal{A}_\eta; f_1)} \\
&= \mathbb{E} \left[ \|\mathbf{U} - \hat{\mathbf{U}}\|_2^2 \mid \mathcal{A}_\eta; f_1 \right] \\
&\stackrel{(b)}{=} \mathbb{E} \left[ \|\mathbf{U} - \hat{\mathbf{U}}\|_2^2 \mid \mathcal{A}_\eta; f_Z \right],
\end{aligned} \tag{196}$$

where (a) follows from (195), and (b) follows from (190). This completes the proof.

## APPENDIX F

### PROOF OF LEMMA 5

Let  $f_{Z,1}(z)$  be the probability density function of the adversarial noise magnitude satisfying the support condition defined in Lemma 4 (i.e., its support is contained within  $[(\eta-1)\Delta, (\eta+1)\Delta]$ ). Let its acceptance probability be  $\Pr(\mathcal{A}_\eta; f_{Z,1}) = \alpha_1$ , where  $\alpha_1 > \alpha$ . The initial state of this distribution is visualized in Figure 17.

We construct a new noise magnitude PDF,  $f_{Z,2}(z)$  as follows

$$f_{Z,2}(z) = \begin{cases} \frac{\alpha}{\alpha_1} f_{Z,1}(z) & \text{if } 0 \leq z \leq (\eta+1)\Delta, \\ \left(1 - \frac{\alpha}{\alpha_1}\right) \delta(z - z_{\text{out}}) & \text{if } z = z_{\text{out}}, \\ 0 & \text{otherwise,} \end{cases} \tag{197}$$

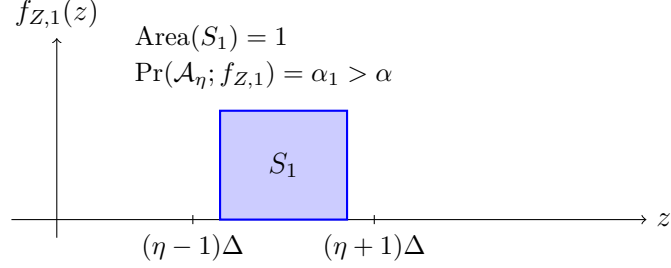


Fig. 17. The initial noise distribution  $f_{Z,1}(z)$  supported entirely within the acceptance region. In this example,  $\alpha_1$  is higher than the target acceptance probability  $\alpha$ .

where  $z_{\text{out}} = (\eta + 2)\Delta$ . The adjustment process is shown in Figure 18, where the valid mass is reduced and the remainder is moved to a zero-acceptance point.

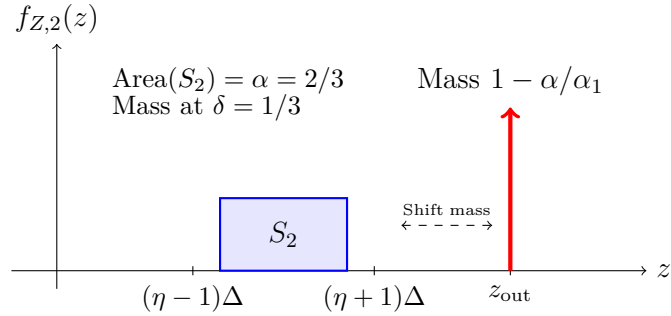


Fig. 18. The adjusted distribution  $f_{Z,2}(z)$ . The original mass is scaled down to exactly  $\alpha$  (e.g.,  $2/3$ ). The discarded mass (e.g.,  $1/3$ ) is concentrated into a Dirac delta at  $z_{\text{out}}$ , ensuring the total integral is 1 while the acceptance probability is exactly  $\alpha$ .

First, we calculate the probability of acceptance for the new distribution using (66). Noting that  $\Phi_N(z_{\text{out}}) = 0$ , we have

$$\begin{aligned}
 \Pr(\mathcal{A}_{\eta}; f_{Z,2}) &= \int_0^{\infty} \Phi_N(z) f_{Z,2}(z) dz \\
 &= \int_0^{(\eta+1)\Delta} \Phi_N(z) \left( \frac{\alpha}{\alpha_1} f_{Z,1}(z) \right) dz + \Phi_N(z_{\text{out}}) \left( 1 - \frac{\alpha}{\alpha_1} \right) \\
 &= \frac{\alpha}{\alpha_1} \underbrace{\int_0^{(\eta+1)\Delta} \Phi_N(z) f_{Z,1}(z) dz}_{\Pr(\mathcal{A}_{\eta}; f_{Z,1}) = \alpha_1} + 0 \\
 &= \frac{\alpha}{\alpha_1} (\alpha_1) = \alpha.
 \end{aligned} \tag{198}$$

Thus, the new noise magnitude PDF satisfies the equality constraint exactly.

Next, we evaluate the conditional MSE using (70). We observe that the weighting function  $\Psi_N(z)$ , defined in (71), is also zero for  $z \geq (\eta + 1)\Delta$ . Therefore,  $\Psi_N(z_{\text{out}}) = 0$ . Thus, we have

$$\begin{aligned} \int_0^\infty \Psi_N(z) f_{Z,2}(z) dz &= \int_0^{(\eta+1)\Delta} \Psi_N(z) \left( \frac{\alpha}{\alpha_1} f_{Z,1}(z) \right) dz + \Psi_N(z_{\text{out}}) \left( 1 - \frac{\alpha}{\alpha_1} \right) \\ &= \frac{\alpha}{\alpha_1} \int_0^{(\eta+1)\Delta} \Psi_N(z) f_{Z,1}(z) dz. \end{aligned} \quad (199)$$

Substituting this into the conditional MSE formula (70) yields

$$\begin{aligned} \mathbb{E} \left[ \|\mathbf{U} - \hat{\mathbf{U}}\|_2^2 \mid \mathcal{A}_\eta; f_{Z,2} \right] &= \frac{1}{4 \Pr(\mathcal{A}_\eta; f_{Z,2})} \int_0^\infty \Psi_N(z) f_{Z,2}(z) dz \\ &= \frac{1}{4\alpha} \left( \frac{\alpha}{\alpha_1} \int_0^{(\eta+1)\Delta} \Psi_N(z) f_{Z,1}(z) dz \right) \\ &= \frac{1}{4\alpha_1} \int_0^\infty \Psi_N(z) f_{Z,1}(z) dz \\ &= \frac{1}{4 \Pr(\mathcal{A}_\eta; f_{Z,1})} \int_0^\infty \Psi_N(z) f_{Z,1}(z) dz \\ &= \mathbb{E} \left[ \|\mathbf{U} - \hat{\mathbf{U}}\|_2^2 \mid \mathcal{A}_\eta; f_{Z,1} \right]. \end{aligned} \quad (200)$$

This completes the proof of the lemma.

## APPENDIX G

### EVALUATION OF THE GAME FOR THE TWO-DIMENSIONAL CASE ( $N = 2$ )

In this section, we evaluate the general results established in Theorem 2 for the specific case of  $N = 2$ . Note that based on (1), we have  $\Gamma(2) = 1$ , and thus based on (3) we have

$$V_2(r) = \frac{\pi^{2/2} r^2}{\Gamma(1 + 2/2)} = \frac{\pi r^2}{\Gamma(2)} = \pi r^2. \quad (201)$$

Next, we evaluate the kernel function  $\mathcal{K}_N(r, c)$ . Recalling the definition in (26), we have

$$\mathcal{K}_N(r, c) = \frac{\pi^{(N-1)/2} r^N}{\Gamma(\frac{N+1}{2})} \int_{c/r}^1 (1 - t^2)^{\frac{N-1}{2}} dt. \quad (202)$$

Substituting  $N = 2$ , the coefficient depends on  $\Gamma(3/2)$ . Using the definition of the Gamma function in (1), we have  $\Gamma(1.5) = \frac{\sqrt{\pi}}{2}$ . Consequently, the coefficient simplifies to

$$\frac{\pi^{(2-1)/2} r^2}{\Gamma(\frac{2+1}{2})} = \frac{\sqrt{\pi} r^2}{\sqrt{\pi}/2} = 2r^2. \quad (203)$$

Thus, the kernel expression becomes

$$\mathcal{K}_2(r, c) = 2r^2 \int_{c/r}^1 \sqrt{1 - t^2} dt. \quad (204)$$

We compute the integral in (204) using the standard substitution  $t = \sin \theta$ , which yields

$$\int \sqrt{1 - t^2} dt = \frac{1}{2} \left( t \sqrt{1 - t^2} + \arcsin(t) \right). \quad (205)$$

Evaluating this from  $c/r$  to 1, and using the identity  $\frac{\pi}{2} - \arcsin(x) = \arccos(x)$ , we obtain

$$\begin{aligned}\mathcal{K}_2(r, c) &= 2r^2 \left[ \frac{\pi}{4} - \frac{1}{2} \left( \frac{c}{r} \sqrt{1 - \frac{c^2}{r^2}} + \arcsin \left( \frac{c}{r} \right) \right) \right] \\ &= r^2 \arccos \left( \frac{c}{r} \right) - c \sqrt{r^2 - c^2}.\end{aligned}\quad (206)$$

With the explicit form of  $\mathcal{K}_2(r, c)$  established in (206), we proceed to evaluate  $\Phi_2(z)$ . First, recalling the definition of the intersection volume in (25), for  $N = 2$  we have

$$\mathcal{V}_{\text{lens}}(\Delta, \eta\Delta, z) = \mathcal{K}_2(\Delta, u_c(z)) + \mathcal{K}_2(\eta\Delta, z - u_c(z)), \quad (207)$$

where  $u_c(z)$  is defined in (27) as

$$u_c(z) = \frac{z^2 + \Delta^2(1 - \eta^2)}{2z}. \quad (208)$$

Next, substituting this into the definition of  $\Phi_N(z)$  in (24), and using the volume  $V_2(\Delta) = \pi\Delta^2$  derived in (201), we obtain

$$\begin{aligned}\Phi_2(z) &= \frac{1}{\pi\Delta^2} \left[ \left( \Delta^2 \arccos \left( \frac{u_c(z)}{\Delta} \right) - u_c(z) \sqrt{\Delta^2 - u_c(z)^2} \right) \right. \\ &\quad \left. + \left( \eta^2 \Delta^2 \arccos \left( \frac{z - u_c(z)}{\eta\Delta} \right) - (z - u_c(z)) \sqrt{\eta^2 \Delta^2 - (z - u_c(z))^2} \right) \right].\end{aligned}\quad (209)$$

Next, we determine the auxiliary functions  $Q_2(r, d)$  and  $J_2(r, d)$ . Specifically, using  $V_1(\rho) = 2\rho$  in (31) with  $N = 2$  yields

$$Q_2(r, d) = \frac{r^2 - d^2}{3} \cdot 2\sqrt{r^2 - d^2} = \frac{2}{3} (r^2 - d^2)^{3/2}. \quad (210)$$

For  $J_2(r, d)$ , substituting  $N = 2$  into (32) gives

$$J_2(r, d) = \frac{1}{2} r^2 \mathcal{K}_2(r, d) + \frac{1}{2} d Q_2(r, d). \quad (211)$$

We now calculate the terms required for  $\Psi_2(z)$ , defined in (28). Note that, based on (29) and (30), we have  $\mathcal{V}_1 = \mathcal{K}_2(\Delta, u_c(z))$  and  $\mathcal{V}_2 = \mathcal{K}_2(\eta\Delta, z - u_c(z))$ . We define  $T_1$  as the first term in the numerator of (28)

$$\begin{aligned}T_1 &\triangleq J_2(\Delta, u_c(z)) + z^2 \mathcal{V}_1 \\ &\stackrel{(a)}{=} \left( \frac{1}{2} \Delta^2 \mathcal{V}_1 + \frac{1}{2} u_c(z) Q_2(\Delta, u_c(z)) \right) + z^2 \mathcal{V}_1 \\ &= \left( \frac{\Delta^2}{2} + z^2 \right) \mathcal{V}_1 + \frac{u_c(z)}{2} Q_2(\Delta, u_c(z)),\end{aligned}\quad (212)$$

where (a) follows from substituting (211) and using the definition of  $\mathcal{V}_1$ . Similarly, we define  $T_2$  as the second term in the numerator of (28)

$$\begin{aligned}
T_2 &\triangleq J_2(\eta\Delta, z - u_c(z)) + 4z^2\mathcal{V}_2 - 2zQ_2(\eta\Delta, z - u_c(z)) \\
&\stackrel{(b)}{=} \left[ \frac{1}{2}\eta^2\Delta^2\mathcal{V}_2 + \frac{1}{2}(z - u_c(z))Q_2(\eta\Delta, z - u_c(z)) \right] \\
&\quad + 4z^2\mathcal{V}_2 - 2zQ_2(\eta\Delta, z - u_c(z)) \\
&= \left( \frac{\eta^2\Delta^2}{2} + 4z^2 \right) \mathcal{V}_2 - \frac{3z + u_c(z)}{2} Q_2(\eta\Delta, z - u_c(z)),
\end{aligned} \tag{213}$$

where (b) follows from substituting (211) and using the definition of  $\mathcal{V}_2$ . Finally, combining  $T_1$  and  $T_2$  and dividing by  $V_2(\Delta) = \pi\Delta^2$  results in the complete expression

$$\begin{aligned}
\Psi_2(z) &= \frac{1}{\pi\Delta^2} \left[ \left( \frac{\Delta^2}{2} + z^2 \right) \mathcal{K}_2(\Delta, u_c(z)) + \left( \frac{\eta^2\Delta^2}{2} + 4z^2 \right) \mathcal{K}_2(\eta\Delta, z - u_c(z)) \right. \\
&\quad \left. + \frac{u_c(z)}{2} Q_2(\Delta, u_c(z)) - \frac{3z + u_c(z)}{2} Q_2(\eta\Delta, z - u_c(z)) \right],
\end{aligned} \tag{214}$$

where  $Q_2$  is given by (210) and  $\mathcal{K}_2$  by (206).

With the explicit expressions for  $\Phi_2(z)$  and  $\Psi_2(z)$  established in (209) and (214), we have fully characterized all the underlying functions required by Theorem 2. While the presence of transcendental terms in  $\Phi_2(z)$  prevents an analytical derivation of the inverse function, the function  $c_\eta(\alpha)$  defined in (22) can be evaluated by applying the numerical procedure described in Remark 2 to these specific 2D case.

## APPENDIX H

### DERIVATION OF GEOMETRIC MOMENTS FOR HYPERSPHERICAL CAPS

We consider the  $N$ -dimensional Euclidean space  $\mathbb{R}^N$  with coordinates  $\mathbf{x} = (x_1, \dots, x_N)$ . Let  $\mathcal{B}_N(r)$  be an  $N$ -ball of radius  $r$  centered at the origin. We recall the definition of the **hyperspherical cap** previously established in (142), as

$$\mathcal{C}_N(r, c) \triangleq \{(x_1, x_2, \dots, x_N) \in \mathbb{R}^N : x_1^2 + x_2^2 + \dots + x_N^2 \leq r^2, x_1 \geq c\}. \tag{215}$$

Specifically, this region is bounded by the spherical surface of radius  $r$  and a hyperplane located at  $x_1 = c$ .

The objective is to derive analytical expressions for two geometric moments of the cap  $\mathcal{C}_N(r, c)$  as functions of the radius  $r$  and the cut location  $c$ . The first moment  $Q_N$ , representing the integral of the first coordinate over the cap volume, is defined as

$$Q_N(r, c) \triangleq \int_{\mathcal{C}_N(r, c)} x_1 dV, \tag{216}$$

and the second moment  $J_N$ , representing the integral of the squared norm over the cap volume, is defined as

$$J_N(r, c) \triangleq \int_{\mathcal{C}_N(r, c)} \|\mathbf{x}\|_2^2 dV. \quad (217)$$

To evaluate these integrals, we utilize the property that a hyperspherical cap can be viewed as a stack of  $(N-1)$ -dimensional balls. For a fixed  $x_1 \in [c, r]$ , the cross-section of the cap is an  $(N-1)$ -ball with radius  $\rho(x_1) = \sqrt{r^2 - x_1^2}$ . The volume of this  $(N-1)$ -ball is given by  $V_{N-1}(\sqrt{r^2 - x_1^2})$ .

#### A. Calculation of the First Moment $Q_N(r, c)$

To evaluate the first moment  $Q_N(r, c)$ , we employ the method of integration by slices perpendicular to the principal axis  $x_1$ , as illustrated in Figure 19. Note that the cross-sectional slice at position  $x_1$  represents the intersection of the  $N$ -ball with the hyperplane, forming an  $(N-1)$ -dimensional ball with radius  $\rho(x_1) = \sqrt{r^2 - x_1^2}$ . Consequently, the differential volume of this slice is given by

$$dV = V_{N-1}(\rho(x_1)) dx_1 = V_{N-1}\left(\sqrt{r^2 - x_1^2}\right) dx_1. \quad (218)$$

The total first moment is obtained by integrating the product of the position  $x_1$  and the differential volume  $dV$  across the extent of the cap from the cut at  $x_1 = c$  to the boundary at  $x_1 = r$ , yielding

$$Q_N(r, c) = \int_c^r x_1 V_{N-1}\left(\sqrt{r^2 - x_1^2}\right) dx_1. \quad (219)$$

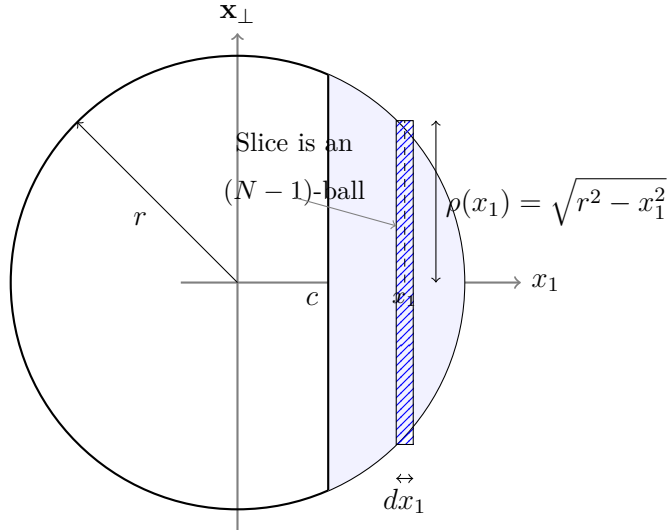


Fig. 19. Integration setup for the  $N$ -dimensional first moment. The cap is decomposed into infinitesimal slices perpendicular to the  $x_1$ -axis. Each slice at position  $x_1$  is an  $(N-1)$ -dimensional ball of radius  $\rho(x_1)$ , with volume  $V_{N-1}(\rho(x_1))dx_1$ .

Recall that the volume of an  $(N-1)$ -ball is given by  $V_{N-1}(r) = C_{N-1}r^{N-1}$  where  $C_{N-1} = \frac{\pi^{(N-1)/2}}{\Gamma(\frac{N+1}{2})}$ .

Thus, we can rewrite (219) as

$$Q_N(r, c) = C_{N-1} \int_c^r x_1 (r^2 - x_1^2)^{\frac{N-1}{2}} dx_1. \quad (220)$$

By employing the substitution  $v = r^2 - x_1^2$ , which implies  $x_1 dx_1 = -\frac{1}{2}dv$ , and observing that the integration limits transform to  $v = r^2 - c^2$  (denoted as the squared intersection height  $h^2$ ) and  $v = 0$ , we obtain

$$Q_N(r, c) = \frac{C_{N-1}}{2} \int_0^{h^2} v^{\frac{N-1}{2}} dv. \quad (221)$$

Evaluating this integral leads to

$$Q_N(r, c) = \frac{C_{N-1}}{2} \left[ \frac{2}{N+1} v^{\frac{N+1}{2}} \right]_0^{h^2} = \frac{C_{N-1}}{N+1} h^{N+1}. \quad (222)$$

Finally, by recognizing that  $V_{N-1}(h) = C_{N-1}h^{N-1}$ , we arrive at the analytical expression

$$Q_N(r, c) = \frac{h^2}{N+1} V_{N-1}(h), \quad (223)$$

where  $h = \sqrt{r^2 - c^2}$ .

### B. Calculation of the Second Moment $J_N(r, c)$

To calculate the second moment  $J_N(r, c)$ , defined in (217), we employ the same slice-based integration method used for the first moment (see Figure 19). Recall that any vector  $\mathbf{x} \in \mathcal{C}_N(r, c)$  can be decomposed into a component along the principal axis ( $x_1$ ) and a component perpendicular to it ( $\mathbf{x}_\perp$ ), such that  $\mathbf{x} = (x_1, \mathbf{x}_\perp)$ , where  $\mathbf{x}_\perp = (x_2, \dots, x_N) \in \mathbb{R}^{N-1}$ . Consequently, the squared Euclidean norm decomposes as  $\|\mathbf{x}\|_2^2 = x_1^2 + \|\mathbf{x}_\perp\|_2^2$ . Substituting this decomposition into the volume integral for the second moment yields

$$J_N(r, c) = \int_{\mathcal{C}_N(r, c)} (x_1^2 + \|\mathbf{x}_\perp\|_2^2) dV. \quad (224)$$

We evaluate this integral by summing the contributions of infinitesimal slices located at position  $x_1$  with thickness  $dx_1$ . Let  $\mathcal{S}_{x_1}$  denote the cross-sectional slice at position  $x_1$ . Geometrically,  $\mathcal{S}_{x_1}$  is an  $(N-1)$ -dimensional ball with radius  $\rho(x_1) = \sqrt{r^2 - x_1^2}$ , and its volume is given by  $\text{Vol}(\mathcal{S}_{x_1}) = V_{N-1}(\rho(x_1))$ . We can write the total integral  $J_N(r, c)$  as a nested integral: an external integral over the scalar variable  $x_1$  ranging from the cut  $c$  to the radius  $r$ , and an internal integral over the vector variable  $\mathbf{x}_\perp$  spanning the slice  $\mathcal{S}_{x_1}$ . More precisely, we have

$$J_N(r, c) = \int_c^r \left[ \int_{\mathcal{S}_{x_1}} (x_1^2 + \|\mathbf{x}_\perp\|_2^2) d\mathbf{x}_\perp \right] dx_1. \quad (225)$$

We now focus on evaluating the term inside the brackets in (225). By linearity, we split this internal integral into an axial component and a perpendicular component. For the axial component, since  $x_1$  is constant with respect to  $\mathbf{x}_\perp$ , we have

$$\int_{\mathcal{S}_{x_1}} x_1^2 d\mathbf{x}_\perp = x_1^2 \int_{\mathcal{S}_{x_1}} 1 d\mathbf{x}_\perp = x_1^2 \text{Vol}(\mathcal{S}_{x_1}) = x_1^2 V_{N-1}(\rho(x_1)). \quad (226)$$

For the perpendicular component, the integral  $\int_{\mathcal{S}_{x_1}} \|\mathbf{x}_\perp\|_2^2 d\mathbf{x}_\perp$  represents the second moment of the slice  $\mathcal{S}_{x_1}$  about its own center. Since  $\mathcal{S}_{x_1}$  is a ball of dimension  $k = N - 1$  with radius  $a = \rho(x_1)$ , we can directly apply the general formula derived in (263),  $M_2(k, a) = \frac{k}{k+2} a^2 V_k(a)$ . Substituting  $k = N - 1$  and  $a = \rho(x_1)$ , we obtain

$$\begin{aligned} \int_{\mathcal{S}_{x_1}} \|\mathbf{x}_\perp\|_2^2 d\mathbf{x}_\perp &= \frac{N-1}{(N-1)+2} \rho(x_1)^2 V_{N-1}(\rho(x_1)) \\ &= \frac{N-1}{N+1} (r^2 - x_1^2) V_{N-1}(\rho(x_1)). \end{aligned} \quad (227)$$

Substituting (226) and (227) back into (225), the integral becomes

$$J_N(r, c) = \int_c^r \left[ x_1^2 V_{N-1}(\rho(x_1)) + \frac{N-1}{N+1} (r^2 - x_1^2) V_{N-1}(\rho(x_1)) \right] dx_1. \quad (228)$$

Simplifying the term in the brackets, the integral splits into two distinct terms

$$J_N(r, c) = \frac{N-1}{N+1} r^2 \int_c^r V_{N-1}(\rho(x_1)) dx_1 + \underbrace{\frac{2}{N+1} \int_c^r x_1^2 V_{N-1}(\rho(x_1)) dx_1}_{I_{x^2}}. \quad (229)$$

Note that, based on the definition, the term  $\int_c^r V_{N-1}(\rho(x_1)) dx_1$  is indeed the volume of the cap, which has been derived in (146), and denoted by  $\mathcal{K}_N(r, c)$ . Thus, we have

$$\int_c^r V_{N-1}(\rho(x_1)) dx_1 = \mathcal{K}_N(r, c). \quad (230)$$

Next, to evaluate  $I_{x^2}$ , defined in (229), we employ the method of integration by parts. The fundamental formula for this technique is given by

$$\int_a^b u dv = [uv]_a^b - \int_a^b v du. \quad (231)$$

We select  $u = x_1$ , and  $dv = x_1 V_{N-1}(\rho(x_1)) dx_1$ , in (231). To find the function  $v$ , we must integrate the expression for  $dv$ . First, we write out the volume term using the formula  $V_{N-1}(a) = C_{N-1} a^{N-1}$ , which yields

$$dv = x_1 \cdot C_{N-1} \left( \sqrt{r^2 - x_1^2} \right)^{N-1} dx_1 = C_{N-1} x_1 (r^2 - x_1^2)^{\frac{N-1}{2}} dx_1. \quad (232)$$

To integrate this, we use the substitution  $w = r^2 - x_1^2$ . Substituting this into the integral for  $v$ , we obtain

$$\begin{aligned}
v &= \int C_{N-1}(w)^{\frac{N-1}{2}} \left( -\frac{1}{2} dw \right) \\
&= -\frac{C_{N-1}}{2} \int w^{\frac{N-1}{2}} dw \\
&= -\frac{C_{N-1}}{2} \left[ \frac{2}{N+1} w^{\frac{N+1}{2}} \right] \\
&= -\frac{C_{N-1}}{N+1} w^{\frac{N+1}{2}}.
\end{aligned} \tag{233}$$

Substituting  $w = r^2 - x_1^2$  back into the expression, and recalling that  $\sqrt{r^2 - x_1^2} = \rho(x_1)$ , we have  $v = -\frac{C_{N-1}}{N+1} \rho(x_1)^{N+1}$ . Since  $V_{N-1}(\rho) = C_{N-1} \rho^{N-1}$ , we have

$$v = -\frac{1}{N+1} \rho(x_1)^2 \left( C_{N-1} \rho(x_1)^{N-1} \right) = -\frac{1}{N+1} \rho(x_1)^2 V_{N-1}(\rho(x_1)). \tag{234}$$

Now that we have explicitly determined  $u$ ,  $du$ , and  $v$ , we substitute them into (231), which leads to

$$I_{x^2} = \left[ -\frac{x_1}{N+1} \rho(x_1)^2 V_{N-1}(\rho(x_1)) \right]_c^r - \int_c^r \left( -\frac{1}{N+1} \rho(x_1)^2 V_{N-1}(\rho(x_1)) \right) dx_1. \tag{235}$$

We evaluate the two parts of this equation separately. First, we analyze the boundary term in (235). At the upper limit  $x_1 = r$ , the slice radius is  $\rho(r) = \sqrt{r^2 - r^2} = 0$ . Since the volume  $V_{N-1}(0) = 0$ , the upper limit contribution is zero. At the lower limit  $x_1 = c$ , the slice radius is the intersection height  $h = \rho(c) = \sqrt{r^2 - c^2}$ . Thus, the evaluation yields

$$\begin{aligned}
\left[ -\frac{x_1}{N+1} \rho(x_1)^2 V_{N-1}(\rho(x_1)) \right]_c^r &= 0 - \left( -\frac{c}{N+1} \rho(c)^2 V_{N-1}(\rho(c)) \right) \\
&= \frac{c}{N+1} h^2 V_{N-1}(h).
\end{aligned} \tag{236}$$

We observe that this expression matches the formula for the first moment derived in Equation (223), where  $Q_N(r, c) = \frac{h^2}{N+1} V_{N-1}(h)$ . Therefore, the boundary term simplifies directly to

$$\left[ -\frac{x_1}{N+1} \rho(x_1)^2 V_{N-1}(\rho(x_1)) \right]_c^r = c Q_N(r, c). \tag{237}$$

Next, we analyze the integral term in (235). We substitute  $\rho(x_1)^2 = r^2 - x_1^2$  into the integrand, which leads to

$$\begin{aligned}
-\int_c^r v du &= \int_c^r \frac{1}{N+1} (r^2 - x_1^2) V_{N-1}(\rho(x_1)) dx_1 \\
&= \frac{1}{N+1} \left( r^2 \int_c^r V_{N-1}(\rho(x_1)) dx_1 - \int_c^r x_1^2 V_{N-1}(\rho(x_1)) dx_1 \right).
\end{aligned} \tag{238}$$

Note that the first integral in (238) is the definition of the cap volume  $\mathcal{K}_N(r, c)$ , derived in (146), while the second integral is exactly our target integral  $I_{x^2}$ , defined in (229). Substituting these identifications back into the expression, we have

$$-\int_c^r v du = \frac{r^2}{N+1} \mathcal{K}_N(r, c) - \frac{1}{N+1} I_{x^2}. \quad (239)$$

By combining (235), (237), and (239), we have

$$I_{x^2} = cQ_N(r, c) + \frac{r^2}{N+1} \mathcal{K}_N(r, c) - \frac{1}{N+1} I_{x^2}. \quad (240)$$

This leads to

$$I_{x^2} = \frac{N+1}{N+2} cQ_N(r, c) + \frac{r^2}{N+2} \mathcal{K}_N(r, c). \quad (241)$$

Now based on (229), (230), and (241), we have

$$\begin{aligned} J_N(r, c) &= \frac{N-1}{N+1} r^2 \mathcal{K}_N(r, c) + \frac{2}{N+1} \left( \frac{N+1}{N+2} cQ_N(r, c) + \frac{r^2}{N+2} \mathcal{K}_N(r, c) \right) \\ &= \frac{N-1}{N+1} r^2 \mathcal{K}_N(r, c) + \frac{2c}{N+2} Q_N(r, c) + \frac{2r^2}{(N+1)(N+2)} \mathcal{K}_N(r, c) \\ &= \frac{Nr^2}{N+2} \mathcal{K}_N(r, c) + \frac{2c}{N+2} Q_N(r, c). \end{aligned} \quad (242)$$

### C. Moments of a Shifted, Left-Oriented Hyperspherical Cap

Let  $\mathcal{B}'_N(r)$  be an  $N$ -ball with radius  $r$  centered at  $\mathbf{z} = (z, 0, \dots, 0)$  on the principal axis. Let the defining hyperplane be located at  $x_1 = u_c$ , such that the cap lies to the left of the center (i.e.,  $u_c < z$ ). The region  $\mathcal{C}_{\text{left}}$  is defined as

$$\mathcal{C}_{\text{left}} = \{\mathbf{x} \in \mathbb{R}^N \mid \|\mathbf{x} - \mathbf{z}\|_2 \leq r \text{ and } x_1 \leq u_c\}. \quad (243)$$

We define the distance parameter  $c$  as

$$c = |u_c - z| = z - u_c. \quad (244)$$

Note that the geometry of this cap (its volume and intersection height) is identical to a standard right-oriented cap cut at distance  $c$ , defined in (215). Specifically, the intersection height is  $h = \sqrt{r^2 - c^2}$ , and the volume is  $\mathcal{K}_N(r, c)$ . The geometry is illustrated in Figure 20.

To utilize the standard results derived previously ( $Q_N$  and  $J_N$ ), which assume a cap centered at the origin oriented to the right, we define a local coordinate system  $(u, \mathbf{u}_\perp)$  centered at  $\mathbf{z}$ :

$$x_1 = u + z, \quad \mathbf{x}_\perp = \mathbf{u}_\perp. \quad (245)$$

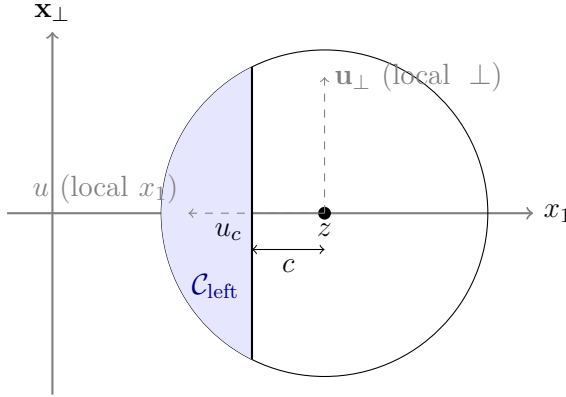


Fig. 20. Geometry of the shifted, left-oriented hyperspherical cap  $\mathcal{C}_{\text{left}}$  (visualized in cross-section). The ball is centered at global coordinate  $x_1 = z$ . The cut is at  $x_1 = u_c$ . The local coordinate  $u$  is defined relative to the center  $z$ , such that the cap extends in the negative  $u$  direction (region  $u \leq -c$ ).

In this local frame, the  $N$ -ball is centered at the origin. The cut location implies that  $x_1 \leq u_c$  transforms to  $u + z \leq u_c$ , which means  $u \leq u_c - z = -c$ . Thus, the region of integration in the local frame is  $\mathcal{C}_{\text{local}} = \{(u, \mathbf{u}_\perp) \mid \|\mathbf{u}\|_2 \leq r \text{ and } u \leq -c\}$ .

We first determine the moments in this local frame using symmetry arguments. The standard result  $Q_N(r, c)$  derived in (223) corresponds to a right-sided cap ( $u \geq c$ ). For a left-sided cap ( $u \leq -c$ ), the geometry is mirrored across the hyperplane  $u = 0$ . Since the integrand  $u$  is an odd function, the sign of the integral flips. More precisely, we have

$$Q_{\text{local}} = \int_{\mathcal{C}_{\text{local}}} u \, dV = -Q_N(r, c). \quad (246)$$

Conversely, the integrand for the second moment is  $\|\mathbf{u}\|_2^2 = u^2 + \|\mathbf{u}_\perp\|_2^2$ . Since  $u^2 = (-u)^2$ , the reflection of the domain does not affect the value of the integral. Thus, it equals the standard second moment. More precisely, we have

$$J_{\text{local}} = \int_{\mathcal{C}_{\text{local}}} \|\mathbf{u}\|_2^2 \, dV = J_N(r, c). \quad (247)$$

We now calculate the moments relative to the global origin  $(0, \mathbf{0})$  by substituting the coordinate transformation  $x_1 = u + z$  into the integrals. The first moment is the integral of the global coordinate  $x_1$  is

$$\int_{\mathcal{C}_{\text{left}}} x_1 \, dV = \int_{\mathcal{C}_{\text{local}}} (u + z) \, dV. \quad (248)$$

By the linearity of integration, we distribute the terms into the local first moment  $Q_{\text{local}}$  and the volume term, as follows

$$\int_{\mathcal{C}_{\text{left}}} x_1 dV = \underbrace{\int_{\mathcal{C}_{\text{local}}} u dV}_{Q_{\text{local}}} + z \underbrace{\int_{\mathcal{C}_{\text{local}}} 1 dV}_{\text{Volume}}. \quad (249)$$

Substituting the local values derived in (246), we obtain the global first moment as

$$\int_{\mathcal{C}_{\text{left}}} x_1 dV = -Q_N(r, c) + z\mathcal{K}_N(r, c). \quad (250)$$

Similarly, for the second moment note that

$$\begin{aligned} \int_{\mathcal{C}_{\text{left}}} \|\mathbf{x}\|_2^2 dV &= \int_{\mathcal{C}_{\text{local}}} (x_1^2 + \|\mathbf{x}_\perp\|_2^2) dV \\ &= \int_{\mathcal{C}_{\text{local}}} ((u + z)^2 + \|\mathbf{u}_\perp\|_2^2) dV. \end{aligned} \quad (251)$$

Note that we have

$$(u^2 + \|\mathbf{u}_\perp\|_2^2) + 2zu + z^2 = \|\mathbf{u}\|_2^2 + 2zu + z^2. \quad (252)$$

Substituting this back into (251), we have

$$\int_{\mathcal{C}_{\text{left}}} \|\mathbf{x}\|_2^2 dV = \underbrace{\int_{\mathcal{C}_{\text{local}}} \|\mathbf{u}\|_2^2 dV}_{J_{\text{local}}} + 2z \underbrace{\int_{\mathcal{C}_{\text{local}}} u dV}_{Q_{\text{local}}} + z^2 \underbrace{\int_{\mathcal{C}_{\text{local}}} 1 dV}_{\text{Volume}}. \quad (253)$$

Finally, substituting the analytical expressions for the local moments from (246) and (247) leads to

$$\begin{aligned} \int_{\mathcal{C}_{\text{left}}} \|\mathbf{x}\|_2^2 dV &= J_N(r, c) + 2z(-Q_N(r, c)) + z^2\mathcal{K}_N(r, c) \\ &= J_N(r, c) - 2zQ_N(r, c) + z^2\mathcal{K}_N(r, c). \end{aligned} \quad (254)$$

## APPENDIX I

### SECOND MOMENT OF AN $N$ -BALL

In this section, we derive the general formula for the second moment (polar moment of inertia) of an  $N$ -dimensional ball with uniform density. Let  $B(N, r)$  denote an  $N$ -ball of radius  $r$  centered at the origin in  $\mathbb{R}^N$ , and let  $V_N(r)$  denote its volume. We seek to calculate the integral of the squared magnitude of the position vector  $\mathbf{u} \in \mathbb{R}^N$  over this volume

$$M_2(N, r) = \int_{B(N, r)} \|\mathbf{u}\|_2^2 dV. \quad (255)$$

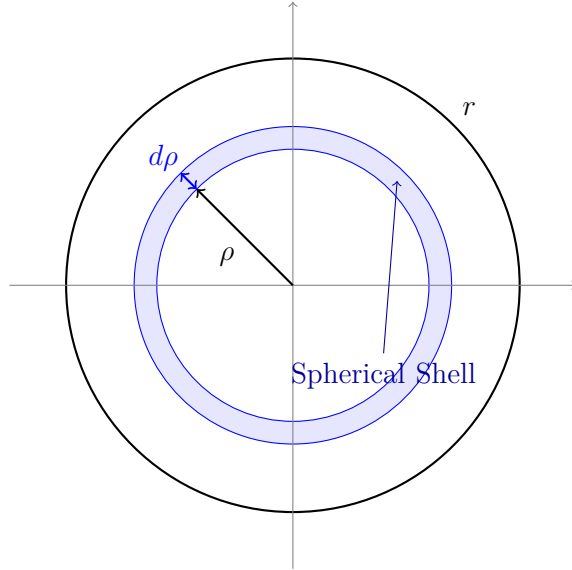


Fig. 21. Decomposition of the  $N$ -ball volume into infinitesimal spherical shells. The integral sums the contributions of shells with radius  $\rho$  and thickness  $d\rho$  from the center to the boundary  $r$ .

We evaluate this integral using spherical coordinates. We decompose the volume of the  $N$ -ball into infinitesimal spherical shells of radius  $\rho$  (where  $0 \leq \rho \leq r$ ) and thickness  $d\rho$ . This decomposition is illustrated in Figure 21.

Recall that the volume of an  $N$ -ball is given by

$$V_N(\rho) = C_N \rho^N, \quad (256)$$

where

$$C_N = \frac{\pi^{N/2}}{\Gamma(\frac{N}{2} + 1)}. \quad (257)$$

The surface area of the  $(N - 1)$ -sphere (the boundary of the  $N$ -ball) at radius  $\rho$ , denoted  $A_{N-1}(\rho)$ , is the derivative of the volume with respect to the radius. Thus, we have

$$A_{N-1}(\rho) = \frac{d}{d\rho} V_N(\rho) = N C_N \rho^{N-1}. \quad (258)$$

Consequently, the differential volume element of a shell at radius  $\rho$  is

$$dV = A_{N-1}(\rho) d\rho = N C_N \rho^{N-1} d\rho. \quad (259)$$

Since the squared magnitude  $\|\mathbf{u}\|_2^2 = \rho^2$  is constant on a spherical shell of radius  $\rho$ , the integral becomes

$$\begin{aligned} M_2(N, r) &= \int_0^r \rho^2 \left( NC_N \rho^{N-1} d\rho \right) \\ &= NC_N \int_0^r \rho^{N+1} d\rho. \end{aligned} \quad (260)$$

This implies that

$$\begin{aligned} M_2(N, r) &= NC_N \left[ \frac{\rho^{N+2}}{N+2} \right]_0^r \\ &= \frac{N}{N+2} C_N r^{N+2}. \end{aligned} \quad (261)$$

We can rewrite this expression to explicitly include the volume of the ball  $V_N(r) = C_N r^N$ . More precisely, we have

$$M_2(N, r) = \frac{N}{N+2} r^2 (C_N r^N) = \frac{N}{N+2} r^2 V_N(r). \quad (262)$$

Therefore, we arrive at the final result

$$\int_{B(N,r)} \|\mathbf{u}\|_2^2 dV = \frac{N}{N+2} r^2 V_N(r). \quad (263)$$

---

**Algorithm 2** Characterizing the Optimal  $N$ -Dimensional Adversarial Noise Distribution

---

- 1: **Input:** Dimension  $N$ , decoding threshold  $\eta$ , bound  $\Delta$ , the utility function  $Q_{\text{AD}}(\cdot, \cdot)$ , and the derived function  $c_\eta(\cdot)$  from Theorem 2.
- 2: **Output:** The optimal noise distribution PDF  $g_{\mathbf{N}_a}^*(\mathbf{x})$ .
- 3: Define  $\Phi_N(z)$  as in (24), and  $\Psi_N(z)$  as in (28).
- 4: Define  $\tilde{\Psi}_N(q) \triangleq \Psi_N(\Phi_N^{-1}(q))$  for  $q \in [0, 1]$ .
- 5: Let  $\tilde{\Psi}_N^*(q)$  denote the upper concave envelope of  $\tilde{\Psi}_N(q)$  over  $q \in [0, 1]$ .

**6: Step 1: Optimal Operating Point Selection**

- 7: Calculate the optimal acceptance probability  $\alpha^*$  that maximizes the adversary's objective

$$\alpha^* = \arg \max_{0 < \alpha \leq 1} Q_{\text{AD}}(c_\eta(\alpha), \alpha).$$

**8: Step 2: Construction of Noise Distribution**

- 9: **if**  $\tilde{\Psi}_N^*(\alpha^*) = \tilde{\Psi}_N(\alpha^*)$  **then**
- 10:   // Case 1: The function lies on its concave envelope.
- 11:   Calculate the optimal noise radius:  $z^* = \Phi_N^{-1}(\alpha^*)$ .
- 12:   Output the distribution uniform over a single  $N$ -sphere of radius  $z^*$ :

$$g_{\mathbf{N}_a}^*(\mathbf{x}) = \frac{1}{S_N(z^*)} \delta(\|\mathbf{x}\|_2 - z^*),$$

where  $S_N(r) = \frac{2\pi^{N/2}}{\Gamma(N/2)} r^{N-1}$ .

- 13: **else**
- 14:   // Case 2: The function lies below its concave envelope.
- 15:   Find probabilities  $q_1 < \alpha^* < q_2$  such that the envelope touches the function at the endpoints:

$$\tilde{\Psi}_N^*(q_1) = \tilde{\Psi}_N(q_1) \quad \text{and} \quad \tilde{\Psi}_N^*(q_2) = \tilde{\Psi}_N(q_2),$$

and is linear in between.

- 16:   Calculate the corresponding radii:  $z_1 = \Phi_N^{-1}(q_1)$  and  $z_2 = \Phi_N^{-1}(q_2)$ .
- 17:   Calculate the mixing weights:

$$\beta_1 = \frac{q_2 - \alpha^*}{q_2 - q_1}, \quad \beta_2 = \frac{\alpha^* - q_1}{q_2 - q_1}.$$

- 18:   Output the mixture distribution uniform over two  $N$ -spheres:

$$g_{\mathbf{N}_a}^*(\mathbf{x}) = \beta_1 \frac{1}{S_N(z_1)} \delta(\|\mathbf{x}\|_2 - z_1) + \beta_2 \frac{1}{S_N(z_2)} \delta(\|\mathbf{x}\|_2 - z_2).$$

- 19: **end if**

---